(3)

Applied Research Laboratory
The Pennsylvania State University

AD-A173 359

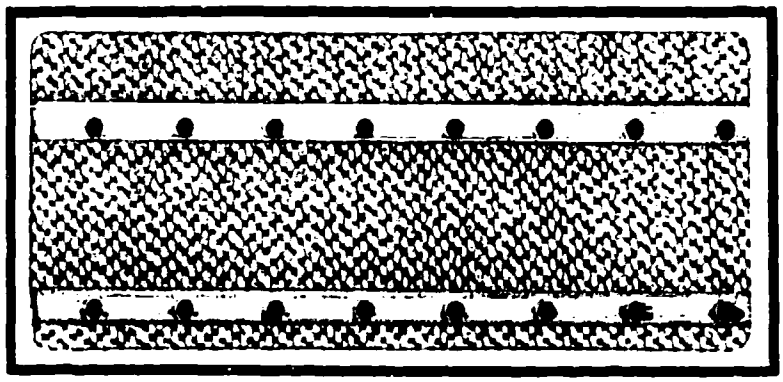

DTIC FILE COPY

DTIC ELECTE
OCT 2 3 1986
A

(ARL-PSU)

TECHNICAL REPORT

86 10 22 050

(3)

The Pennsylvania State University
Intercollege Research Programs and Facilities
APPLIED RESEARCH LABORATORY
P. O. Box 30
State College, PA 16804

WALL PRESSURE FLUCTUATIONS AND ACOUSTICS IN TURBULENT PIPE FLOW

by

M. A. Daniels, G. C. Lauchle

Technical Report TR 86-006

September 1986

Supported by: Naval Scientific Technical Exchange Program

L. R. Hettche, Director
Applied Research Laboratory

Unclassified
SECURITY CLASSIFICATION OF THIS PAGE

AD-A173359

REPORT DOCUMENTATION PAGE

1a. REPORT SECURITY CLASSIFICATION Unclassified	1b. RESTRICTIVE MARKINGS
2a. SECURITY CLASSIFICATION AUTHORITY	3. DISTRIBUTION/AVAILABILITY OF REPORT Approved to public release; distribution unlimited
2b. DECLASSIFICATION/DOWNGRADING SCHEDULE	
4. PERFORMING ORGANIZATION REPORT NUMBER(S)	5. MONITORING ORGANIZATION REPORT NUMBER(S)
6a. NAME OF PERFORMING ORGANIZATION Applied Research Laboratory The Pennsylvania State Univ.	6b. OFFICE SYMBOL (If applicable) ARL
7a. NAME OF MONITORING ORGANIZATION Naval Sea Systems Command Department of the Navy	
6c. ADDRESS (City, State, and ZIP Code) P. O. Box 30 State College, PA 16804	7b. ADDRESS (City, State, and ZIP Code) Washington, DC 20362
8a. NAME OF FUNDING/SPONSORING ORGANIZATION Naval Sea Systems Command	8b. OFFICE SYMBOL (If applicable) NAVSEA
9. PROCUREMENT INSTRUMENT IDENTIFICATION NUMBER	
8c. ADDRESS (City, State, and ZIP Code) Department of the Navy Washington, DC 20362-	10. SOURCE OF FUNDING NUMBERS PROGRAM ELEMENT NO. / PROJECT NO / TASK NO. / WORK UNIT ACCESSION NO.
11. TITLE (Include Security Classification) Wall Pressure Fluctuations and Acoustics in Turbulent Pipe Flow	
12. PERSONAL AUTHOR(S) M. A. Daniels and G. C. Lauchle	
13a. TYPE OF REPORT M.S. Thesis	13b. TIME COVERED FROM _____ TO _____
14. DATE OF REPORT (Year, Month, Day) August 1986	15. PAGE COUNT 116
16. SUPPLEMENTARY NOTATION	

17. COSATI CODES		
FIELD	GROUP	SUB-GROUP

18. SUBJECT TERMS (Continue on reverse if necessary and identify by block number)
turbulent boundary layer, acoustics, pressure spectrum experimental, signal processing, noise, coherence function, glycerine, transducer

19. ABSTRACT (Continue on reverse if necessary and identify by block number)

Measurements of the turbulent boundary layer (TBL) wall pressure spectrum and the facility's propagating acoustic field were conducted in the Boundary Layer Research Facility (glycerine tunnel) of the Applied Research Laboratory at The Pennsylvania State University. Subminiature, piezo-resistive-type pressure transducers were used for these measurements. A detailed calibration of the pressure transducers was conducted using a standing wave tube. Measured sensitivities of the transducers were within 0.5 dB of factory specifications and measured phase differences between individual transducers were insignificant. The turbulent boundary layer wall pressure spectrum was obtained using a novel signal-processing

20. DISTRIBUTION/AVAILABILITY OF ABSTRACT ☒ UNCLASSIFIED/UNLIMITED ☐ SAME AS PPT ☐ OTIC USERS	21. ABSTRACT SECURITY CLASSIFICATION Unclassified
22a. NAME OF RESPONSIBLE INDIVIDUAL	22b. TELEPHONE (Include Area Code) / 22c. OFFICE SYMBOL

DD FORM 1473, 84 MAR — 83 APR edition may be used until exhausted. All other editions are obsolete.

SECURITY CLASSIFICATION OF THIS PAGE
Unclassified

19 ABSTRACT (continued)

technique that allowed a minimization of both acoustic and vibration-induced noise. This technique uses pairs of transducer difference signals from an axisymmetric array of three flush-mounted pressure sensors and permits the cancellation of the propagating acoustic and vibrationally induced pressure fields. A measurement involving the coherence function between these transducer signals was shown to validate the measured TBL wall pressure spectra and all assumptions used in the development of the measurement technique. Non-dimensionalized spectra of the TBL fluctuating wall pressure measured in this investigation are compared to those measured in previous investigations. These comparisons have substantiated a maximum, normalized transducer diameter for the complete resolution of the high-frequency part of the TBL wall pressure spectrum. In this study, using glycerine as the working fluid, the transducer diameter is less than four (4) wall units, a factor of nine (9) smaller than ever before achieved.

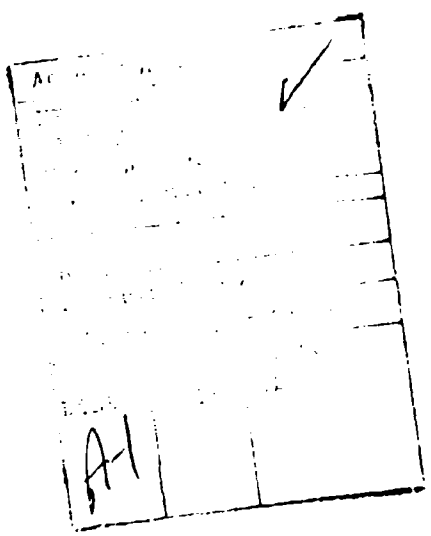

ABSTRACT

Measurements of the turbulent boundary layer (TBL) wall pressure spectrum and the facility's propagating acoustic field were conducted in the Boundary Layer Research Facility (glycerine tunnel) of the Applied Research Laboratory at The Pennsylvania State University. Subminiature, piezo-resistive-type pressure transducers were used for these measurements. A detailed calibration of the pressure transducers was performed using a standing wave tube. Measured sensitivities of the transducers were within 0.5 dB of factory specifications and measured phase differences between individual transducers were insignificant. The TBL wall pressure spectrum was obtained using a novel signal-processing technique that allowed a minimization of both acoustic and vibration-induced noise. This technique uses pairs of transducer difference signals from an axisymmetric array of three flush-mounted pressure sensors and permits the cancellation of the propagating acoustic and vibrationally induced pressure fields. A measurement involving the coherence function between these transducer signals was shown to validate the measured TBL wall pressure spectra and all assumptions used in developing the measurement technique. Non-dimensionalized spectra of the TBL fluctuating wall pressure measured in this investigation are compared to those measured in previous investigations. These comparisons substantiated a maximum, normalized transducer diameter for the complete resolution of the high-frequency part of the TBL wall pressure spectrum. In this study, using glycerine as the working fluid, the transducer diameter is less than four (4) wall units, a factor of nine (9) smaller than ever before achieved.

TABLE OF CONTENTS

		Page
ABSTRACT		iii
LIST OF TABLES		vii
LIST OF FIGURES		viii
GLOSSARY		xi
ACKNOWLEDGMENTS		xii
Chapter		
1	INTRODUCTION	1
1.1	Turbulence-Induced Pressure Fields	1
1.2	Statement of the Objective	5
1.3	Scope of the Thesis	6
2	MEASUREMENT TECHNIQUE AND ANALYSIS	8
2.1	Introduction	8
2.2	Array Description	8
2.3	Model Assumptions and Considerations	10
2.4	Analysis: The Finite Fourier Transform	11
2.5	TBL Spectrum From Cross-Difference Signals	12
2.6	Analysis of Vibrationally Induced Terms	15
2.7	Estimation of Vibrational Spectral Quantities	19
2.8	Cross-Spectral Measurements: Acoustic and Vibratory Noise	21
2.9	Estimation of Vibrational Terms	23

TABLE OF CONTENTS (Continued)

Chapter		Page
3	PRESSURE SENSORS AND CALIBRATION TECHNIQUES	24
	3.1 Introduction	24
	3.2 Pressure Sensor Description	24
	3.3 Calibration and Phase Measurement Techniques	30
	3.3.1 Calibration Tube Assembly	31
	3.3.2 Water Versus Glycerine Calibration Mediums	31
	3.4 Data Acquisition and Reduction	34
	3.5 Results	36
	3.6 Conclusions	37
4	THE GLYCERINE TUNNEL AND WALL PRESSURE MEASUREMENTS	42
	4.1 Introduction	42
	4.2 The Experimental Facility	44
	4.2.1 Tunnel Mean Velocity	47
	4.2.2 Wall Shear Stress Measurements	49
	4.2.3 TBL Measurement Array and Data Acquisition System	51
	4.3 TBL Wall Pressure Spectra	53
	4.4 Correlation of the TBL in the Cross-Difference Spectrum	66
	4.5 Tunnel Background Noise	73
	4.6 Conclusions and Areas of Future Research	82

TABLE OF CONTENTS (Continued)

	Page
APPENDIX 1 : SPECTRAL DENSITY VIA THE FINITE FOURIER TRANSFORM	84
APPENDIX 2 : SOUND PROPAGATION IN CIRCULAR TUBES	89
APPENDIX 3 : RANDOM AND BIAS ERRORS IN THE CROSS-DIFFERENCE SIGNAL SPECTRUM	92
APPENDIX 4 : CORCOS' CORRECTIONS TO THE ESTIMATED TBL WALL PRESSURE SPECTRUM	95
BIBLIOGRAPHY	97

LIST OF TABLES

Table		Page
3.1	Endevco Factory Nominal Sensitivities of Transducers with a 10-Volt Excitation	28
3.2	Endevco Typical Specifications, Series 8514 Transducer with a 10-Volt Power Supply	29
4.1	Comparison of the Measured and Corrected Normalized Wall Pressure r.m.s. Levels	65
A2.1	Roots of $J_m'(\alpha_{mv})$	90
A3.1	Estimation Errors in the Measured Spectral Density Functions	93
A4.1	Attenuation Factors for a Round Transducer	95

LIST OF FIGURES

Figure		Page
2.1	Array and Sensor Locations	9
2.2	Ideal Single Input/Single Output System	15
2.3	Vibrational Noise Model	20
2.4	Vibrational Noise Model	23
3.1	TBL Pressure Fluctuations and Sensor Size	25
3.2	Schematic Diagram of the 4-Arm Bridge of the Sensors	26
3.3	Typical Transducer Sensitivity Shift (mV/Pa/Input Volt) Due to Varying Supply Voltage	27
3.4	Input Supply Voltage Versus Time Under Full Loading (All Three Sensors)	28
3.5	Physical Dimensions of Subminiature Transducers	29
3.6	Calibration Tube and Transducer Assemblies	32
3.7	Water and Glycerine Transducer Output Voltage Versus Frequency	34
3.8	Source Input Voltage Spectrum	35
3.9	Data Acquisition System and Tube Calibrator	36
3.10	Measured Sensitivity of Sensor KW45, Average=-227.6 dB	38
3.11	Measured Sensitivity of Sensor KW35, Average=-227.2 dB	39
3.12	Measured Sensitivity of Sensor KW38, Average=-227.8 dB	39

LIST OF FIGURES (Continued)

Figure		Page
3.13	Measured Phase Difference between Sensors KW45 and KW35	40
3.14	Measured Phase Difference between Sensors KW45 and KW38	40
3.15	Measured Phase Difference between Sensors KW35 and KW38	41
4.1	Measured Kinematic Viscosity of Glycerine as Per Standard Method ASTM D445-83	43
4.2	Closed Circuit Glycerine Tunnel	45
4.3	Static Pressure Measurement Locations of Mean Flow Velocity, with Nozzle Contraction Ratio of 16:1	47
4.4	15-PSI, Differential Pressure Transducer Calibration	48
4.5	Tunnel Velocity Versus Glycerine Temperature	49
4.6	Wall Shear Stress Versus Glycerine Temperature	50
4.7	5-PSI, Differential Transducer Calibration Results	51
4.8	Cross-sectional View of Plug Assembly	52
4.9	Difference Signal Versus COP Difference Signal Spectrum	54
4.10	G_{tbl} Versus Glycerine Temperature	56
4.11	Normalized Wall Pressure Spectral Density, re: τ_w and D	58
4.12	Normalized Wall Pressure Spectral Density, re: ρ, δ and U	59

LIST OF FIGURES (Continued)

Figure		Page
4.13	Turbulent Boundary Layer Similarity Plot of the Wall Pressure Spectrum	62
4.14	Inner Boundary Layer Similarity Plot of the Wall Pressure Spectrum	63
4.15	Dependence of the Normalized r.m.s. Value of the Wall Pressure Fluctuations upon the Normalized Transducer Diameter	65
4.16	Typical Coherence Function between Transducer Difference Signals	70
4.17	Typical Cross-Difference (TBL) and Difference Spectra	72
4.18	Spectral Plots of the Auto, Cross and TBL Pressure Fluctuations at 35.0° C	74
4.19	Spectral Plots of the Auto, Cross and TBL Pressure Fluctuations at 46.1° C	75
4.20	Typical Phase Response between Transducer Difference Signals at 35.0 ° C	76
4.21	Typical Phase Response between Transducer Signals at 35.0° C	77
4.22	Typical Phase Response between Transducer Difference Signals at 46.1 ° C	78
4.23	Typical Phase Response between Transducer Signals at 46.1° C	79
4.24	Typical Auto and Coherent Output Power Spectra	81

GLOSSARY

$a(r,\theta,t)$, $b(r,\theta,t)$, $c(r,\theta,t)$	transducer time varying output voltages
$A(f)$, $B(f)$, $C(f)$	Fourier transformed quantities of $a(t)$, $b(t)$, and $c(t)$, respectfully
c	sound speed
COP	coherent output power function
d, D	transducer diameter, pipe diameter
d^+	normalized transducer diameter, $u_\tau d/\upsilon$
$E[...]$	expected value operator
f	frequency, cycles/second
f^+	normalized frequency, $f\upsilon/u_\tau^2$
G_{XX}, G_{XY}	auto and cross-spectral density functions
$H(j\omega)$	complex transfer function
j	$\sqrt{-1}$
J_m	Bessel function of order m
k	acoustic or sonic wavenumber, ω/c
k_c	convective wavenumber, ω/U_c
M	transducer sensitivity, Volt/μPa
r	radial distance and transducer radius
$u'_i(t)$	local time varying measured acceleration levels
u_τ	wall friction of shear velocity
U	mean tunnel velocity

Greek terms and symbols.

γ_{XY}	ordinary coherence function between x and y
θ	usual angular coordinate
λ	acoustic wavelength, c/f
υ	fluid kinematic viscosity
ρ	fluid density
τ	time shift variable
τ_w	wall shear stress
φ_{AB}	measured phase difference
ω	radian frequency, $2\pi f$
∇	the "del" operator
$\int$	integral sign

ACKNOWLEDGMENTS

I would first like to thank Dr. Gerald Lauchle who suggested this thesis topic and was crucial in the understanding and interpretation of the data. I would also like to thank him for his instructive aid in the successful completion of this manuscript. Thanks are also due to my other thesis committee members, Dr. Courtney Burroughs and Dr. Steven Deutsch, for their constructive comments and critical review of the final thesis manuscript. Other thanks are due to the many individuals who aided in getting the glycerine tunnel back up in working order after its long rest period. Among these people, special thanks are given to Mr. Wilden Nuss and Mr. Nevin Fngle for their aid in setting up and testing the electronical instrumentation used throughout this investigation.

This work was performed at the Applied Research Laboratory under contract with the Naval Sea Systems Command and was supported by the Applied Research Laboratory Exploratory and Foundational Research Program.

Chapter 1
INTRODUCTION

1.1 Turbulence-Induced Pressure Fields

The pressure induced by boundary-layer turbulence has generated much concern, arising primarily from the unsteady loads it induces on flexible panels and the noise that it radiates (due to pressure fluctuations in the fluid, or indirectly from panel vibration). Panel vibration is driven by the spatially integrated turbulent boundary layer (TBL) pressure field, weighted against the structure's response function, so that the integral scales of the pressure fluctuations are important measures of boundary layer turbulence. Essentially, the correlation area of the pressure producing turbulent eddies determines the mean-square level of the applied force field.

The subject of wall pressure fluctuations beneath turbulent boundary layers has been extensively studied [for reviews see Corcos (1964), Haddle and Skudrzyk (1969), and Willmarth (1975)]. From these analytical and experimental investigations, it is now widely accepted that the energy associated with TBL wall pressure fluctuations is distributed over wide frequency and wavenumber ranges. Three distinct wavenumber regions of the turbulent pressure fluctuations have been identified; they are, in order of increasing wavenumber, the sonic, low wavenumber and convective regions, respectfully.

The lowest wavenumber region (longest wavelengths) of the TBL pressure fluctuations consists of wavenumbers less than and equal to the sonic wavenumber ($k=\omega/c$) of the fluid, where ω is the radian frequency and c, the sound speed in the fluid. This pressure field, although very weak, radiates as true sound and is caused by the interaction of the turbulence

with itself. Many investigators have addressed this sound field with major contributions from Lighthill (1952, 1954), Haddle and Skudrzyk (1969), and Tam (1975). A few of the many other experimental studies of this TBL-induced sound field include Nishi et al.(1970), Skudryzk and Haddle (1960), Meecham (1965), Vecchio and Wiley (1973) and Lauchle (1976).

Wall pressure fluctuations at wavenumbers greater than sonic wavenumber (k) and smaller than the convective wavenumber ($k_c=\omega/U_c$, where U_c is the convection velocity), describe the low wavenumber region of the TBL pressure fluctuations. It is presumed that large-scale coherent motions in the TBL are characterized by bursts and sweeps of turbulent energy and contribute significantly to the pressure fluctuations in this low wavenumber region (e.g., Kline et al. (1963), and Blackwelder and Kaplan (1976)). Although comprising a very small portion of the total TBL's wavenumber-frequency spectral energy it is thought that these large-scale motions in the TBL are major causes of excessive structural fatigue. Analytical models for the pressure field at these low wavenumbers are given by Chase (1980), Maestrello (1965,1967), and Wetting (1976). Extensive measurements of the wall pressure fluctuations in this low wavenumber region do not exist because of the inherent experimental difficulty with such measurements. For example, spatial filters are needed to eliminate both very low and high convective wave contributions. Farabee and Geib (1976), Willis (1970), Blake and Chase (1971), and Martin and Leehey (1977) have performed some of these measurements; however, reasonable agreement between experimental results and theoretical predictions are less than satisfactory.

The final region of the TBL wavenumber spectrum consists of wavenumbers that lie in a narrow ridge, centered about the convective

wavenumber (k_c) of the flow. Pressure fluctuations in this convective region arise from the interaction of the turbulence and the mean shear. Current models suggest that this region is composed of the dominant TBL fluctuating energy and comprises the major part of the r.m.s. wall pressure. This so-called "convective ridge" energy arises because small-scale turbulent motions within the TBL convect over a surface at a preferred convection velocity (typically 0.7 to 0.8 times the free-stream velocity). However, these small-scale eddies are correlated for very short distances and decay due to the viscous damping effects of the fluid. In fact, the distances that these pressure producing eddies convect is directly proportional to their size. The pressure field along this convective ridge has perhaps received the most attention, beginning with the theoretical modeling by Kraichnan (1956a, b). Willmarth (1975) gives an account of the most significant contributions to this area.

Although the energy contained in this pressure ridge dominates the wavenumber-frequency spectrum, its accurate measurement over a wide frequency range is not a trivial matter. Early experimental studies, particularly those of Willmarth (1956) and Corcos (1963,1964) recognized the necessity of "small" pressure transducers in conducting TBL wall pressure fluctuation measurements. The convective domain is primarily dominated (spatially) by small-scale eddies. Therefore, finite-sized pressure sensors--which average over space--need to be at least as small as the smallest eddies; otherwise, an attenuation of the high-frequency (small wavelength) spectral contributions (particularly those in this convective ridge) will occur. Kolmogoroff (see Hinze, 1959, for discussion) deduced both length and velocity scales for these smallest eddies. He found that the size of the smallest eddies is inversely

proportional to the 1/4th power of the dissipation rate of turbulent energy. Conversely, he found that the velocity scale is directly proportional to the 1/4th power of this same dissipation rate. Therefore, by combining these two quantities in a Reynolds number fashion it is easily demonstrated that these smallest eddies scale as υ/u_τ, where υ is the kinematic viscosity and u_τ is the friction (or shear) velocity. Emmerling (1973) was the first investigator to verify experimentally that the smallest scales of the turbulence are indeed the same order as the viscous length scale υ/u_τ. The parameter that most accurately describes the degree of spectral resolution for a given wall pressure measurement is therefore, $d^+=u_\tau d/\upsilon$, where d is the pressure transducer's active diameter. Clearly, d^+ must be of order one to resolve the smallest scale pressure fluctuations, e.g. Emmerling (1973).

As stated, many of the early wall pressure fluctuation measurements [Willmarth (1956), Willmarth and Wooldridge (1962), and Bull and Willis (1961), among others] suffered from transducer spatial averaging problems. In order to alleviate these problems, Corcos (1963) developed a correction factor that could be applied directly to the measured TBL spectral levels. Corcos' correction factors, however, were based on the similarity parameter $\omega r/U_c$ (where r=d/2) and not on d^+. In another investigation Blake (1970) customized an 1/8-inch condenser microphone by placing a cap, perforated with an 1/32-inch diameter hole over its center. With this type of approach, Blake hoped to resolve the high-frequency part of the TBL wall pressure spectrum. Blake's results clearly indicated that the TBL pressure fluctuations contained a larger frequency content (smaller scale pressure fluctuations) than what had been measured previously. However, the effect of the hole on the TBL wall pressure spectrum was not clearly

understood. That is, was the observed higher frequency content of the TBL wall pressure spectrum attributed to the pressure fluctuations in the TBL or, was it due to some other anomalous contribution from the pin-hole. Bull and Thomas (1976) later addressed this question by comparing the TBL wall pressure spectrum measured by a microphone with a pin-hole cap (pin-hole microphone), to that measured with a quartz-type transducer of the same diameter as the pin-hole. Their findings indicated that the increase in the frequency content of the TBL wall pressure spectrum were, in part, attributable to the hole and the small resonance cavity that existed between the perforated cap and transducer diaphragm. Subsequent investigations of the TBL wall pressure spectrum have followed, together with controversies centered on the parameters that best describe the ultimate in transducer resolution and the scaling of the TBL wall pressure spectrum.

Without the use of pin-hole type pressure transducers, Schewe (1983) was the first investigator to obtain wall pressure fluctuation data for $d^+<50$. His lowest quoted value is a d^+ of 19, and he states that his measurements of the TBL wall pressure spectrum are representative of a true point measurement; that is, there should be no attenuation of the TBL spectrum's high-frequency content. In this investigation, TBL wall pressure spectra are obtained using a unique facility and data processing technique. The transducer spatial resolution achieved is significantly better than any previous investigation; a d^+ of 2.1 is demonstrated.

1.2 Statement of the Objective

The uniqueness of the TBL wall pressure measurements conducted in this investigation lie in the fluid and the facility in which they were made. All

data obtained in previous investigations were obtained in either water or air. This investigation, however, uses glycerine as the working fluid. Glycerine has a kinematic viscosity (υ), at room temperature, of almost 1000 times that of water and roughly 50 times that of air. Because of this, the smallest normalized transducer diameter ($d^+=2.1$) to date has been achieved. Therefore, the high-frequency spectral energy of the TBL can be investigated by the acquisition and comparison of the spectral data at a d^+ which is a factor of nine (9) smaller than that achieved in the Schewe investigation. Also, the unique way in which the flow Reynolds number is altered (viscosity is primarily the independent variable rather than the mean flow velocity) allows for a better understanding of the scaling laws that characterize the TBL wall pressure spectrum.

Investigations involving single point measurements of the TBL wall pressure spectra are often plagued with low-frequency facility noise. The measurement technique used in this investigation minimizes these effects while maintaining the integrity of the measured TBL pressure spectrum. In addition, a measurement involving the coherence function between a set of (co-planar) transducer difference signals is shown to validate the TBL wall pressure spectra (especially at low frequencies).

1.3 Scope of the Thesis

This chapter introduced some fundamental aspects of turbulence and the basic types of noise associated with it. The problems to be addressed in subsequent chapters were also described and the anticipated results discussed.

Chapter 2 concentrates on the techniques used to measure the turbulent boundary layer (TBL) wall pressure fluctuations. This selected technique is

an improvement on a method previously used by Horne and Hansen (1981), in which an axisymmetric, flush-mounted, pressure transducer array is used to minimize the farfield acoustic effects in the TBL wall pressure spectrum.

The types of pressure transducers used through this investigation are described in Chapter 3. Also described is transducer calibration scheme. The measured sensitivities and relative phase responses of the pressure transducers are given.

Chapter 4 presents data on the measured TBL wall pressure spectrum at a number of flow Reynolds numbers and compares these results, in non-dimensional form, to those obtained by other investigators. Also described are important scaling parameters that aid in the understanding of the TBL wall pressure spectrum. This chapter concludes with a discussion of the facility generated background noise.

Chapter 2

MEASUREMENT TECHNIQUE AND ANALYSIS

2.1 Introduction

Measurements of turbulent boundary layer (TBL) pressure fluctuations with flush (wall) mounted pressure sensors are frequently contaminated with facility generated and vibrationally induced noise. A novel technique described by Wambsganss (1979) utilized a two sensor arrangement that discriminated between the propagating (facility) and nonpropagating (TBL) pressure components in a fully, turbulent pipe flow. However, this early technique involved uncertainties when combining various source (TBL) terms.

Refined techniques were developed later by Wilson (1979), and investigators Horne and Hansen (1981). Both of these techniques involved an axisymmetric, three sensor configuration that resolved earlier ambiguities and greatly improved the integrity (Wilson) and moreover, the ease of acquiring data (Horne and Hansen). All of these methods however, neglected the vibrationally induced pressure signal that can dominate the output of flush-mounted pressure sensors (especially at low frequencies). The following describes a more complete analysis and represents a further refinement to the latest method of Horne and Hansen. This new refinement includes the effect of tunnel wall vibration and offers a correction, if needed--due to vibrational effects--to the measured TBL pressure spectra.

2.2 Array Description

Consider the flush-mounted array depicted below in Figure 2.1. The outputs $a(r_1, \theta, t)$, $b(r_1, \theta, t)$, $c(r_1, \theta, t)$ define the time varying output

voltages of hydrophones at locations 1, 2, and 3, respectfully. The hydrophones are in direct communication with the TBL and the signals are represented as a linear combination of various source terms (Equations 2.1, 2.2, and 2.3).

$$a(r_1,\theta,t) = a_{Ac}(r_1,\theta,t) + a_{u'}(r_1,\theta,t) + a_{tbl}(r_1,\theta,t) + a_e(r_1,\theta,t) \quad (2.1)$$

$$b(r_1,\theta,t) = b_{Ac}(r_1,\theta,t) + b_{u'}(r_1,\theta,t) + b_{tbl}(r_1,\theta,t) + b_e(r_1,\theta,t) \quad (2.2)$$

$$c(r_1,\theta,t) = c_{Ac}(r_1,\theta,t) + c_{u'}(r_1,\theta,t) + c_{tbl}(r_1,\theta,t) + c_e(r_1,\theta,t) \quad (2.3)$$

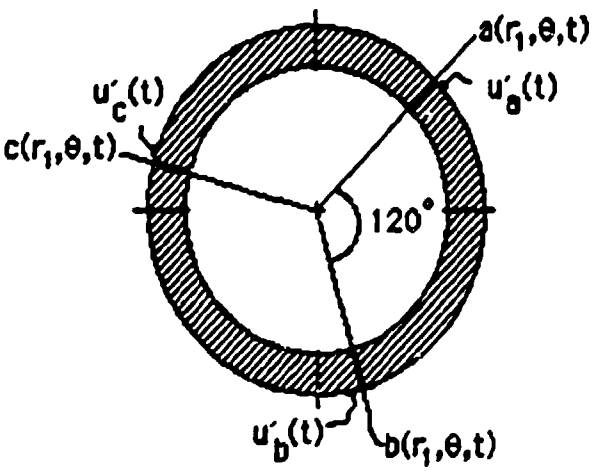

Figure 2.1: Array and Sensor Locations.

In the above equations subscripts Ac, u', tbl, and e, refer to individual sources that describe the total signal measured at 1, 2, and 3 due to the facility generated, vibrationally induced, TBL pressure fluctuations and electronic noise, respectively. The outputs $u'_a(t)$, $u'_b(t)$, and $u'_c(t)$ describe the time varying vibrations measured by accelerometers located on the tunnel wall near each respective hydrophone location. Finally, all outputs are considered to be stationary, random processes of zero mean.

2.3 Model Assumptions and Considerations

The foremost, of the model assumptions is that all facility generated noise propagates as plane waves, constant in amplitude and phase in any plane perpendicular to the flow in the test section. If all major sources of the acoustic or, propagating pressure field are located several diameters up or downstream from the test section then--for frequencies below the cutoff, f_{CO} (Appendix 2)--this foremost assumption should be valid. This premise implies that by simply subtracting any pair of hydrophone outputs (e.g. $a(r_1,\theta,t) - b(r_1,\theta,t)$), virtually all acoustic or, propagating pressure contributions can be eliminated. Also, if the primary objective is to determine the spectrum of the TBL wall pressure fluctuations then the following restrictions on the measurement system apply:

1) All hydrophones must have the same receiving sensitivities
2) All hydrophones must be electronically matched in phase
3) Hydrophone separation distances must be greater than the maximum correlation length of the TBL pressure fluctuations (generally accepted to be on the order of the boundary-layer thickness).

If either of the first two criteria are not true, then the acoustic or, propagating component of the pressure field will not be effectively cancelled. In addition, if item three is not met then an attenuation of the local TBL-induced pressure signal will result. Therefore, all hydrophones are assumed matched in phase, equal in receiving sensitivity and their

separation distances are maximized to allow negligible attenuation in the local TBL pressure fluctuation levels (see Chapter 4 for further discussion on correlation length scales). Summarizing the above concepts suggests that the following source related terms are either correlated or, uncorrelated:

1) Acoustic source terms are uncorrelated with TBL source terms
2) TBL pressure fluctuations at a given location are uncorrelated with those at <u>other</u> locations
3) Acoustic terms are <u>fully</u> correlated between hydrophones
4) Electronic source terms are uncorrelated between hydrophones and with <u>all</u> other non-electronic terms.

2.4 <u>Analysis : The Finite Fourier Transform</u>

The Fourier transform of a nonperiodic function x(t) can be represented as (note that the upper case lettering refers to the transformed quantity),

$$X(f) = F\{ x(t) \} = \int_{-\infty}^{\infty} x(t)\, e^{-2\pi j f t}\, dt. \qquad (2.4)$$

It is not possible to obtain data over an infinite record length, therefore the Fourier transform of x(t) must be approximated by integrating over a finite record of length T. For example, x(t) is approximated as,

$$x(t) = \{ x_k(t) [H(t) - H(t-T)] \} \quad 0 < k < n \quad (2.5)$$

where, nT is the total record length of x(t), k is an individual record of length T, and H(t) is the Heaviside Function defined as,

$$H(t) = 0. \qquad \text{for } t < 0$$
$$H(t) = 1. \qquad \text{for } t > 0.$$

Substituting Equation 2.5 into Equation 2.4 yields the finite Fourier transform of the k^{th} record of $x_k(t)$ (= x(t,k)).

$$X(f, T, k) = F[\, x(t, k)\,] = \int_{-\infty}^{\infty} x(t, k)\,[\, H(t) - H(t - T)\,]\, e^{-2\pi j f t}\, dt$$

$$= \int_{0}^{\infty} x(t, k)\, e^{-2\pi j f t}\, dt - \int_{T}^{\infty} x(t, k)\, e^{-2\pi j f t}\, dt$$

$$= \int_{0}^{T} x(t, k)\, e^{-2\pi j f t}\, dt. \qquad (2.6)$$

2.5 TBL Spectrum From Cross-Difference Signals

The finite Fourier transform of the difference signals between two pairs of hydrophones is the autospectral density of the TBL pressure fluctuations. This analysis is shown as follows.

From Equation 2.6, the finite Fourier transform of the difference signals between the hydrophone outputs at locations 1 and 2, and, 1 and 3 can be constructed and, is represented by Equation 2.7. However, in Equation 2.7 the dependency on the spatial coordinates r, and θ have been suppressed for convenience (i.e. the Fourier transform is evaluated where time is the variable).

$$[\,A(f,T,k) - B(f,T,k)\,] = \int_0^T \{[a_{AC}(t) + a_{U'}(t) + a_{tbl}(t) + a_e(t)] - [b_{AC}(t) + b_{U'}(t) + b_{tbl}(t) + b_e(t)]\} e^{-2\pi j f t}\, dt. \tag{2.7}$$

and,

$$[\,A(f,T,k) - C(f,T,k)\,] = \int_0^T \{[a_{AC}(t) + a_{U'}(t) + a_{tbl}(t) + a_e(t)] - [c_{AC}(t) + c_{U'}(t) + c_{tbl}(t) + c_e(t)]\} e^{-2\pi j f t}\, dt. \tag{2.8}$$

In terms of their individual transformed quantities Equations 2.7 and 2.8 become, where the arguments have been suppressed for simplification,

$$D_{A-B}(f,T,k) \equiv [\,A(f,T,k) - B(f,T,k)\,] = A_{tbl} - B_{tbl} + A_{Ac} - B_{Ac} + A_{U'} - B_{U'} + A_e - B_e \tag{2.7a}$$

and,

$$D_{A-C}(f,T,k) \equiv [\,A(f,T,k) - C(f,T,k)\,] = A_{tbl} - C_{tbl} + A_{Ac} - C_{Ac} + A_{U'} - C_{U'} + A_e - C_e. \tag{2.8a}$$

Appendix 1 shows that the autospectral density function, $G_{xx}(f)$ and cross-spectral density function $G_{xy}(f)$ can be represented by the respective

products of their Fourier transformed time functions x(t) and y(t). Therefore, the cross-spectral density function between the Fourier transformed difference signals (Equations 2.7a and 2.8b) is given by,

$$G_{A-B,A-C}(f) = 2 \lim_{T\to\infty} E[(A - B)^* (A - C)]/ T. \qquad (2.9)$$

Expanding the terms inside the expectation operation of Equation 2.9 gives,

$$G_{A-B,A-C}(f) = \lim_{T\to\infty} \frac{1}{T} E\{[A^*_{tbl} - B^*_{tbl} + A^*_{u'} - B^*_{u'} + A^*_{e} - B^*_{e}] [A_{tbl} - C_{tbl} + A_{u'} - C_{u'} + A_{e} - C_{e}]\}. \qquad (2.10)$$

In Equation 2.10 the expected value of all uncorrelated terms will tend to zero so that,

$$G_{A-B,A-C}(f) = 2 \lim_{T\to\infty} \frac{1}{T} \{E[A^*_{tbl} A_{tbl}] + E[A^*_{u'} A_{u'}] - E[A^*_{u'} C_{u'}] + E[B^*_{u'} C_{u'}] - E[B^*_{u'} A_{u'}] - E[B^*_{u'} A_{u'}] + E[A^*_{u'} A_{tbl}] - E[A^*_{u'} C_{tbl}] + E[B^*_{u'} C_{tbl}] - E[B^*_{u'} A_{tbl}] + E[A^*_{tbl} A_{u'}] - E[A^*_{tbl} C_{u'}] + E[B^*_{tbl} C_{u'}] - E[B^*_{tbl} A_{u'}] + E[A^*_{e} A_{e}]\}. \qquad (2.11)$$

Solving Equation 2.11 for the expected value of the turbulent boundary layer pressure fluctuations at location 1, and by combining similar quantities it easily shown that,

$$G_{A_{tbl}}(f) = G_{A-B,A-C}(f) - 2 \lim_{T\to\infty} E[(A_{u'} - B_{u'})^*(A_{u'} - C_{u'})] / T$$

$$- 2 \lim_{T\to\infty} E[(A_{u'} - B_{u'})^*(A_{tbl} - C_{tbl})] / T$$

$$- 2 \lim_{T\to\infty} E[(A_{tbl} - B_{tbl})^*(A_{u'} - C_{u'})] / T - G_{A_e}(f). \qquad (2.12)$$

2.6 Analysis of Vibrationally Induced Terms

Suppose that a hydrophone's output, y(t) is due only to its local acceleration, u'(t). Then with all extraneous noise absent, the hydrophone's output can be modeled as an "ideal," single input/output system, as depicted in Figure 2.2.

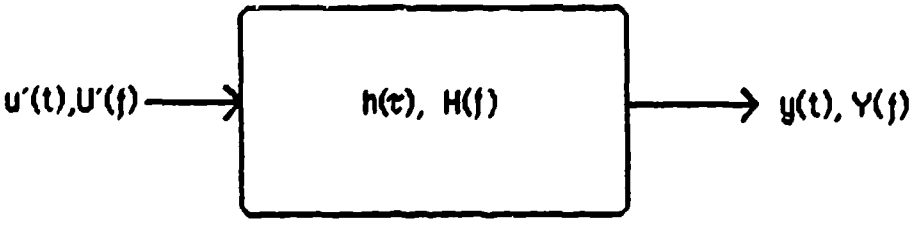

Figure 2.2: Ideal Single Input/Single Output System.

For this ideal single input/output system y(t) is given by the convolution of the impulse response function, $h(\tau)$ with the system input u'(t) or, using the Fourier transform,

$$Y(f) = H(f)\, U'(f), \qquad (2.13)$$

where the upper case lettering refers to the usual Fourier transformed quantities. From Equation 2.13 it follows that,

$$Y^*(f) = H^*(f)\, U'^*(f)$$

$$Y^*(f)\, Y(f) = H^*(f)\, H(f)\, U'^*(f)\, U'(f) \qquad (2.14)$$

and,

$$U'^*(f)\, Y(f) = H(f)\, U'^*(f)\, U'(f). \qquad (2.15)$$

Multiplying Equations 2.14 and 2.15 by 2/T, letting T tend to infinity, and taking the expected values give the usual spectral relationships,

$$G_{yy}(f) = |\, H(f)\,|^2\, G_{u'u'}(f) \qquad (2.16)$$

$$G_{u'y}(f) = H(f)\, G_{u'u'}(f). \qquad (2.17)$$

Clearly, H(f) is a complex function and for convenience will be represented as,

$$H(f) = |\, H(f)\,|^2\, e^{-j\theta(f)}$$

where,

$$\theta(f) = \tan^{-1}[\, \mathrm{Im}\{ G_{xy}(f) \,/\, \mathrm{Re}\{ G_{xy}(f) \} \}.$$

Using these and previous results, the transfer functions between the locally measured accelerations ($u'_a(t)$, $u'_b(t)$, $u'_c(t)$) and the respective hydrophone's vibrational outputs can be constructed and are given by the following spectral relationships,

$$H_A(f) = A_{u'}(f) / U'_A(f) \qquad (2.18a)$$

$$H_B(f) = B_{u'}(f) / U'_B(f) \qquad (2.18b)$$

$$H_C(f) = C_{u'}(f) / U'_C(f). \qquad (2.18c)$$

In practice, these transfer functions are measured under a no-flow condition (all non-vibrational source terms are forced to zero) using some form of mechanical excitation. Solving Equations 2.18 (where frequency variables have been suppressed) for their vibrational outputs result in,

$$A_{u'}(f) = U' H_A \qquad (2.19a)$$

$$B_{u'}(f) = U' H_B \qquad (2.19b)$$

$$C_{u'}(f) = U' H_C \qquad (2.19c)$$

Substituting Equations 2.19 into Equation 2.12 yields,

$$G_{A_{tbl}}(f) = G_{A-B,A-C}(f)$$

$$- 2 \lim_{T\to\infty} E[(U'_A H_A - U'_B H_B)^* (U'_A H_A - U'_C H_C)] / T$$

$$- 2 \lim_{T\to\infty} E[(U'_A H_A - U'_B H_B)^* (A_{tbl} - C_{tbl})] / T$$

$$- 2 \lim_{T\to\infty} E[(A_{tbl} - B_{tbl})^* (U'_A H_A - U'_C H_C)] / T - G_{A_e}(f). \qquad (2.21)$$

In the above equation, terms that involve the turbulent boundary layer pressure fluctuations are not directly measurable; however, there exists quantities that involve these source terms which can be measured. By substituting,

$$A_{tbl}(f,T,k) - C_{tbl}(f,T,k) = A - C - (A_{u'} - C_{u'}) - (A_e - C_e)$$

and,

$$A_{tbl}(f,T,k) - B_{tbl}(f,T,k) = A - B - (A_{u'} - B_{u'}) - (A_e - B_e).$$

into Equation 2.21, we find,

$$\begin{aligned} G_{A_{tbl}}(f) = {} & G_{A-B,A-C}(f) \\ & + 2 \lim_{T\to\infty} \frac{1}{T} E[(U'_A H_A - U'_B H_B)^* (U'_A H_A - U'_C H_C)] \\ & - 2 \lim_{T\to\infty} \frac{1}{T} E[(U'_A H_A - U'_B H_B)^* (A - C)] \\ & - 2 \lim_{T\to\infty} \frac{1}{T} E[(A - B)^* (U'_A H_A - U'_C H_C)] - G_{A_e}(f). \end{aligned} \tag{2.22}$$

If the measured complex transfer functions in the above equation are not equal in magnitude, and phase over the desired frequency range (e.g. $H_A \neq H_B \neq H_C$) then all expected value terms in Equation 2.22 must be expanded to yield the desired measurable, spectral quantities. Expanding Equation 2.22, and taking the limit of individual terms as T tends to infinity will then yield the following expression for the TBL pressure fluctuations in terms of other measurable spectral quantities,

$$G_{A_{tbl}}(f) = G_{A-B,A-C} - H^*_A G_{U'_A A} + H^*_A G_{U'_A C}$$
$$+H^*_B G_{U'_B A} - H^*_B G_{U'_B C} - H_A G_{AU'_A}$$
$$+H_C G_{AU'_C} + H_A G_{BU'_A} - H_C G_{BU'_C}$$
$$+|H_A|^2 G_{U'_A U'_A} - H^*_A H_C G_{U'_A U'_C}$$
$$- H^*_B H_A G_{U'_B U'_A} + H^*_B H_C G_{U'_B U'_C} - G_{A_e} \quad (2.23)$$

However, if the complex transfer functions are equal in magnitude and phase ($H_A=H_B=H_C=H$) for all frequencies of interest then, Equation 2.22 reduces to,

$$G_{A_{tbl}}(f) = G_{A-B,A-C} - G_{A_e} - H^* G_{U'_A-U'_B,A-C}$$
$$- H G_{A-B,U'_A-U'_C} + |H|^2 G_{U'_A-U'_B,U'_A-U'_C} \quad (2.24)$$

2.7 Estimation of Vibrational Spectral Quantities

It is possible to gain insight into the relative magnitude of the vibrationally related terms in Equation 2.24 without actually measuring them. Consider the system model shown in Figure 2.3.

In this model y(t) represents the output due to the difference between two hydrophone signals, and n(t) is that part of y(t) due to the difference between TBL source terms only. Finally, x(t) represents the signal due the difference between the respective hydrophone's accelerometers outputs.

The true, uncontaminated vibrational difference signal output, v(t) of the two hydrophones is therefore obtained by the convolution of $h(\tau)$ with x(t). All electronic source terms are assumed negligible in this model.

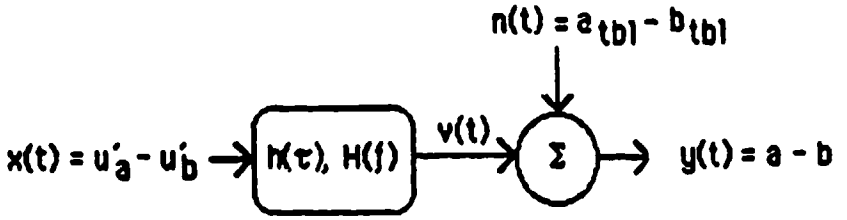

Figure 2.3 : Vibrational Noise Model

From Figure 2.3 it is clear that,

$$G_{YY}(f) = G_{NN}(f) + G_{VV}(f)$$
$$G_{VV}(f) = |H(f)|^2 G_{XX}(f)$$
$$G_{XY}(f) = H(f)\, G_{XX}(f).$$

The ordinary coherence function between x(t) and y(t) is defined as,

$$\gamma^2_{XY}(f) = \frac{|G_{XY}(f)|^2}{G_{XX}(f)\, G_{YY}(f)} \leq 1.$$

From the above relationships it follows directly that,

$$G_{VV}(f) = \frac{|G_{XY}(f)|^2}{G^2_{XX}(f)}\, G_{XX}(f) = \gamma^2_{XY}(f)\, G_{YY}(f).$$

The above equation is termed the coherent output power (COP) spectrum between y(t) and x(t) and, represents the power spectrum of v(t) with the

linear effects of n(t) removed. Therefore, if the COP spectrum of y(t) is much less than the autospectrum of y(t) ($G_{yy}(f)$), the dominant source term is n(t) or, that part of y(t) due to the TBL pressure fluctuations. In other words, if the ordinary coherence function between x(t) and y(t) is much less than unity, the output y(t) is dominated by the local TBL pressure fluctuations and all vibrational terms in Equations 2.24 and 2.25 may be neglected. If this is true, then Equation 2.24 reduces to,

$$G_{tbl}(f) = G_{A-B,A-C}(f) - G_{A_e}(f). \qquad (2.25)$$

This equation for $G_{tbl}(f)$ represents the true turbulent boundary layer wall pressure spectrum with all extraneous noise removed. The electronic noise spectrum, G_{A_e} is easily determined by a direct measurement of the output at sensor a, with the facility off and is usually negligible.

2.8 Cross-Spectral Measurements: Acoustic and Vibratory Noise

Measuring the cross-spectral density function between any two hydrophones will yield only those noise sources that are correlated between the two points of measurement. In other words, the local TBL pressure fluctuations will be conditioned out of the cross-spectrum assuming the measurement points are not in close proximity. For example, consider the cross-spectrum between hydrophone signals a and b,

$$G_{AB}(f) = 2 \lim_{T\to\infty} \frac{1}{T} E[(A_{tbl} + A_{Ac} + A_{U'} + A_e)^* (B_{tbl} + B_{Ac} + B_{U'} + B_e)]. \qquad (2.27)$$

Expanding the expectation operation and keeping only non-zero terms gives,

$$G_{AB}(f) = 2 \lim_{T\to\infty} \frac{1}{T} \{ E[A^*_{tbl} B_{U'}] + E[A^*_{U'} B_{tbl}] + E[A^*_{U'} B_{U'}] + E[A^*_{Ac} B_{Ac}] + E[A^*_{Ac} B_{U'}] + E[A^*_{U'} B_{Ac}] \}. \quad (2.28)$$

Recalling that,

$$A_{tbl}(f) = A - A_{U'} - A_e - A_{Ac}$$

$$B_{tbl}(f) = B - B_{U'} - B_e - B_A.$$

Substituting these expressions into Equation 2.28 and collecting like terms yields the following expression,

$$G_{AB}(f) = 2 \lim_{T\to\infty} \frac{1}{T} \{ E[A^* B_{U'}] + E[A^*_{U'} B] - E[A^*_{U'} B_{U'}] + E[A^*_{Ac} B_{Ac}] \}. \quad (2.28)$$

From Equation 2.19 the above equation reduces to,

$$G_{AB}(f) = H_B G_{AU'_B} + H^*_A G_{U'_{AB}} - H^*_A H_B G_{U'_A U'_B} + G_{A_{Ac} B_{Ac}} \quad (2.30)$$

The fourth term on the right hand side (R.H.S.) of Equation 2.30 represents the true propagating acoustic pressure field and propagates as plane waves throughout the test section (i.e. constant in magnitude and phase). All other terms on the R.H.S. of Equation 2.30 represent a pseudo-acoustic field due to the local wall and/or transducer vibrations.

2.9 Estimation of Vibrational Terms

Again, using an analysis that is similar to the one used previously, it is possible to determine the relative magnitude of the vibrational contamination present in the cross-spectrum of sensors, a and b (without measuring the transfer functions $H_A(f)$ and $H_B(f)$). Consider the model shown in the Figure 2.4 .

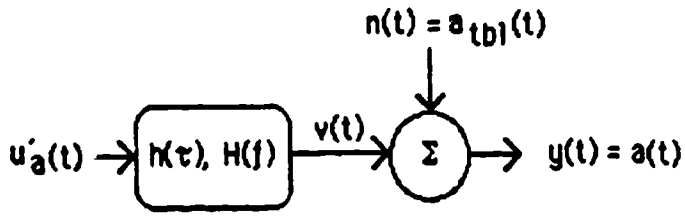

Figure 2.4: Vibrational Noise Model.

In Figure 2.4, y(t) represents the output from a single hydrophone, n(t) is part of y'(t) due to the local TBL pressure fluctuations, v(t) is the hydrophone's vibrationally induced output and $u'_a(t)$ is the corresponding accelerometer's vibrational output. The electronic noise source term is neglected. Measuring the coherent output power (COP) spectrum between y(t) and u'(t) will then determine the amount of vibrational contamination present in y(t). If the COP spectrum is much less (<10dB) than the autospectrum of y(t), all vibrational terms in Equation 2.30 can be neglected. If this is true then Equation 2.31 will reduce to,

$$G_{AB}(f) = G_{A_{Ac}B_{Ac}} = G_{Acoustic} \qquad (2.31)$$

The above equation represents all facility generated noise that propagates as plane acoustic waves in the test section.

Chapter 3

PRESSURE SENSORS AND CALIBRATION TECHNIQUES

3.1 Introduction

In Chapter 2 a measurement technique was developed that describes how an axisymmetric, pressure sensor array can discriminate between the propagating (acoustic) and nonpropagating (turbulent boundary layer, TBL) pressure fluctuations in a fully developed, turbulent pipe flow. However, a prerequisite and critical aspect of this measurement technique is that 1) the phase difference between pressure sensors, and 2) the receiving sensitivities of each sensor match. Moreover, the facility in which the TBL pressure measurements are to be made uses glycerine as the working fluid. Therefore, possible differences between water and glycerine hydrophone sensitivities may exist and is investigated.

This chapter describes the type of pressure sensors used and also, the calibration schemes employed in clarifying the above sensor requirements.

3.2 Pressure Sensor Description

In order to minimize possible phase and sensitivity differences between pressure sensors, high quality, resistive-type sensors from the ENDEVCO Corporation were chosen. Resistive-type sensors have a purely real input impedance and should theoretically introduce no phase delays in the output signal. Also, high quality pressure sensors should have a flat frequency response (to first resonance) and more importantly, the sensitivities should vary little from sensor to sensor. Another aspect of the pressure sensors that was mentioned in Chapter 1 was that the sensor's facial diameter has to be small, in relation to the smallest size of the TBL

pressure producing eddies. If the sensor's diameter is large, then local, spatial averaging of the pressure producing eddies will result producing a mean output voltage that approaches zero (see Figure 3.1).

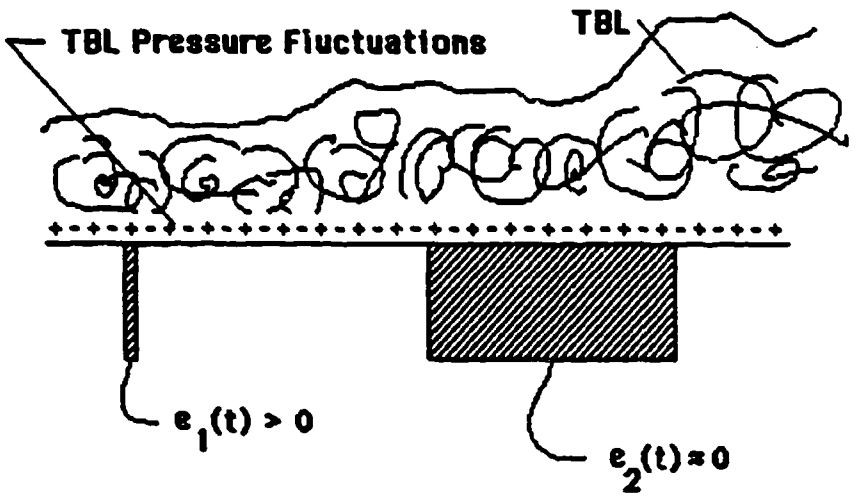

Figure 3.1: TBL Pressure Fluctuations and Sensor Size.

Therefore, subminiature pressure sensors with a casing diameter of 1.57 millimeters (mm) were selected (ENDEVCO, Model Number 8514-10). It should be noted however, that the active sensing elements of each transducer are much smaller. Galib and Zandina (1984) have used these types of transducers for TBL wall pressure measurements and have concluded (through testing) that the active area is probably as small as 0.5 mm. All sensors are rated to 6.8944×10^4 N/m^2 with a corresponding full scale output of 300 mV. Also, each sensor can withstand transient inputs of 6.8944×10^5 N/m^2 without damage and outputs remain linear for pressures up to three (3) times the full scale (F.S.) output. Due to the harsh thermal environment that exists in the Glycerine Tunnel, each transducer

was thermally compensated for temperatures between -17.7° and 93.3°C. Each sensor was specially ordered with a double coating of "Parylene C," (a factory sealant) that provided more than adequate sealing. The transducers consist of a zero balanced, four-active-arm, strain gage bridge, diffused into a molded silicon diaphragm (see Figure 3.2). Thermal compensation resistors (R_1, R_2) and the complete bridge circuit are all housed in the same nickel-iron alloy case. Powering the transducers with a 10 volt DC source is recommended; however, appreciable shift in output sensitivity is not observed at even half the recommended supply voltage (see Figure 3.3).

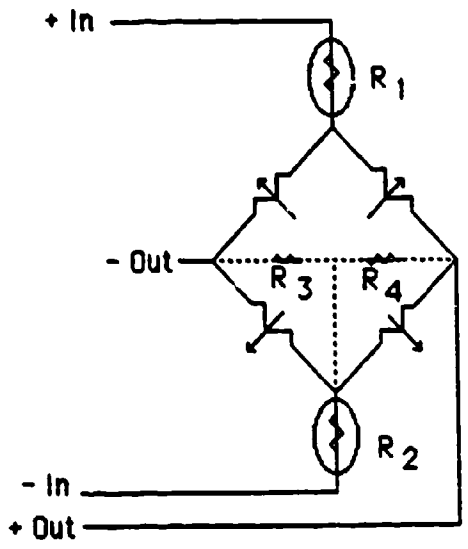

Figure 3.2: Schematic Diagram of the 4-Arm Bridge of the Sensors.

The power supply requirement was fulfilled with eight 1.25-volt, dry-cell, rechargeable nickel-cadmium batteries (10-volt total supply). A major advantage of batteries over commercial DC power supplies is the

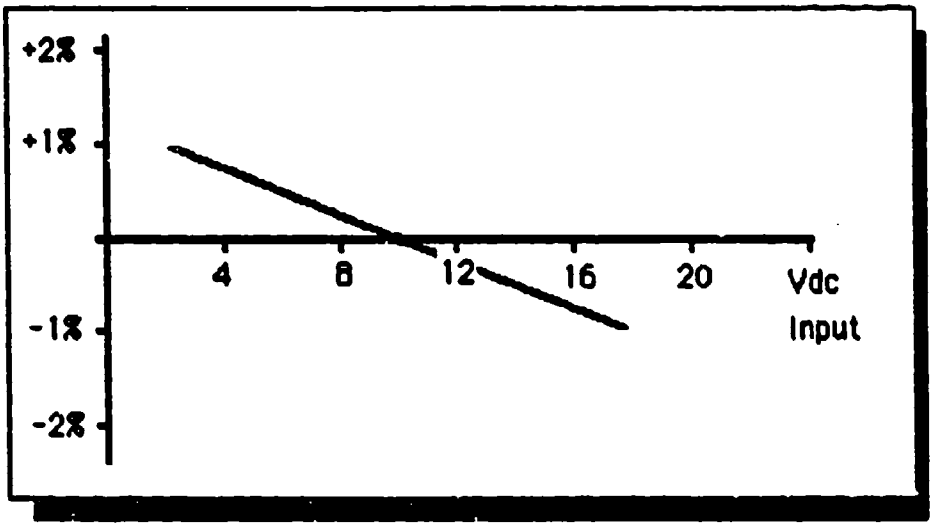

Figure 3.3: Typical Transducer Sensitivity Shift (mV/Pa/Input Volt) Due to Varying Supply Voltage.

elimination of all 60 cycle related noise. The current needed to power each sensor was small (6mA/sensor), enabling the powering of all three sensors simultaneously. The power supply unit was tested and found capable of supplying the required input voltage for up to seven (7) hours of continuous operation without recharging (Figure 3.4). Factory supplied free-field pressure sensitivities for each sensor and other typical performance specifications are given below in Tables 3.1 and 3.2 (note that all factory specifications are with a 10-volt supply). Shown in Figure 3.5 are the physical dimensions of a typical, 8514-10 unit. A removable screen that consists of eleven extremely small slots protects the silicon diagram from undesired impacts and is not shown. However, the transducer properties and performance are uneffected by the screen's presence.

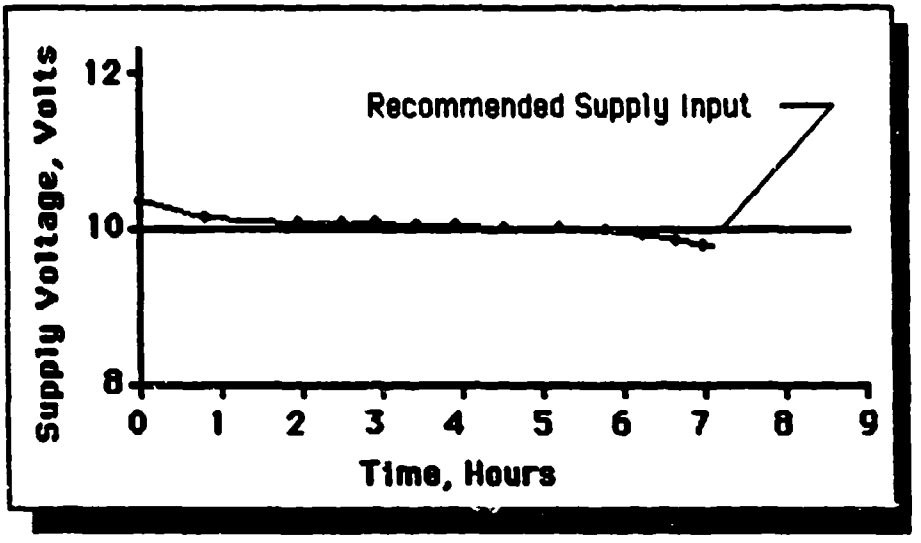

Figure 3.4: Input Supply Voltage Versus Time Under Full Loading (All Three Sensors).

Table 3.1: Endevco Factory Nominal Sensitivities of Transducers with a 10-Volt Excitation.

Sensor Model Number	Sensitivity dB, re 1V/µPa
KW45	- 227.3
KW35	- 227.9
KW38	- 228.6

Table 3.2: Endevco Typical Specifications, Series 8514 Transducer with a 10-Volt Power Supply.

Performance	8514-10
Range	0 - 6.8944 × 10^4 N/m^2
Resonance Frequency	140,000 Hertz
Linearity @ FSO	± 0.5 % of FSO
Linearity @ 3 x FSO	± 1.0 % of FSO
Hysteresis	0.1 % of FSO
Zero Shift @ 3 x overrange	0.1 %
Zero Shift w/ temperature ref. 23.9 ° C	± 3 % of FSO @ max. rated temp.
Sensitivity Shift w/ temp. ref. 23.9 ° C	± 4 % FSO @ max. rated temp.
Warm up Time	15 seconds
Acceleration Sensitivity:	
Lateral	0.4137 N/m^2 /g
Longitudinal	10342 N/m^2 /g
Burst Pressure:	
Burst Differential	± 6.8944 × 10^5 N/m^2

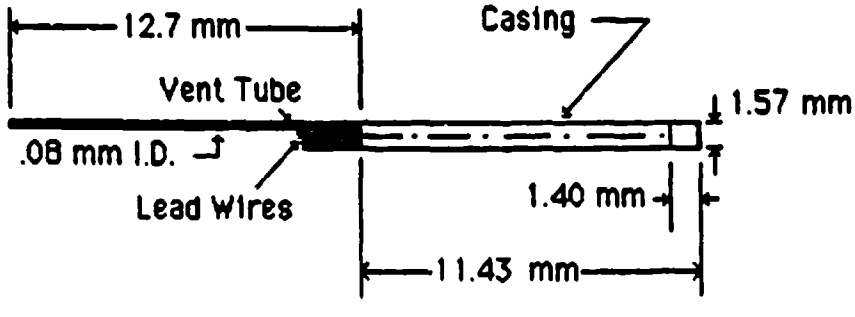

Figure 3.5: Physical Dimensions of Subminiature Transducers.

3.3 Calibration and Phase Measurement Techniques

Considerable attention was given to the various methods of transducer calibration. However, for reasons of simplicity, reliability and relative accuracy, the "comparison calibration," method that utilized a known standard transducer was employed. The sensitivity of an unknown transducer is found by subjecting both the unknown and the standard to the same incident pressure field and recording the output voltages of each unit at various frequencies (f). Then, the sensitivity of the unknown ($M_{unknown}$) transducer is computed from,

$$M_{unknown}(f) = M_{standard}(f) \frac{V_{unknown}(f)}{V_{standard}(f)} . \quad (3.1)$$

Phase calibration imposed an additional restriction on the calibration device. In order to keep the phase of the incident pressure wave at the face of each sensor the same, a plane wave sound field is needed. This was accomplished by utilizing a thick-walled, glass tube as the calibrator. For a cylindrical, rigid-walled tube, the cutoff frequency for plane, axially symmetric wave propagation can be obtained and is shown in Appendix 2 to be,

$$f_{co} = 0.293\ c / R. \quad (3.2)$$

In the above equation, c represents the sound speed of the calibration medium and R, the radius of the tube. In the case of the 5.08 centimeter (I.D.) tube used for these calibrations a corresponding cutoff frequency

was computed. If water filled, the cutoff frequency of the tube is 17,000 Hertz and, 22,800 Hertz if glycerine filled. These frequencies represent an upper limit to which calibrations and moreover, phase data are accurate.

3.3.1 Calibration Tube Assembly

The calibration tube and assemblies (Figure 3.6) were vertically positioned and a piezo-ceramic source (projector) placed and sealed into the lower end of the tube. A large, cylindrical shaped transducer was chosen as the source. Its facial diameter was 4.76 centimeters (cm) and had a length of 3.81 cm. Although the transmitting response of the source transducer was not critical because a comparison calibration method was used, the received signal from the source was always at least 10 dB above the background noise level (i.e. noise present at receiver with source off). The opposite end of the tube was customized to accommodate either all three small area transducers or, the standard LC-10 hydrophone.

The small area transducers were all housed in a single assembly unit and were circumferentially placed 120-degrees apart. This assembly was placed in the far end of the calibration tube and rested on a vibration isolating o-ring. The LC-10 hydrophone had a similar assembly and could also be positioned in the far end of the tube. Both assemblies, when installed were located 10 feet from the source.

3.3.2 Water Versus Glycerine Calibration Mediums

Comparison calibration techniques reference all measurements to the original calibration medium of the standard. Therefore, because the standard (LC-10) used in these calibrations was (factory) calibrated in water, the calibration results of 8514-10 transducers would--regardless

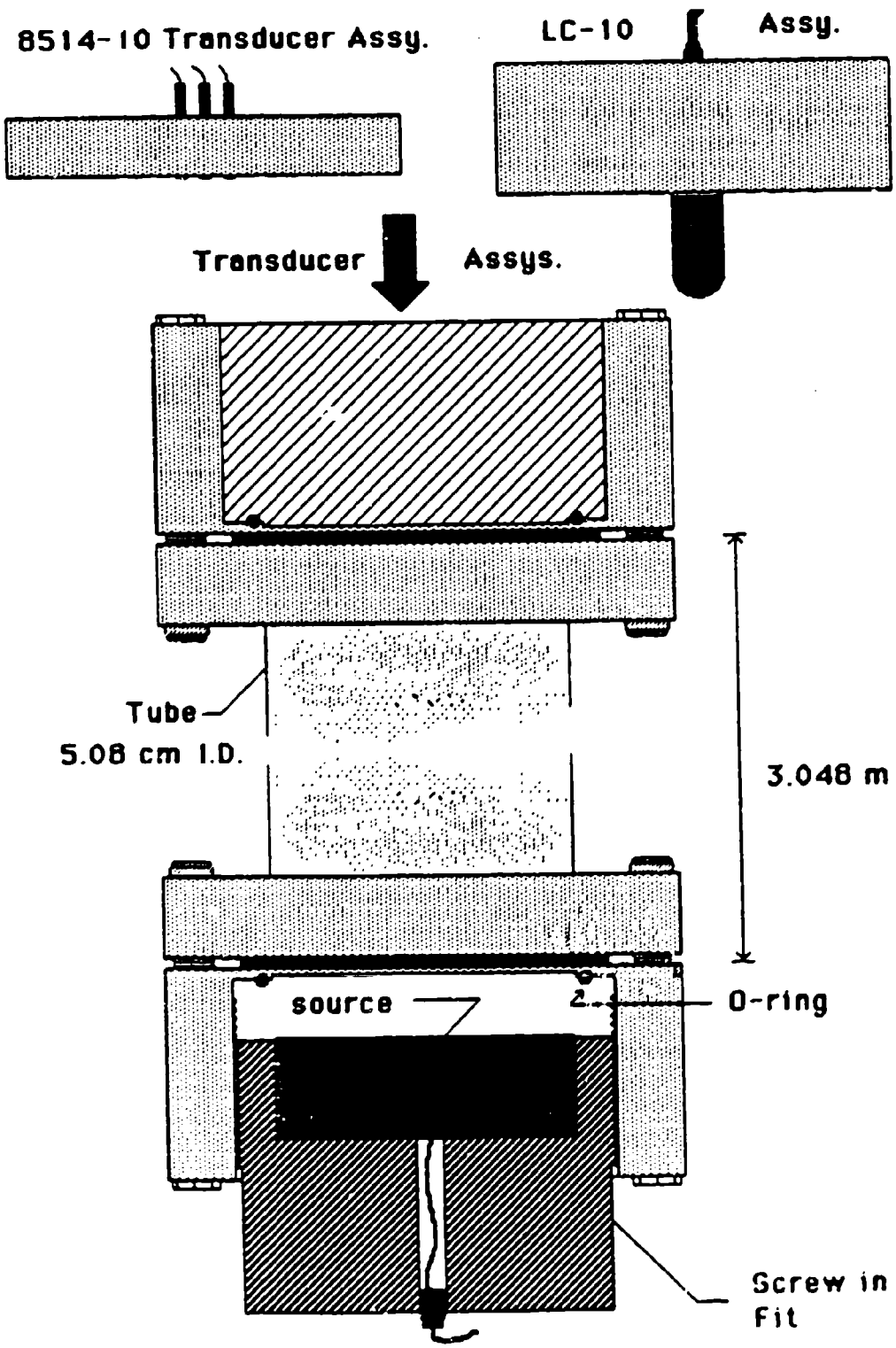

Figure 3.6 Calibration Tube and Transducer Assemblies

of calibration medium--be referenced to water. Since the characteristic acoustic impedances between water and glycerine ($\rho c_{water} / \rho c_{glycerine}$ = 0.592) differ, possible discrepancies in calibrations involving these two mediums were considered.

Air and water methods of transducer calibration will yield the same results at audio frequencies if:

1) the transducer's radiation impedance can be neglected and,
2) the transducer is small enough compared to the acoustic wavelength of the medium so that diffraction effects can be neglected.

The above criteria suggest that if $ka \ll 1$, where k is the acoustic wavenumber and a, the transducer radius then, the transducer's sensitivity should be independent of the calibration medium.

To test this, the output voltage of a 8514-10 transducer was recorded (with a white noise source input) when the calibration tube when filled with both, water and then, glycerine mediums. Results shown in the above Figure 3.7, suggests no difference in calibration will occur over the specified frequency range if water, rather than glycerine were used as the calibration medium. Therefore, because of its relative handling ease water was chosen as the calibration fluid.

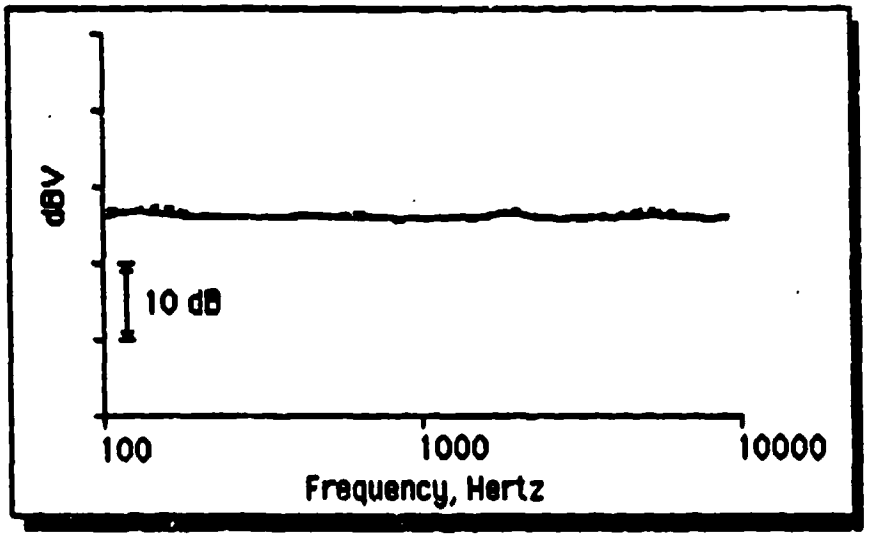

Figure 3.7: Water and Glycerine Transducer Output Voltage Versus Frequency.

3.4 Data Acquisition and Reduction

Calibration and phase data were needed over a broad range of frequencies (0 to 10 kHz). This was accomplished by using broad-band noise as input to the source. In this way, a quick method of calibration over the desired frequency range was possible using FFT processing.

The output of a General Radio random noise generator was amplified and used to drive the source transducer. This input was monitored on a dual channel Spectral Dynamics 360 spectral analyzer (SD360) and was flat over the frequency range of interest (Figure 3.8). Outputs from the hydrophones (small area and LC-10) were individually, bandpassed filtered and amplified via a Brookdeal, differential filter/amplifier. Half power points of the highpass and lowpass filters were set at 1 and 10,000 Hertz, respectfully. These outputs, were then processed on the SD360 spectral analyzer. All analyzer data was averaged 512 times over a frequency range of 0 to 10,000 Hertz.

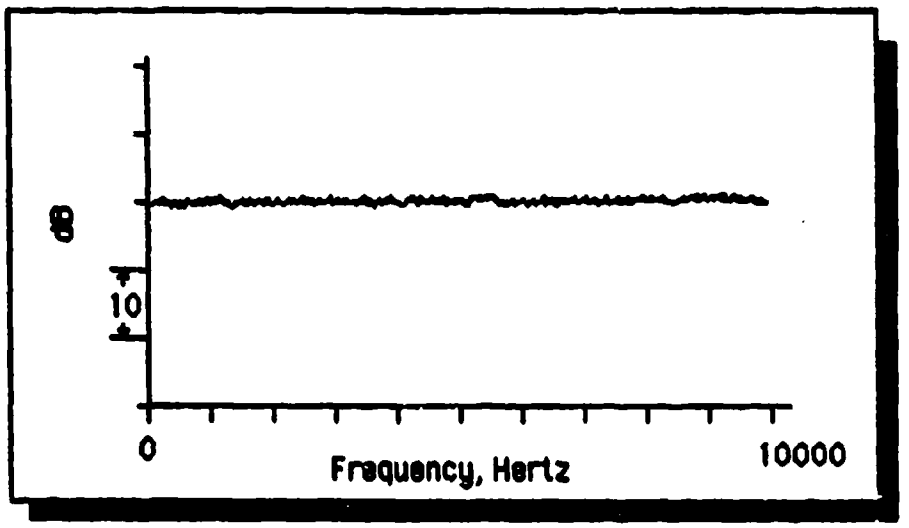

Figure 3.8: Source Input Voltage Spectrum.

This frequency range of calibration set the corresponding bandwidth of the Hanning, analysis window to 20 Hertz. After processing, all data were sent to the ARL/VAX 782 computer for reduction. Figure 3.9 depicts the data acquisition system employed throughout the calibrations.

Sensitivities of the small area transducers were obtained by recording their output voltages. Then, for the same source input, the small area transducers (8514-10) were replaced with the standard LC-10 and its output voltage was recorded. These data were then processed on the VAX computer according to equation 3.1, yielding the desired sensitivities.

The phase relationships between the small area transducers were calculated directly by the SD360. That is, the phase differences were obtained by measuring the cross-spectral density function ($G_{AB}(f)$) between two pressure sensors. The phase difference ($\varphi_{AB}(f)$) was then calculated from,

$$\varphi_{AB}(f) = \frac{IM[\,G_{AB}(f)\,]}{RE[\,G_{AB}(f)\,]}.$$

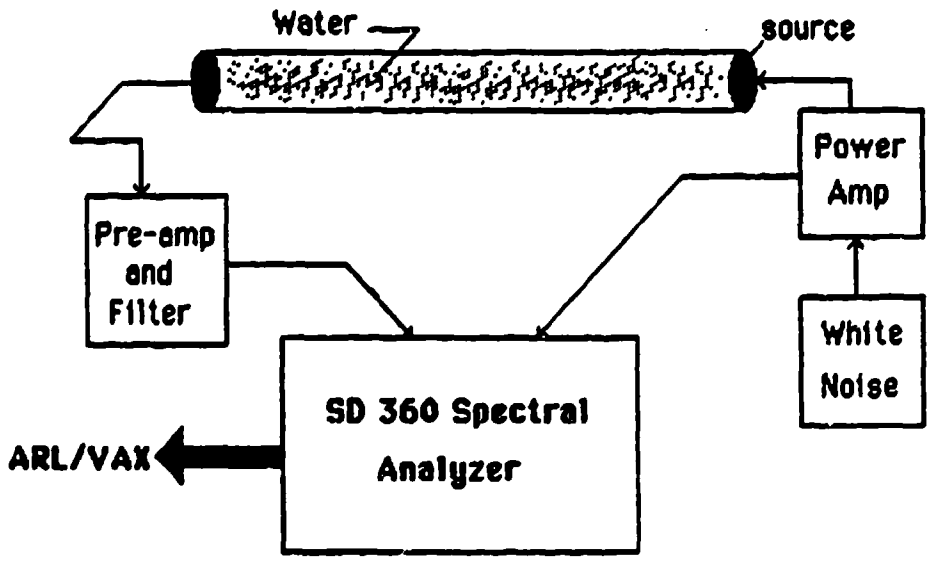

Figure 3.9: Data Acquisition System and Tube Calibrator.

Phase differences were then plotted on the SD360's analog plotter for all three cross-spectral combinations of the small area transducers.

3.5 Results

The measured sensitivities of the small area transducers are shown as a function of frequency in Figures 3.10, 3.11 and 3.12. Due to the relatively flat frequency response in the measured sensitivities of all three pressure sensors, averaged values are given. These averaged values of the small area transducers are all within 0.5 dB of the factory supplied calibrations.

Shown in Figures 3.13, 3.14 and 3.15 are the measured phase differences between the small area transducers. All plots, for the frequency range specified show a negligible (phase) shift in the received signal between paired sensor outputs.

3.6 Conclusions

The techniques employed in measuring the sensitivities and phase relationships of the small area transducers provided an excellent way to check the factory specifications and theoretical considerations. The measured sensitivities between sensors varied only, 0.5 dB over the frequency range of calibration and phase differences between the sensor outputs were insignificant. Overall, the sensors proved to be quality devices and meet all of the requirements for the measurement of turbulent boundary layer wall pressure fluctuations.

A plane wave environment was achieved by utilizing a tube as a calibration device. The calibrator proved that accurate free-field calibrations and phase measurements are possible over a wide frequency range (0 to 10kHz) without the traditional use of anechoic chambers.

Also, because of the tube's small volumetric size, transducer calibration is easily performed in any number of test mediums (e.g. water, oil, air, etc.). Variations in transducer sensitivity due to different calibration mediums can be investigated, and accounted for by simply measuring and comparing the output voltage of the transducer when immersed in both mediums. The sensitivity of the transducer in the new calibration medium (medium 2) is given simply by the following relationship,

$$M_{medium_2}(f) = M_{medium_1}(f) \times \frac{V_{medium_2}(f)}{V_{medium_1}(f)}.$$

Although no differences in sensitivity between water and glycerine calibration mediums were observed for the small area transducers used in this investigation, larger transducers may produce different results because of possible changes in impedance characteristics.

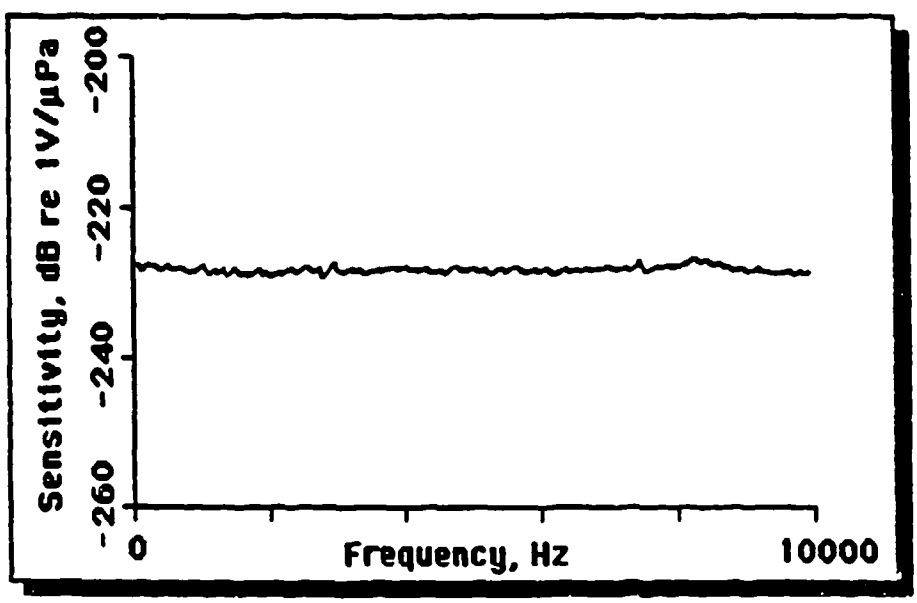

Figure 3.10: Measured Sensitivity of Sensor KW45, Average = -227.6 db.

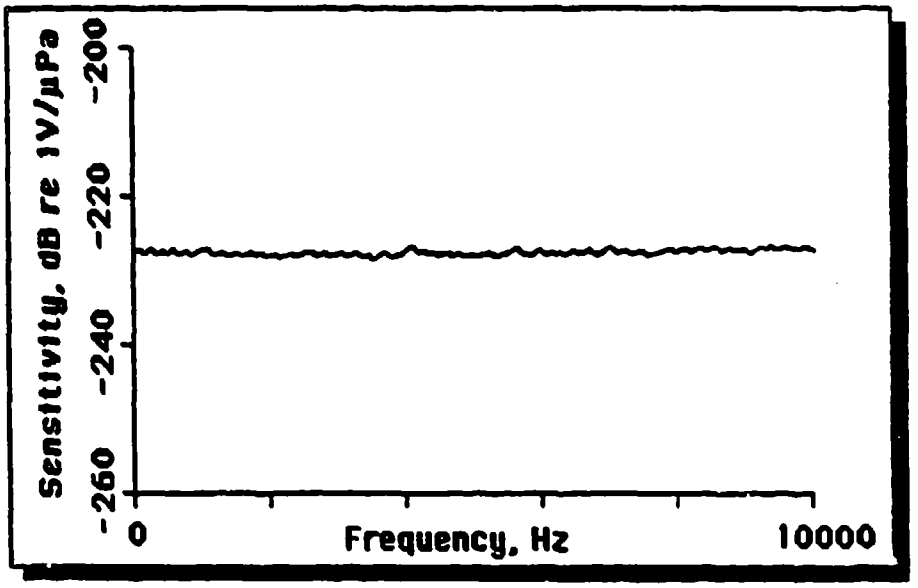

Figure 3.11: Measured Sensitivity of Sensor KW35, Average = -227.2 db

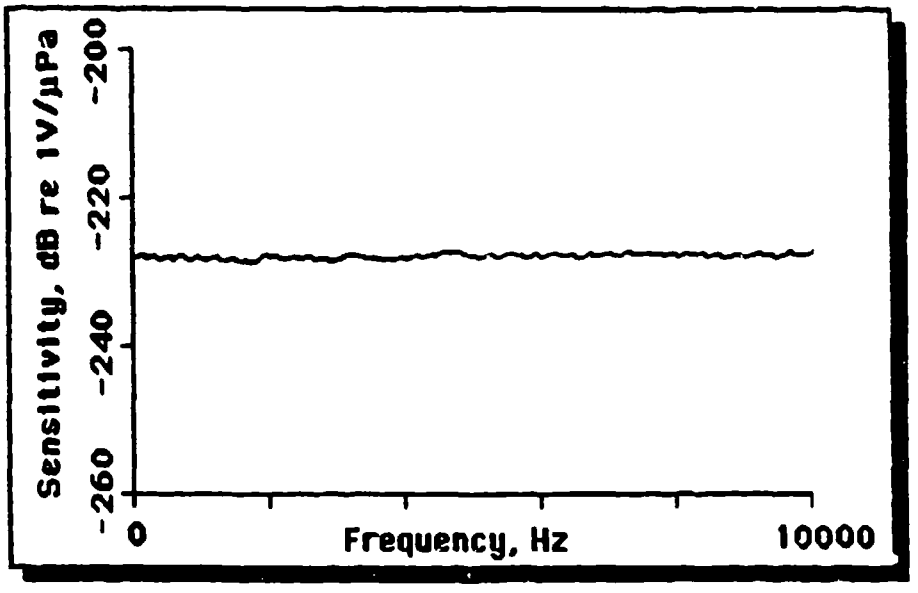

Figure 3.12: Measured Sensitivity of Sensor KW38, Average = -227.8 db.

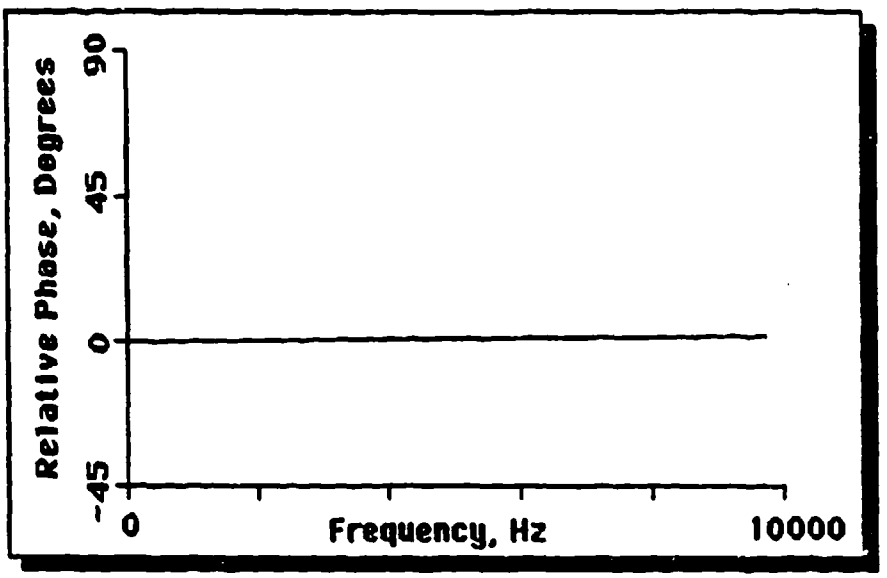

Figure 3.13: Measured Phase Difference between Sensors KW45 and KW35.

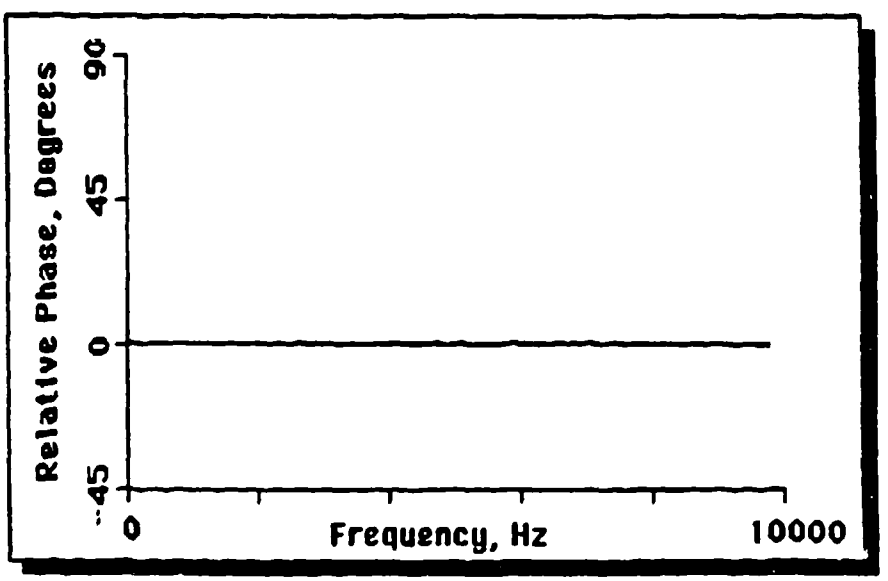

Figure 3.14: Measured Phase Difference between Sensors KW45 and KW38.

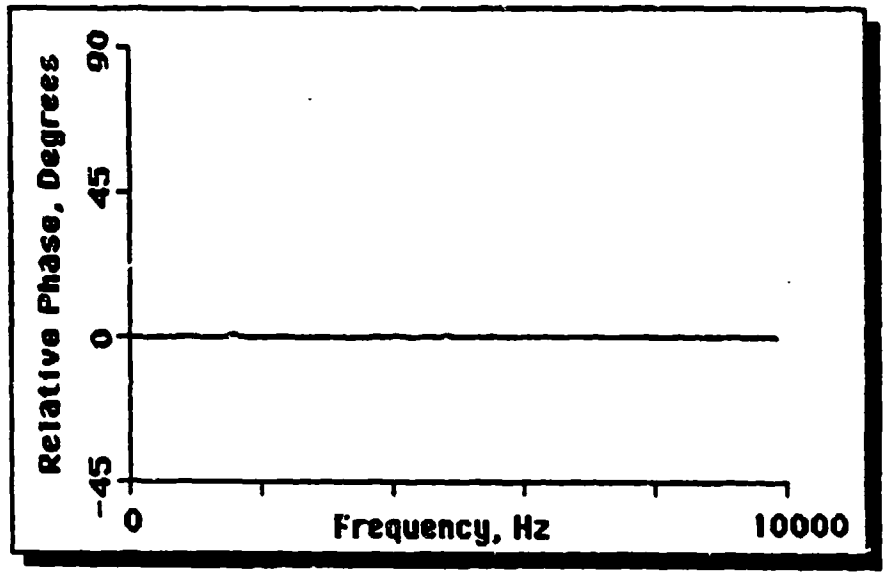

Figure 3.15: Measured Phase Difference between Sensors KW35 and KW38.

Chapter 4

THE GLYCERINE TUNNEL AND WALL PRESSURE MEASUREMENTS

4.1 Introduction

This chapter describes the facility in which the turbulent boundary layer (TBL) wall pressure fluctuation measurements were made. These include measurements of key parameters that help characterize the TBL wall pressure spectrum. This involved measuring the mean flow velocity (U) and wall shear stress (τ_w) as functions of glycerine temperature. Also, because empirical formulae exist for calculating the wall shear stress, theoretical and measured values of this parameter are compared.

This chapter also describes how the TBL wall pressure spectrum is influenced by the Reynolds Number of the flow. Reynolds Number, is a parameter that characterizes all types of viscous flows (internal and external) and is a ratio of a fluid's inertial to viscous forces. Turbulent flow at the centerline of a pipe is predominantly influenced by the fluid's inertia. Moving radially outward from the centerline, viscous forces become more influential until, at the wall the flow velocity becomes zero. The Glycerine tunnel is a unique facility in that the Reynolds Number ($Re_D = UD/\upsilon$) is varied by changing the fluid's viscosity (υ) rather than the mean flow velocity. The viscosity of the glycerine is very temperature sensitive (see Figure 4.1) and therefore, controlled by the fluid's temperature. Because of this, the TBL wall pressure spectrum can be measured over a wide range of Reynolds numbers while maintaining an almost constant mean flow velocity. This provides a novel means for investigating the scaling of the TBL wall pressure spectra in terms of inner (viscous) variables. For example, the viscosity (instead of the mean flow velocity) in this case

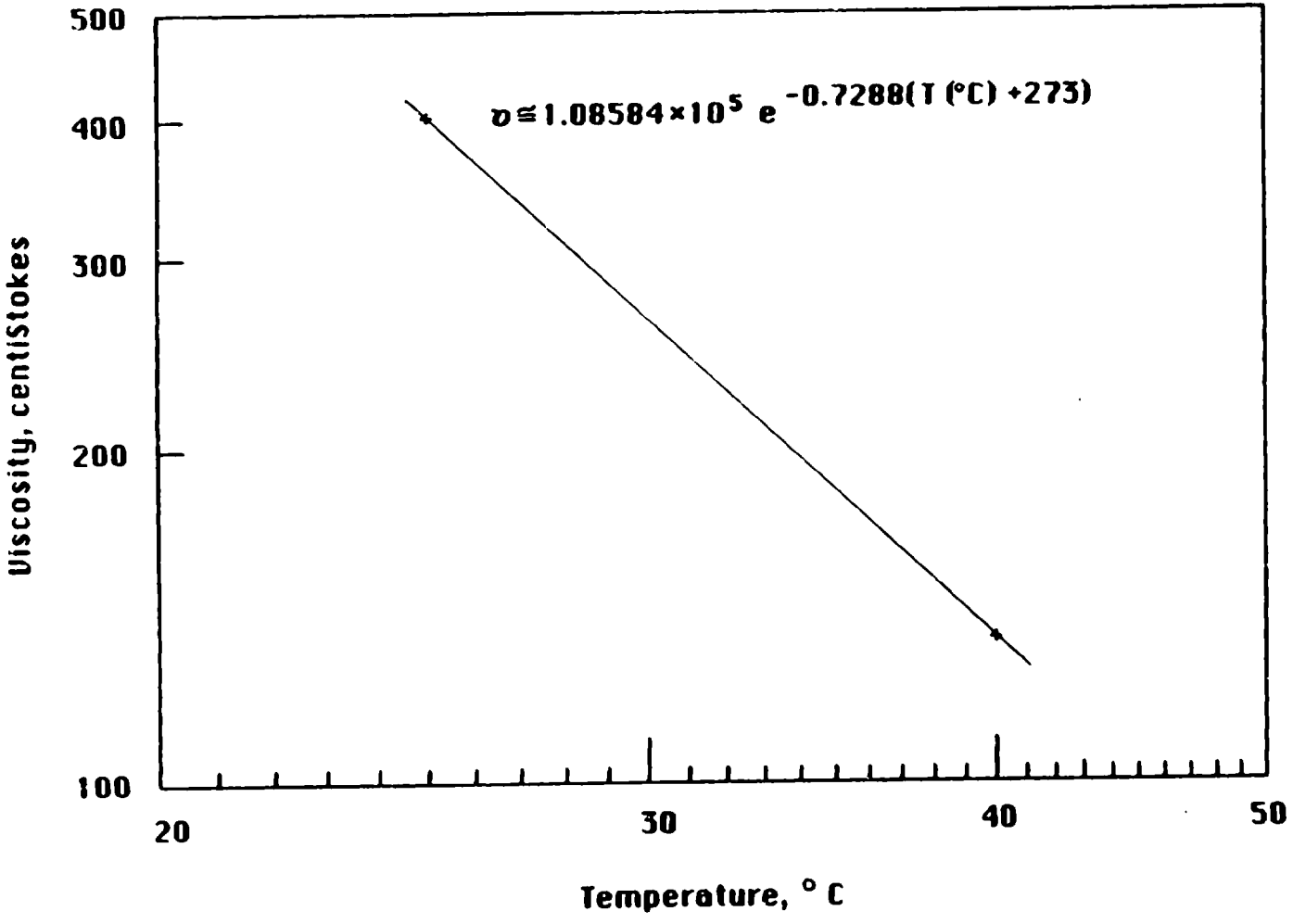

Figure 4. 1 : Measured Kinematic Viscosity of Glycerine as Per Standard Method ASTM D445-83.

represents the independent variable which in turn affects τ_w, u_τ, and the normalized viscous time scale ℓ^+ ($= \ell u/u_\tau$).

Verification of one of the model's foremost assumptions namely, that the TBL pressure fluctuations are uncorrelated between sensors is shown. This vastly improves the data integrity, especially at very low frequencies (< 10 Hertz), and indirectly proves that the other TBL measurement assumptions, described in Chapter 2, are correct.

Measurement of the acoustic background noise in the facility was investigated as part of an assessment of the adequacy of the glycerine tunnel for future low-wavenumber, wall pressure spectra research. This noise is shown to be very intense for the facility in its current configuration. However, the extreme power of the measurement technique in its ability to extract the desired TBL pressure spectrum in the presence of this severe, contaminating acoustic noise, was demonstrated. Causes of the major noise sources is considered, along with their possible solutions.

Finally, a few suggestions of possible new areas of research are proposed.

4.2 The Experimental Facility

The experimental facility (Figure 4.2) is a closed circuit tunnel that uses glycerine as the working fluid. The glycerine employed in the facility is commercially available and in this investigation tested to 96.5% purity.

The test section is 7.6 meters (24.9 feet) long and has a diameter of 284.5 millimeters (11.2 inches). The test section is also honed to a 16-rms microinch finish so that all pertinent smooth pipe formulae apply. Fluid (glycerine) is circulated by a 75 kilowatt constant speed (900 rpm), centrifugal pump, located in the downstream leg of the test facility.

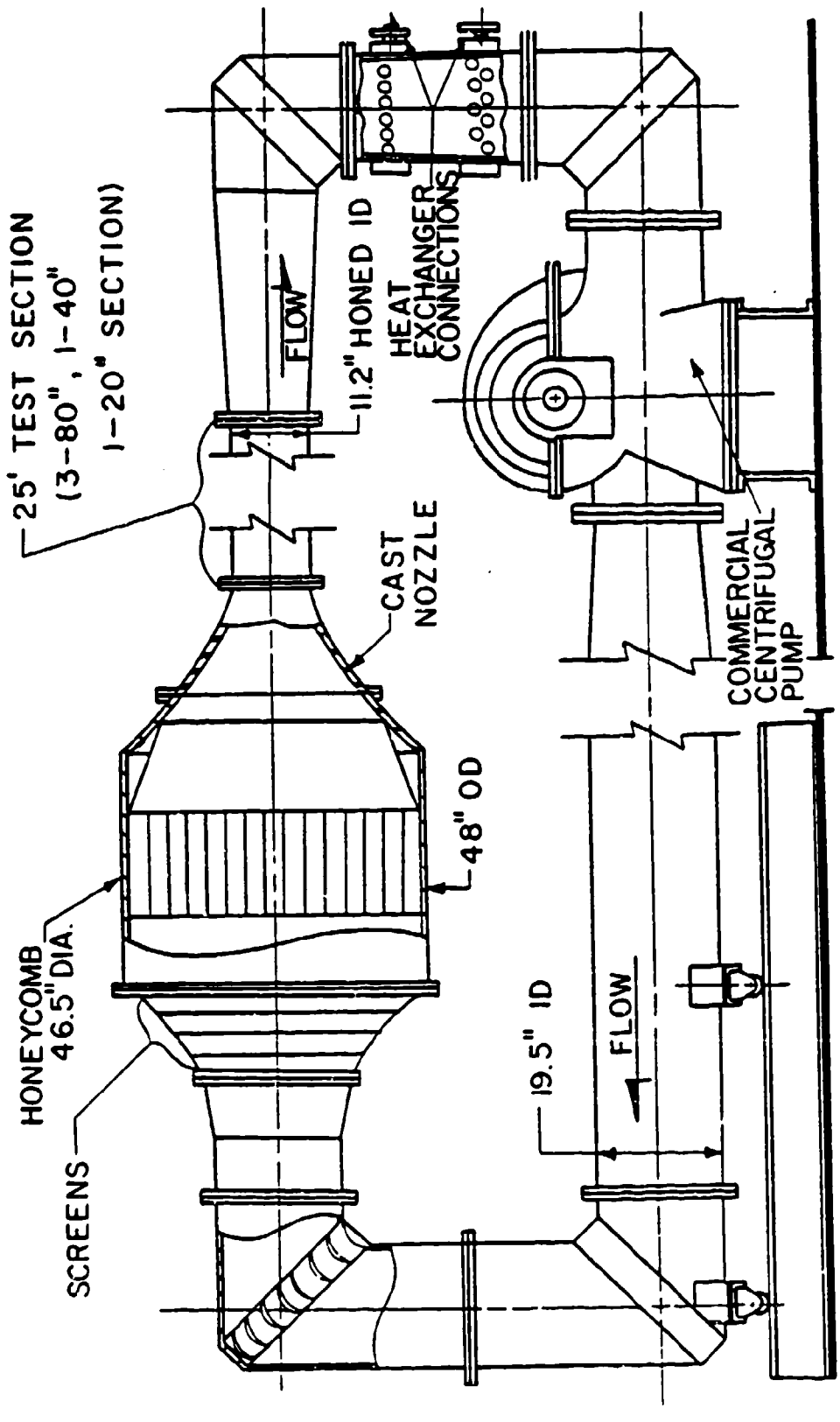

Figure 4.2 : Closed Circuit Glycerine Tunnel.

The laminar/turbulent transition location of the boundary layer is fixed at the entrance to the test section by a trip ring. Fluid exiting the nozzle section of the facility encounters an abrupt increase in cross-sectional area thus, tripping the flow into turbulence at the test section entrance. The onset of turbulence and the location of the transition zone were investigated experimentally by Bakewell (1965). Bakewell's results indicated that, for pipe diameter Reynolds numbers above 8000, fully developed turbulent flow exists throughout the length of the test section.

Reynolds numbers are varied by controlling the temperature of the glycerine. Cooling is accomplished through a large, reverse flow, heat exchanger located in a separate leg, just downstream of the test section. Heated fluid is discharged into the heat exchanger and after cooling, recirculated into the main flow of the facility. Constant flow temperatures can then be maintained by systematically controlling the cooling water flow rate in the heat exchanger. Tunnel temperatures are monitored by a digital thermometer, that is located in the diffuser section of the tunnel.

The tunnel is covered with a single, 4-inch wrap of fiberglass insulation (tunnel test section has 8 inches). Bakewell investigated the thermal gradient that exists normal to the flow in the test section. He found that the temperature gradient was minimized with the above specified insulation thicknesses. Therefore, a uniform temperature profile is assumed throughout the tunnel test section.

Because glycerine is an extremely viscous fluid, small air bubbles tend to become suspended in the fluid during the tunnel filling operation. To alleviate this problem, consecutive cycling of the tunnel over a period of three (3) days was required. The subsequent drop in the viscosity of the fluid with heating allows all entrapped air bubbles to escape through the

low, and high pressure observation domes of the facility. This is then verified by visually observing the glycerine (during tunnel operation) through the translucent domes.

4.2.1 Tunnel Mean Velocity

The mean flow velocity (U) was obtained as a function of glycerine temperature by measuring the static pressure drop (P_1 -P_2) across the nozzle section of the tunnel (Figure 4.3) for various glycerine temperatures. The Glycerine tunnel is configured with small, static pressure taps that begin at the settling section and proceed in 0.3048 meter increments along the entire length of the test section. Two, small lengths of capillary tubing were attached to two of these taps (P_1 and P_2), and the respective high (P_1) and low pressure (P_2) sides of a 15 PSI, Bell and Howell differential transducer. The transducer was calibrated as a

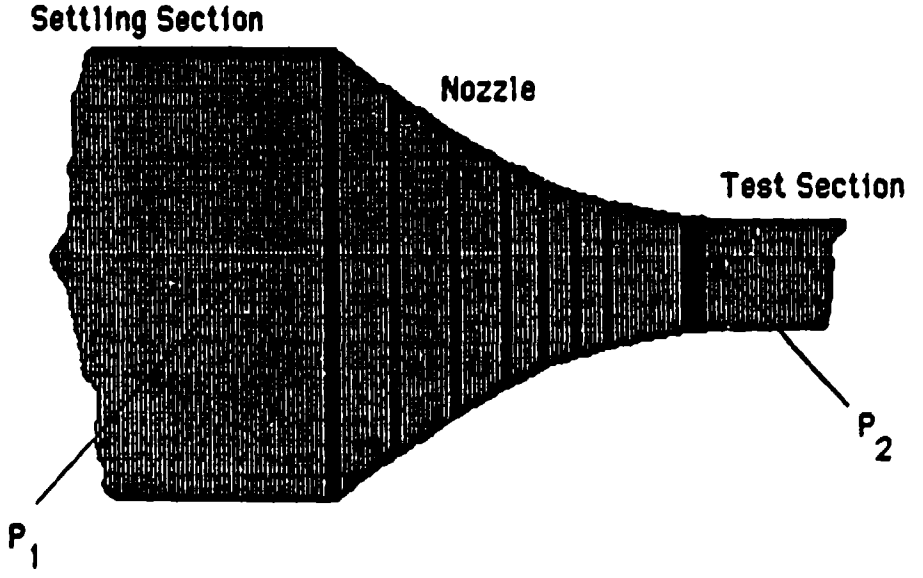

Figure 4.3: Static Pressure Measurement Locations of Mean Flow Velocity, with Nozzle Contraction Ratio of 16:1.

function of output voltage versus constant, input pressure differentials and is shown below in Figure 4.4.

The mean flow velocity was then determined by combining Bernoulli's equation with the conservation of mass law. This yielded the following relationship between the square of the average velocity and the pressure differential ($P_1 - P_2$). In the following equation, A_1 and A_2 are the respective cross-sectional areas at pressure locations P_1 and P_2 (see previous Figure 4.3).

$$U_2^2 = U^2 = \frac{2(P_1 - P_2)}{\rho[1 - (A_2/A_1)^2]} . \qquad (4.1)$$

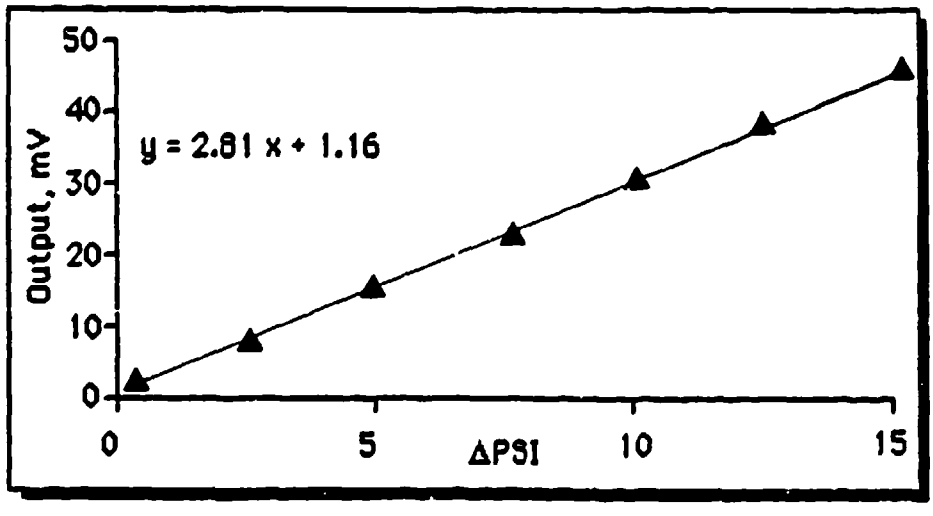

Figure 4.4: 15-PSI, Differential Pressure Transducer Calibration.

Due to the large contraction ratio (16:1) of the tunnel nozzle, the square of the area ratio (1:256) in the denominator of Equation 4.1 can be ignored.

From this, Equation 4.1 reduces to,

$$U^2 \approx \frac{2}{\rho} (P_1 - P_2). \qquad (4.2)$$

The calculated mean flow velocity versus glycerine temperature is plotted below (Figure 4.5) for glycerine temperatures ranging from 35°C to 46.1°C.

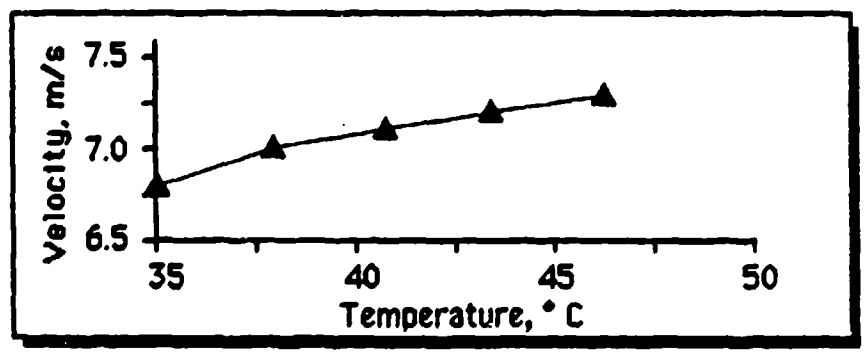

Figure 4.5: Tunnel Velocity Versus Glycerine Temperature.

4.2.2 Wall Shear Stress Measurements

The wall shear stress was measured at the same glycerine temperature (Reynolds number) as that used by Bakewell and also, at a number of other temperatures. This was accomplished by measuring the static pressure drop that occurred between two points along the wall of the test section. The wall shear stress is then obtained from the following relationship (Schlichting (1979)),

$$\tau_w = \frac{\Delta P\, D}{4\, L}. \qquad (4.3)$$

In Equation 4.3, D is the pipe diameter, and ΔP the pressure difference measured between two points separated by a distance, L along the pipe wall. The static pressure drop was obtained from two pressure taps located 5.7, and 7.3 meters downstream from the nozzle entrance. Flexible, hypodermic tubing was attached to the high and low pressure fittings of a 5-PSI, Bell and Howell differential pressure transducer and to the respective tunnel, pressure taps. The pressure differential $(P_1 - P_2)$ was then recorded while varying the tunnel temperature. Values of the measured wall shear stress were then calculated from Equation 4.3 and are compared to the theoretical wall shear stress values in Figure 4.6. Theoretical values were obtained from the previously measured average flow velocities and the following relationship for τ_{wall} (Schlichting),

$$\tau_w = 0.03955\, \rho\, U^{7/4}\, \upsilon^{1/4}\, D^{-1/4}$$

Both theoretical and measured values are shown as a function of glycerine temperature and are in reasonable agreement.

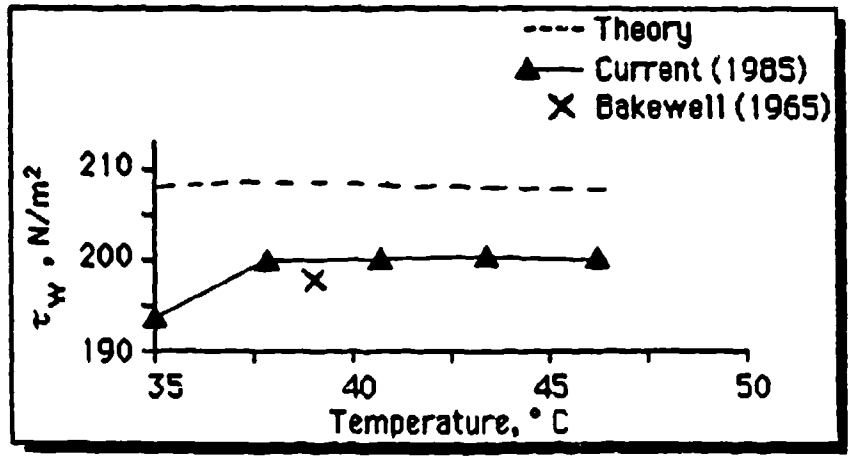

Figure 4.6: Wall Shear Stress Versus Glycerine Temperature.

Calibration of the Bell and Howell 5-PSI transducer was also done and is shown as a function of millivolt output, for constant pressure differential input in Figure 4.7. As with the 15-PSI transducer, an excellent linear relationship between output voltage and pressure differential input was observed.

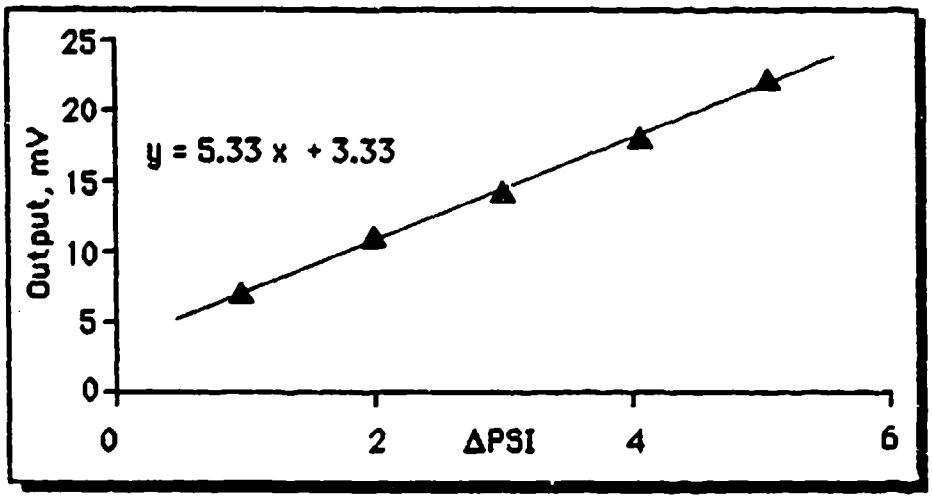

Figure 4.7: 5-PSI, Differential Transducer Calibration Results.

4.2.3 TBL Measurement Array and Data Acquisition System

The measurement array consisted of three Endevco, model number 8514-10, pressure transducers (described in Chapter 3) and also, three Endevco brand, piezo-electric accelerometers (nominal sensitivities of 45 mV/g). The array was located approximately 7.5 meters downstream from the entrance to the test section, in the fully developed, turbulent flow region of the pipe.

The transducers were mounted in individual cylindrical, plug-type assemblies. These assemblies were inserted into accommodating sleeves located along the tunnel wall and separated circumferentially by

120-degrees. The sleeves were equipped with gate valves, allowing the removal of the plugs without draining the tunnel. Alignment bolts were also positioned on the outer portion of each sleeve assembly to allow proper alignment of each plug with the inner tunnel wall. However, due to excessive play (≈1 cm) in the bolt mechanism proper, flush alignment of the plug with the inner tunnel wall could only be achieved through tactile verification. The pressure transducers were sealed into the face of each plug assembly with RTV sealant and were in direct communication with the flow. Accelerometers, were used to measure the local vibrations of each plug subassembly and were mounted on the back of the subassembly of each transducer (see Figure 4.8).

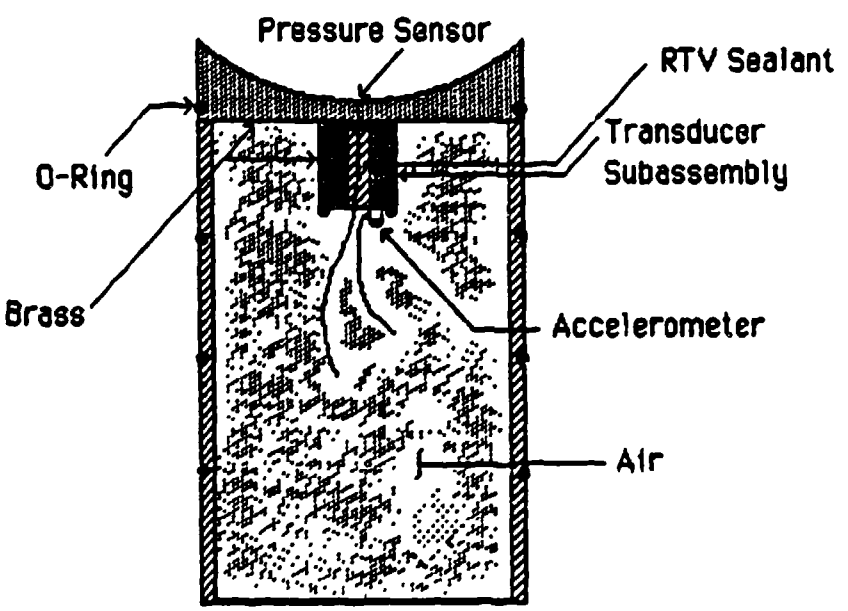

Figure 4.8: Cross-sectional View of Plug Assembly.

The 10-volt power supply used in the calibration of the transducers was also used in the actual tests. Also, the same cables and preamplifiers were used to ensure that all calibration results remained unchanged.

All voltage signals--transducer and accelerometer--were filtered and amplified on Brookdeal Differential Amplifiers before processing on a Spectral Dynamics (SD) 375 real-time spectral analyzer. The half power points of the high and lowpass filters were set at 1 Hertz and 1000 Hertz, respectfully. The SD 375's analysis bandwidth was set by the maximum frequency of analysis. For example, the SD 375 analyzer stores and displays 400 bins of information; this sets the bandwidth of analysis at,

$$B.W. = f_{max} / 400.$$

Throughout this investigation a Hanning ($\cos^2$) analysis window was used because of its characteristic side lobe suppression (18 dB/octave) and relatively narrow main lobe bandwidth. Various types of spectra were chosen from a selection menu on the SD 375 and after analyzing, were either sent to a hard copy digital plotter or, to the ARL/VAX 782 computer via a standard IEEE data bus.

4.3 TBL Wall Pressure Spectra

Before the TBL pressure fluctuations were measured an estimation of the vibrational contamination, present in the difference signals was obtained. This estimate was acquired by measuring the coherent output power (COP) spectrum between the difference signal of two pressure sensors and, the difference signal of their corresponding accelerometer outputs. As pointed out in Chapter 2, if the COP spectrum is significantly less than the autospectrum of the pressure difference signal then all vibrationally induced pressure terms can be ignored. Figure 4.9 shows a typical plot of the autospectrum of a pressure difference signal and the

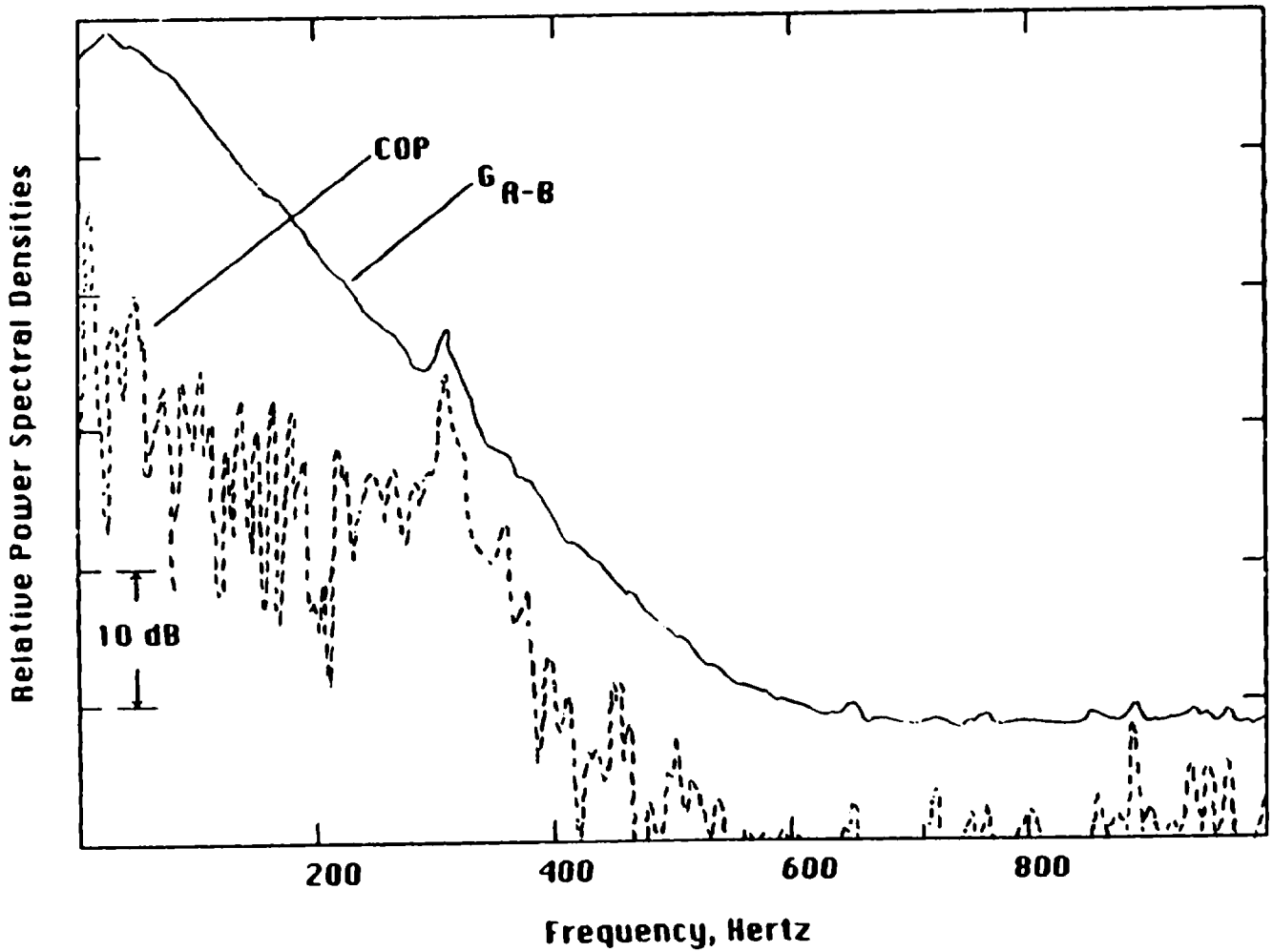

Figure 4.9: Difference Signal Versus COP Difference Signal Spectrum.

corresponding COP spectrum. As Figure 4.9 indicates, all vibrationally induced pressure terms are essentially removed in the difference signal. This implies that the power spectrum of the TBL wall pressure fluctuations is given simply by the cross-spectrum between two, pressure difference signals (electronic noise source terms included). For example,

$$G_{A_{tbl}}(f) = G_{A-B,A-C} + G_{A_e}.$$

The turbulent boundary layer (TBL) wall pressure spectra were obtained as a function of glycerine temperature by the method outlined previously in Chapter 2. Measurement of the electronic noise spectrum was found to be insignificant (70 dB down) so that,

$$G_{A_{tbl}}(f) = G_{A-B,A-C}.$$

Difference signals were obtained from the Brookdeal Differential Amplifiers and the corresponding cross-spectral density functions were obtained from the SD 375 spectral analyzer. Figure 4.10 shows the TBL pressure spectrum for various glycerine temperatures where 256 consecutive ensemble averages were taken. These results indicate that as the temperature of the flow increases, the frequency content of the wall pressure spectrum also increases. However, the peak levels of the power spectra for the various glycerine temperatures remain essentially constant, independent of Reynolds number. An explanation of this observation can be attributed to changes in the viscosity of the fluid that occurred over the temperature range tested. At the lower tunnel (glycerine) temperatures, the small-scale eddies that produce the higher frequency content of the TBL

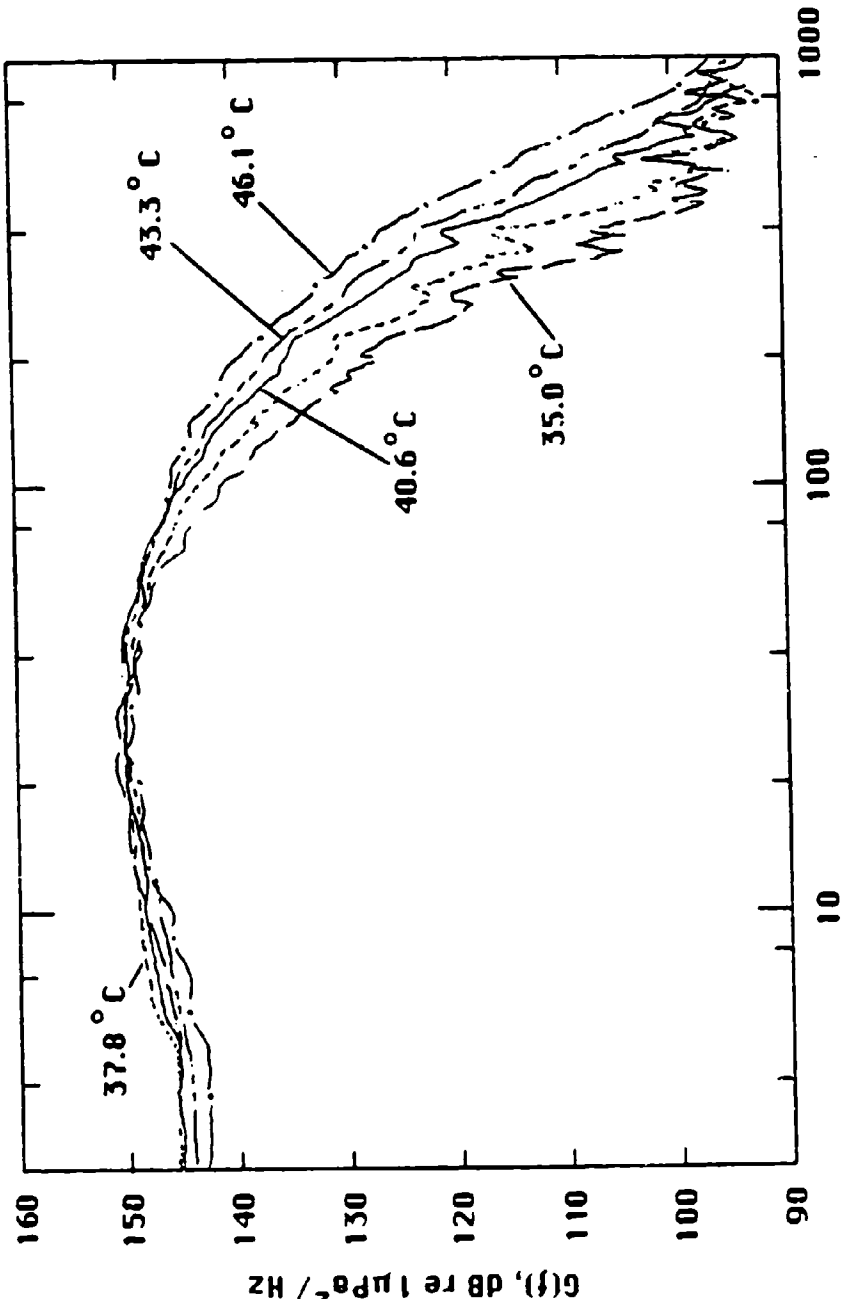

Figure 4.10: G_{tbl} Versus Glycerine Temperature.

pressure spectrum are more easily damped by the fluid's higher viscosity. As the temperature increases the viscosity decreases thereby allowing more of the smaller scale eddies to exist which in turn, generate higher frequency energy. This premise is further substantiated by Figures 4.11 and 4.12. Both of these plots show previously used non-dimensionalizing methods for characterizing the TBL wall pressure spectra in various test mediums--air, water and glycerine.

Figure 4.11 suggests that the amplitude of the TBL pressure spectrum scales with the inner flow parameter τ_w, and outer flow parameters, U and pipe diameter, D. The frequency, f is scaled in the usual Strouhal fashion where the length scale is taken as the pipe diameter and velocity as U. Figure 4.12, scales the frequency in a similar fashion where δ is D/2. However, the amplitude of the pressure fluctuations is scaled entirely on outer flow parameters ρ, U and D. Although reasonable data collapse is not achieved in either scaling case, an interesting result can be noted. As the viscosity (υ) of the medium is reduced, an increase in the frequency content of the TBL pressure spectrum is observed. That is, water having the smallest kinematic viscosity of the three mediums shown, also has the highest frequency content of the TBL pressure spectrum. Glycerine on the other hand, has the lowest frequency content of the TBL pressure spectrum and as expected, the highest viscosity. Also, both figures suggest that the scaling of the amplitude of the TBL pressure fluctuations is not critical. That is, both methods of amplitude scaling produce similar results. However, it is considerably more understandable to scale the amplitude of the pressure fluctuations with τ_w, since this parameter describes the physics of the flow locally, at the transducer location. In general, it is expected that the proper way to scale the TBL wall pressure

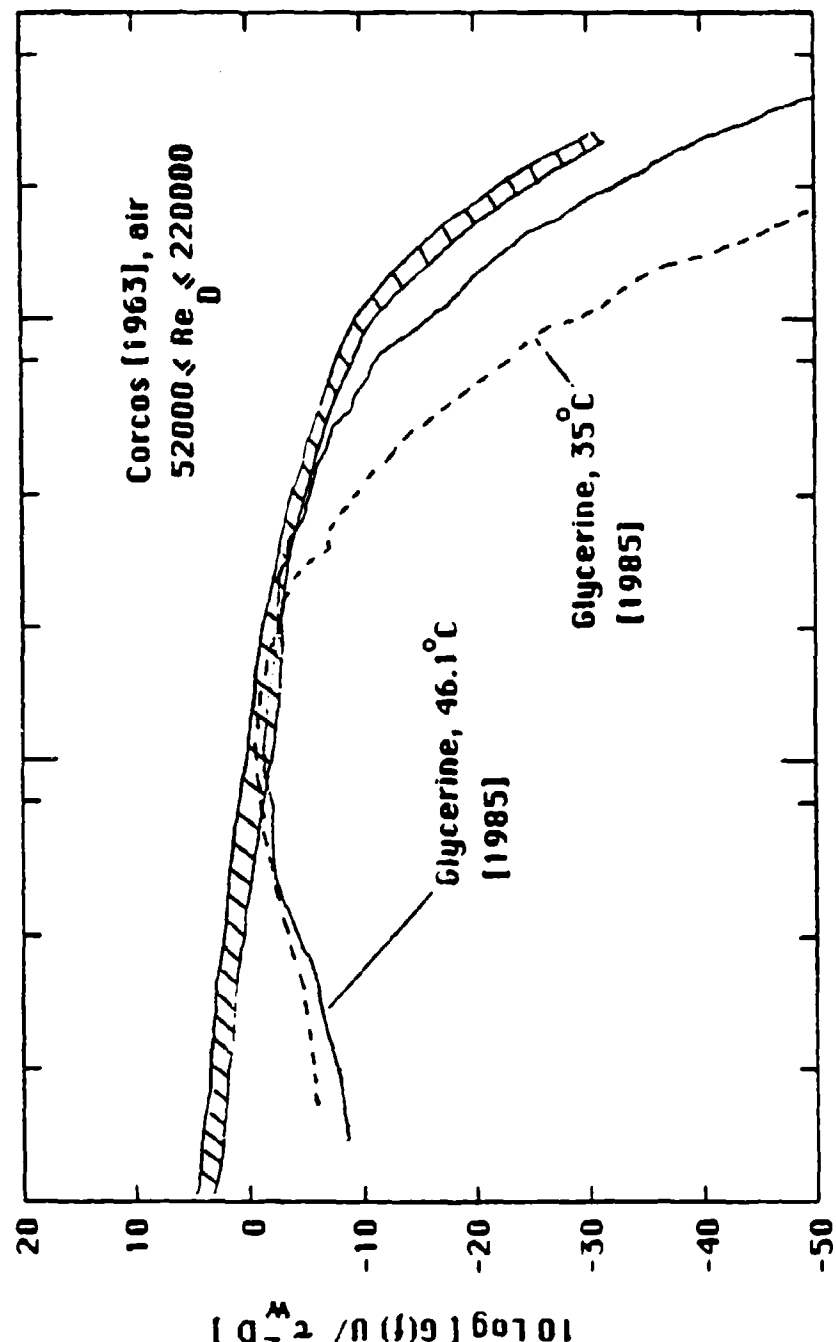

Figure 4.11: Normalized Wall Pressure Spectral Density, re: τ_w and D.

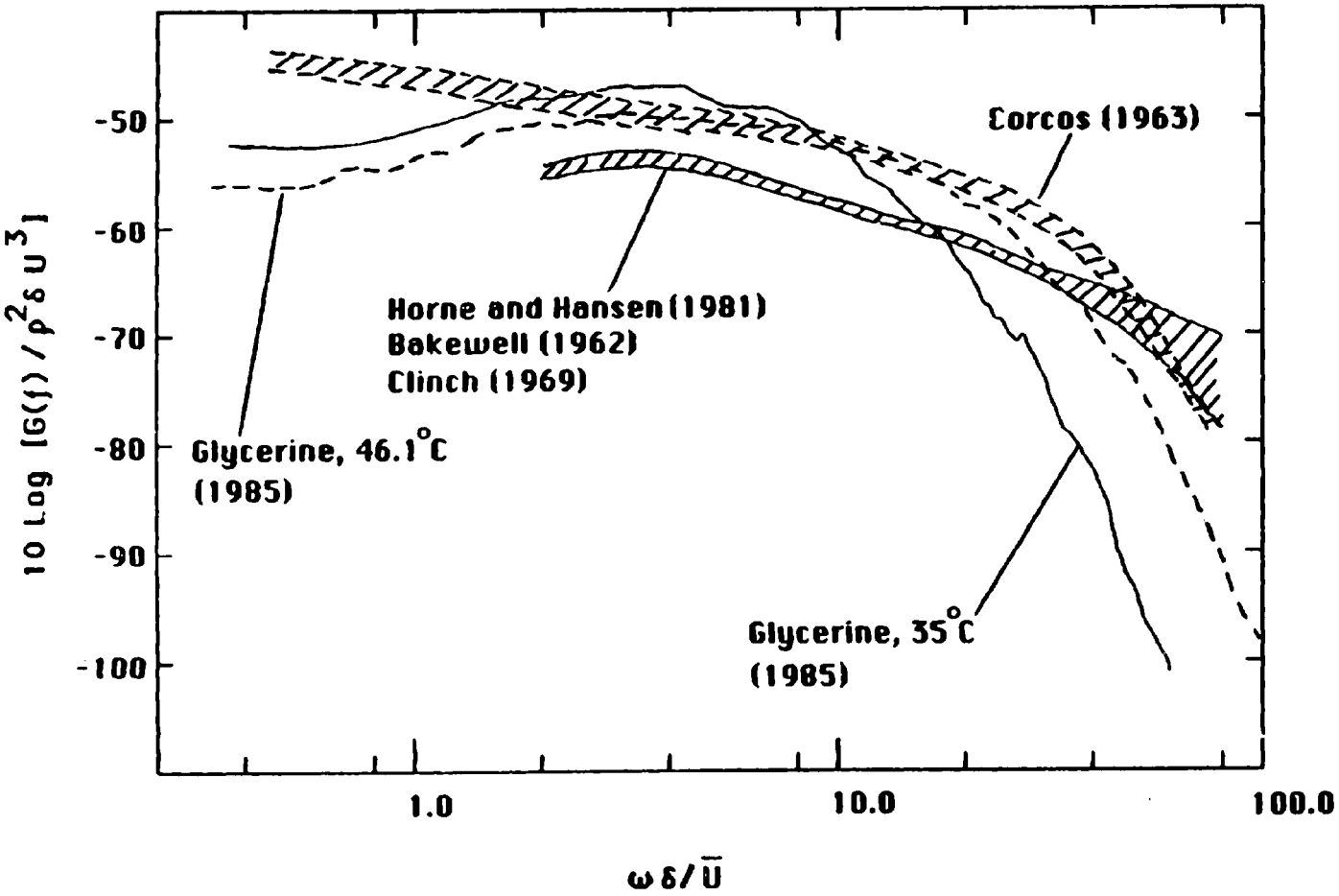

Figure 4.12: Normalized WallPressure Spectral Density, re: ρ, δ and $\bar{U}$.

spectra (both magnitude and frequency) is entirely with inner wall variables, taking due account of the resolution imposed by the finite size of the measurement transducer.

In many previous investigations, the major parameter used to characterize the transducer resolution has been d/δ^*. Where d, represents the hydrophone diameter and δ^*, the displacement thickness. Schloemer (1966) recognized, as early as 1966, that a "small" transducer must be small relative to the viscous scale, or "wall unit" (υ/u_τ), where u_τ is the friction velocity. This idea was later expanded upon by Fabula in the work published by Patrick(1977) in 1977. Willmarth (1975) also points out the importance of this form of scaling, that was later used extensively by Schewe (1983). Fabula contended that the d/δ^* method of normalization fails to describe the fundamental characteristics of turbulent boundary layer flow. Fabula argued that the ultimate transducer resolution is more correctly attained by a maximum value of $u_\tau d/\upsilon$ ($= d^+$) rather than d/δ^*. In other words, d^+ is a transducer resolution parameter that is based on inner boundary layer similarity considerations, while d/δ^* is appropriate for a transducer resolution parameter based on the outer boundary layer (lower frequencies). In fully developed turbulent pipe flow δ^*, is fixed at roughly $1/7^{th}$ the pipe radius. From this it is possible to see that even if d/δ^* equals a constant, d^+ can vary considerably over a given Reynolds number range which, varies (with d/δ^* fixed) from medium to medium. The parameter, d^+ can be thought of as a quantity that relates the transducer size to the height of the viscous sublayer region in the turbulent boundary layer ($y^+=yu_\tau/\upsilon \leq 5$). Fabula proposed that the ultimate in transducer resolution is achieved when $u_\tau d/\upsilon \leq 10$. However, Schewe (1983) states complete resolution of the essential structure of the turbulent pressure

fluctuations with a measured value of d^+ =19. Values of this parameter for data obtained in the current investigation ranged from $2.1 \leq u_\tau d/\upsilon \leq 4.4$. Therefore, these data provide the best spatial resolution of the TBL wall pressure fluctuations measured to date; they represent a true "point" measurement. (It should be noted that the transducer's casing diameter was used in the normalization and the actual value of d^+ is most likely smaller by a factor of 3, Galib and Zandina (1984)).

Inner wall scaling requires that the frequency be non-dimensionalized by the viscous time scale. Therefore, the frequency of the wall pressure spectrum is now scaled as $f\upsilon/u_\tau^2$. Figure 4.13, while using the same amplitude scaling as in Figure 4.11 uses the inner flow, frequency scaling. This figure clearly shows the dramatic effect transducer size has on the measured spectra. As d^+ decreases, more high-frequency (small-scale) information is detected by the transducer.

For completeness, Blake's(1970) and Schewe's (1983)data, obtained for turbulent flat plate flow, is compared to the data obtained in the Glycerine tunnel in Figure 4.14. In this figure, the pressure amplitude and frequency are scaled entirely on inner flow parameters. Although internal pipe flows differ from external flat plate flows for a number of reasons; the physical causes of the pressure fluctuations should be similar. Therefore, heuristically speaking, if the parameters that characterize the pressure fluctuations are explicitly known then direct comparisons of the resulting TBL pressure fluctuations for different flow geometries is somewhat justified. At values of $d^+>20$ (Blake) spatial filtering of the TBL pressure fluctuations is apparently occurring because of the observed attenuation of the high-frequency spectral energy. For values of $d^+ < 20$, the present data and those of Schewe agree quite well; attenuation of the high-frequency

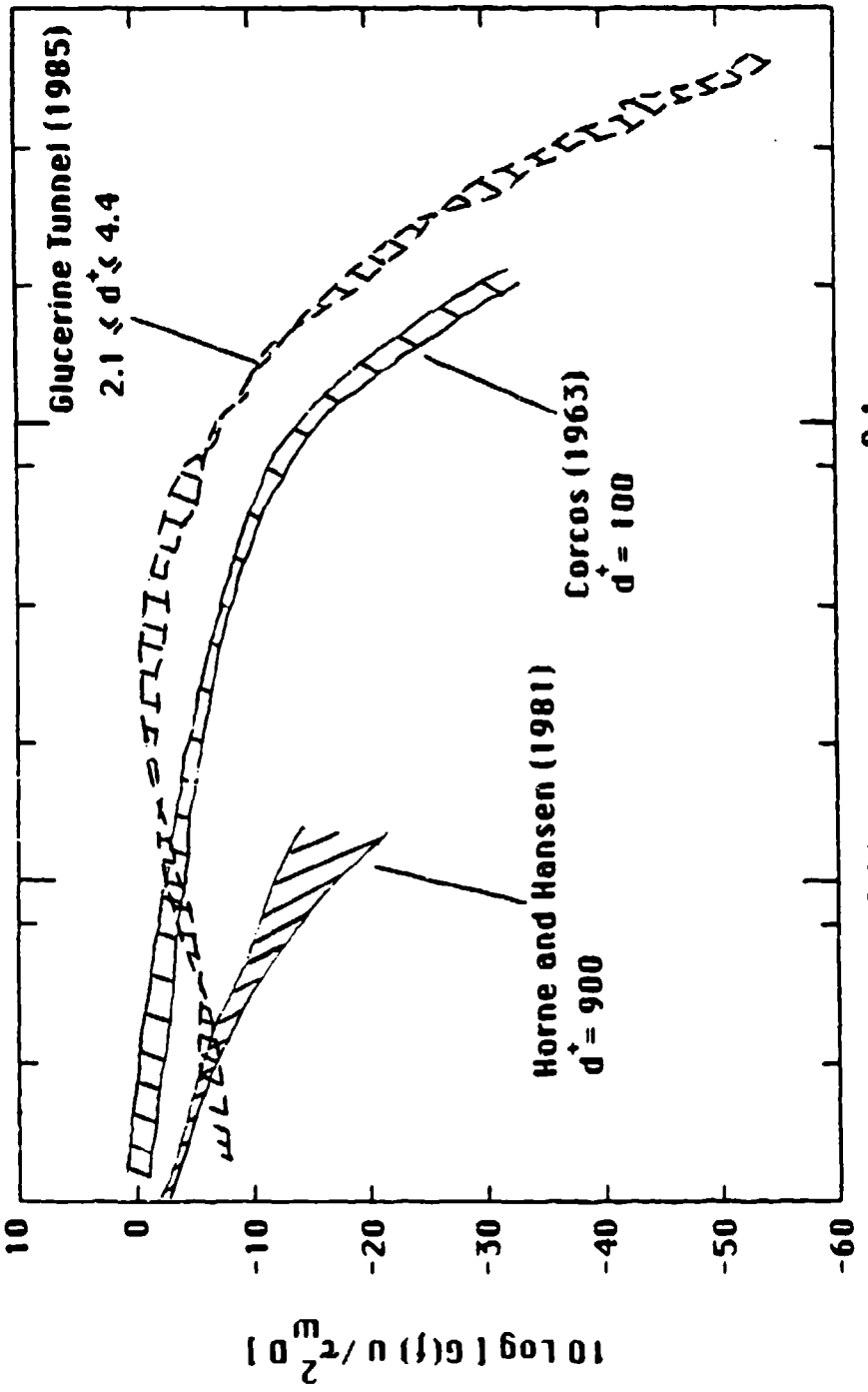

Figure 4.13: Turbulent Boundary Layer Similarity Plot of the Wall Pressure Spectrum.

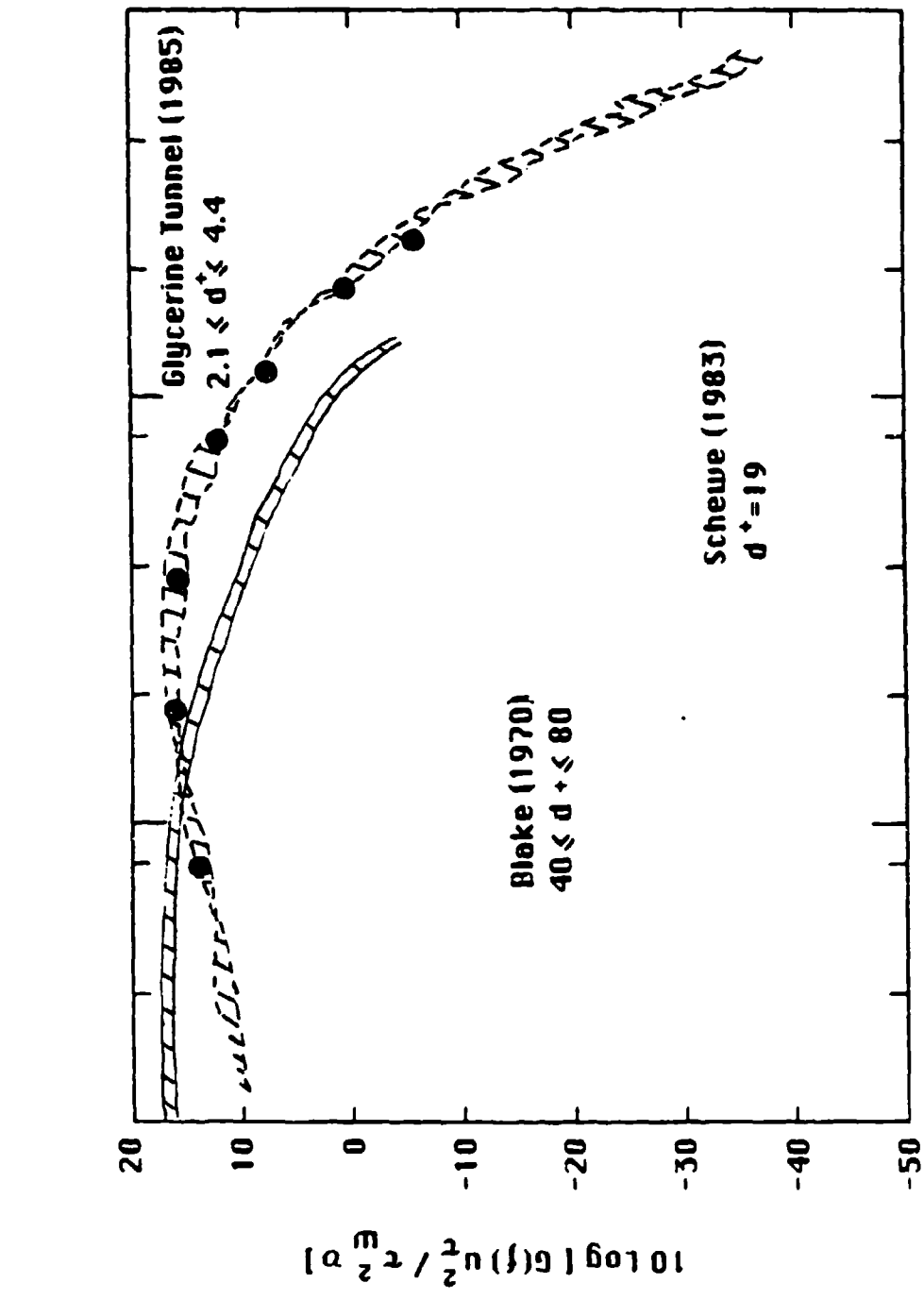

Figure 4.14: Inner Boundary Layer Similarity Plot of the Wall Pressure Spectrum.

content of the TBL pressure fluctuations is virtually non-existent. Schewe's contention, that the complete resolution of the TBL pressure fluctuations exists when $d^+ \leq 19$ is therefore substantiated by the agreement observed between the two sets of data. It appears that no further increase in transducer resolution is expected for values of d^+ smaller than 20. This confirms that transducer resolution depends primarily on values of $u_\tau d/\upsilon$ and not on d/δ^*. Scaling the wall pressure spectra in the manner used in Figure 4.14 allows the direct comparison of various types of flow geometries; for example, pipe and flat plate flows. It also suggests that the wall pressure fluctuations are mainly controlled by the physics of the flow in the inner wall region.

The r.m.s. value of the TBL pressure fluctuations is obtained by integrating the wall pressure spectrum over all frequencies and represents a measure of the intensity of the process. Figure 4.15 illustrates the dependence of the r.m.s. pressure on d^+. Here, the r.m.s. pressure is non-dimensionalized by the dynamic head, q_∞.

Corcos (1963) proposed a correction to account for the finite size measurement transducer (see Appendix 4). This correction is a function of the non-dimensional frequency, $\omega R/U_C$ and is applied directly to the spectral magnitude of the TBL pressure fluctuations. From measurements of the wavenumber-frequency response of a circular pressure sensor, virtually no correction is needed for values of $\omega R/U_C < 1.0$. From this result and those from Appendix 4, no correction should be needed for any of the measurements reported here for the Glycerine tunnel where, $\omega_{max} R/U_C = 0.6$ (ω_{max} was taken as the 50 dB down point in TBL wall pressure spectrum). In Table 4.1, both corrected, and uncorrected values of the r.m.s. pressure for Schewe's data is presented and compared to those

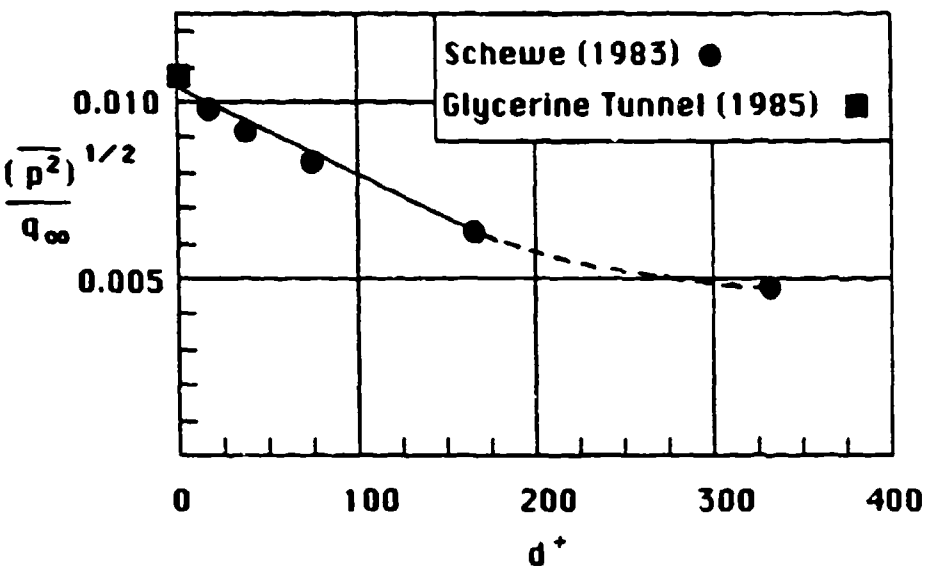

Figure 4.15: Dependence of the Normalized r.m.s. Value of the Wall Pressure Fluctuations upon the Normalized Transducer Diameter.

		p_{rms} / q_∞	
Investigator	d^+	Measured	Corrected
Schewe	19	0.0098	0.0105
Current	2.1	0.0106	0.0106
Current	4.4	0.0107	0.0107

Table 4.1: Comparison of the Measured and Corrected Normalized Wall Pressure r.m.s. Levels.

measured in the Glycerine tunnel. As indicated, the r.m.s. value of the wall pressure fluctuations is well resolved and equal to 0.0107 q_{∞}.

4.4 Correlation of the TBL in the Cross-Difference Spectrum

The hypothesis that the TBL pressure fluctuations were uncorrelated between pressure sensors is a major assumption of the TBL measurement technique described in Chapter 2. This model assumption may not be entirely valid at very low frequencies and, if not, may actually attenuate the low-frequency part of the TBL wall pressure spectrum. A relatively simple analysis can be performed to show that if the above assumption is fully valid then the value of the coherence function between any pair of (pressure sensors) difference signal outputs should equal 0.25 over the frequency range of validity. Moreover, this analysis also shows that the vibration-induced and acoustical pressure components are removed in the subtraction of any two pressure sensor signals.

To start, assume that the instantaneous pressure sensor outputs are represented as a(t), b(t) and c(t). Also, assume that all acoustic and vibrationally induced pressure signals are entirely cancelled when any two pressure sensor outputs are subtracted. Then using the same notation as in Chapter 2, the Fourier transformed quantities between pressure difference signals, a(t) - b(t) and a(t) - c(t) can be represented as,

$$A(f) - B(f) = A_{tbl}(f) - B_{tbl}(f)$$

and

$$A(f) - C(f) = A_{tbl}(f) - C_{tbl}(f).$$

The coherence function between the difference signals, A(f) - B(f) and, A(f) - C(f) is therefore given by (where the tbl subscripts are suppressed),

$$\gamma_{xy}^2 = \frac{|G_{xy}|^2}{G_{xx}\,G_{yy}} = \frac{|G_{A-B,A-C}|^2}{G_{A-B}\,G_{A-C}} . \quad (4.4)$$

In terms of expected values Equation 4.4 can be rewritten as,

$$\gamma_{xy}^2 = \frac{|E[(A-B)^*(A-C)]|^2}{E[(A-B)^*(A-B)]E[(A-C)^*(A-C)]} . \quad (4.5)$$

Expanding the expectation operations yields,

$$\gamma_{xy}^2 = \frac{|E[A^*A] - E[A^*C] - E[B^*A] + E[B^*C]|^2}{(E[A^*A] - E[B^*A] - E[A^*B] + E[B^*B])(E[A^*A] - E[C^*A] - E[A^*C] + E[C^*C])} . (4.6)$$

Assuming that the turbulent boundary layer (TBL) pressure fluctuations are uncorrelated between measuring points, any expected value involving two different quantities will tend to zero. For example,

$$E[A^*B] = E[B^*C] = \ldots = 0.$$

Equation 4.6 will then reduce to,

$$\gamma^2_{xy} = \frac{E[A^*A]E[A^*A]}{(E[A^*A]+E[B^*B])(E[A^*A]+E[C^*C])} \quad (4.7)$$

Also, because the flow is axisymmetrical, the autospectra of the turbulent boundary layer pressure fluctuations will be the same at locations a, b and c. This implies that (recall that the "tbl" subscript is suppressed),

$$E[A^*A] = E[B^*B] = E[C^*C].$$

Equation 4.7 then reduces to,

$$\gamma_{xy}{}^2 = \frac{E[A^*A]E[A^*A]}{(E[A^*A]+E[A^*A])(E[A^*A]+E[A^*A])} = 0.25 \quad (4.8)$$

From this analysis it can be stated that if :

1) the difference signal effectively removes all acoustic and vibrationally induced pressure signals, and
2) the pressure sensor separation distance is large enough to permit the TBL pressure fluctuations to remain uncorrelated between pressure sensors then,

the value of the coherence function between any pair of difference signals should equal 0.25. A simple measurement will therefore either prove or, disprove the validity of the TBL measurement assumptions.

A typical measurement of the coherence function between two pairs of difference sig , is shown in Figure 4.16 where 256 spectral averages were taken. At very low frequencies (< 10 Hertz) the coherence function is essentially 0.25 implying that all vibrational and acoustic components of the pressure field are cancelled thereby, leaving only the TBL pressure fluctuations. As the frequency of the coherence function increases above 20 Hertz, deviations from 0.25 begin to appear. These deviations are most likely due to the increasing loss of the coherent structure in the vibrationally induced pressure field and, not in the propagating acoustic field because the (duct) cutoff frequency for axially plane wave propagation is approximately 4100 Hertz. This means that all acoustic noise should remain perfectly correlated between pressure sensors for frequencies as high as 4100 Hertz. The effect of the vibration contamination is most prevalent at lower tunnel temperatures and, for frequencies above 200 Hertz, as shown in Figure 4.16. These vibrational effects appear as spectral peaks and valleys in the TBL pressure spectra (see Figure 4.10), but only represent a small fraction of the total spectral energy.

Another way of determining how well the TBL pressure spectrum was measured is by comparing the power spectrum of a difference signal to cross-difference spectrum. From previous relationships it is easily shown that,

$$G_{A-B}(f) = 2 \lim_{T \to \infty} [\, E(A_{tbl} - B_{tbl})^{*}(A_{tbl} - B_{tbl})] / T = 2\, G_{tbl}(f) \,.$$

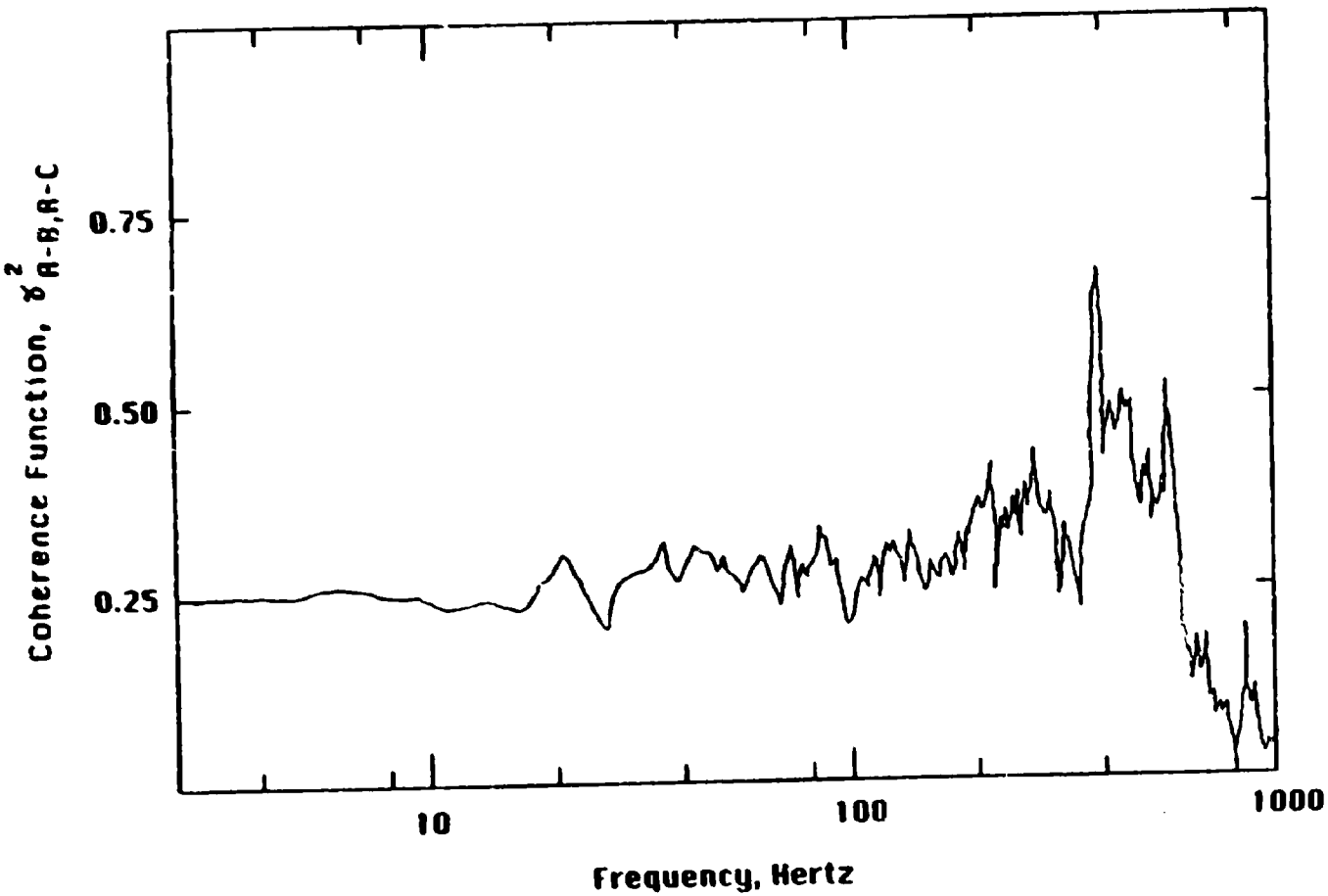

Figure 4.16: Typical Coherence Function between Transducer Difference Signals.

and from Chapter 2,

$$G_{A-B,A-C}(f) = G_{tbl}(f).$$

Therefore, the power spectrum of a difference signal should be 3 dB above the cross-difference spectrum (G_{TBL}). Typically, Figure 4.17 shows these two power spectra. As expected, the power spectrum of the difference signal A(f)-B(f), is nominally 3 dB above that of the TBL spectrum over the entire frequency range shown.

The above analyses and their results are significant in that, vibration contamination usually causes considerable errors in the measurement of the TBL wall pressure spectrum at very low frequencies and has generally made accurate conventional measurements (using single pressure transducers) of these types impossible (Willmarth (1975)). However, TBL wall pressure measurements that involve transducer difference signals can not only remove significant amounts of acoustic and vibratory noise from the TBL wall pressure spectrum (Section 4.3), but also, provide a direct way to check the integrity of the data acquired (especially at very low frequencies). Data integrity of the TBL wall pressure spectrum can now be established with a measurement of the coherence function between difference signal pairs. This measurement will equal 0.25 for the precise measurement of the TBL wall pressure spectrum. It should be noted, that this difference signal approach to measure the TBL wall pressure spectrum is not limited to axisymmetric flows; this type of measurement technique will work as long as the transducer array is positioned normal to the mean flow field. These measurement techniques are the preferred way to measure the TBL wall pressure spectrum.

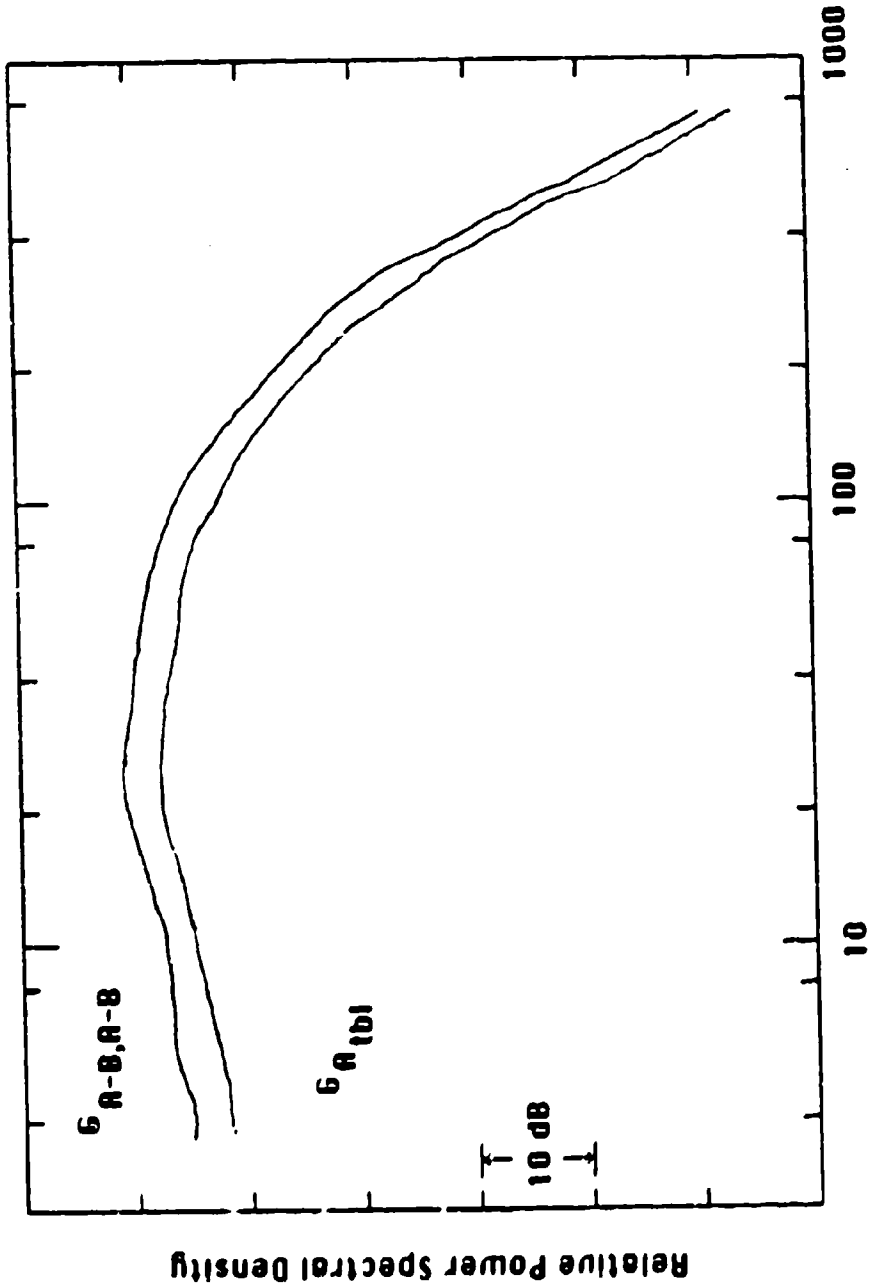

Figure 4.17: Typical Cross-Difference (TBL) and Difference Spectra.

4.5 Tunnel Background Noise

At the onset of this experimental investigation it was hoped that the noise associated with the tunnel operation would be many orders of magnitude below that created by the TBL wall pressure fluctuations. Because measurements of the low-wavenumber content of the TBL have yet to be performed with any degree certainty, it was an early goal of this investigation to qualify the glycerine tunnel for such measurements. Unfortunately, instead of qualifying the Glycerine tunnel as a candidate for future low-wavenumber research, measurements of the acoustic and vibrational noise spectra have indicated that these two sources dominate the output of all flush-mounted pressure sensors. Figures 4.18, and 4.19 show three different power spectra measured in the glycerine tunnel, at temperatures of 35° and 46.1° C. Both plots indicate typical results of the TBL pressure spectrum (G_{tbl}), the acoustic or, cross-spectrum (G_{AB}) and, the power spectrum measured by a single transducer (G_{AA}). These results--at both temperature extremes--clearly indicate the power of the cross-difference TBL measurement technique and the high-level noise present in the facility. Over most of its frequency range, the TBL pressure spectrum is 10 to 15 dB below that of the acoustic (and single transducer spectrum) noise spectrum, and at 46.1°C, as much as 30 dB below.

Figures 4.20, 4.21, 4.22, and 4.23 depict the corresponding phase angles of the TBL pressure spectrum and the acoustic noise spectrum at glycerine temperatures of 35 and 46.1° C, respectfully. All phase plots of the TBL pressure fluctuations show essentially zero phase shift for frequencies up to 150 Hertz. At higher frequencies (>150 Hertz) and especially for glycerine temperatures of 35°C, large deviations from zero occur in the phase of the TBL spectrum.

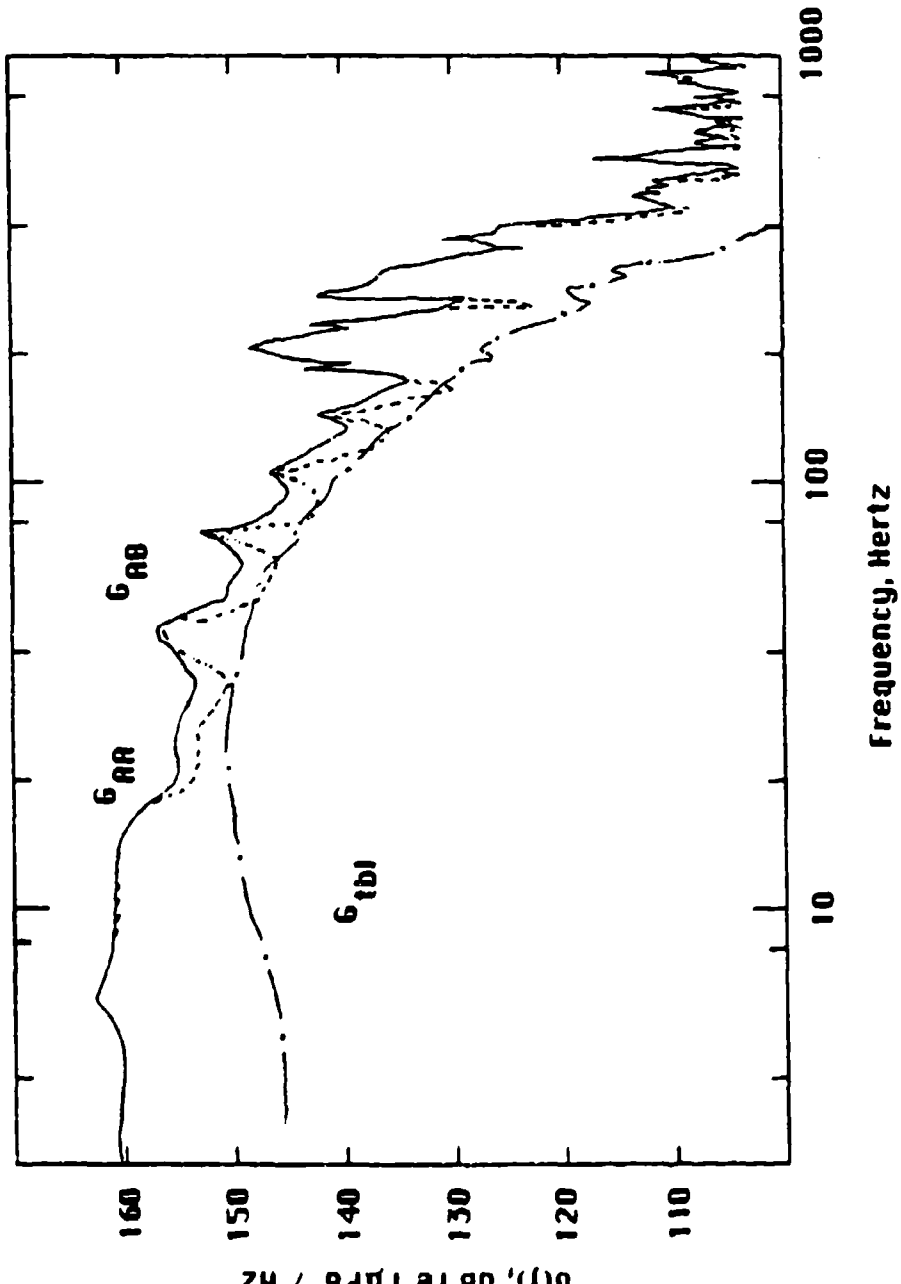

Figure 4.18: Spectral Plots of the Auto, Cross and TBL Pressure Fluctuations at 35.0°C

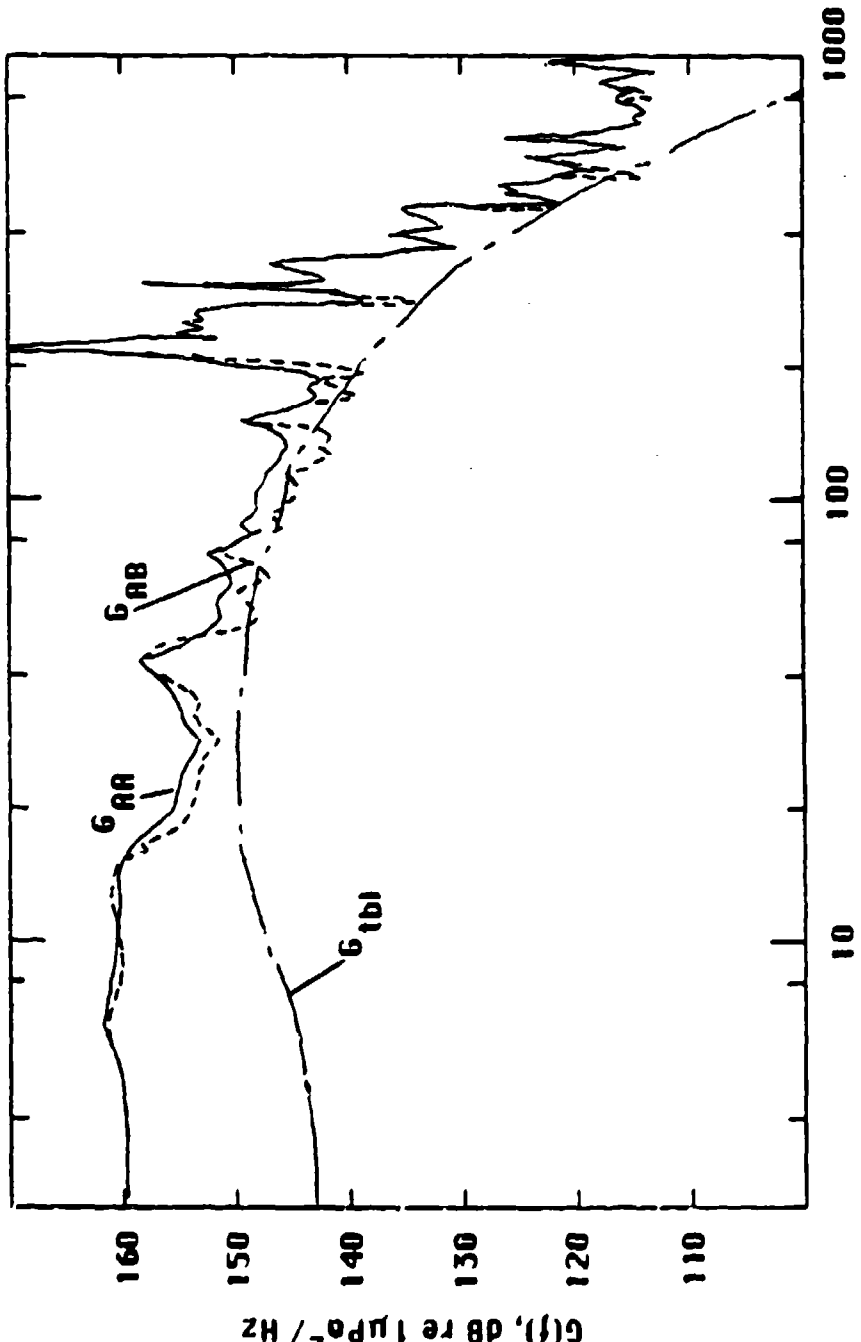

Figure 4.19: Spectral Plots of the Auto, Cross and TBL Pressure Fluctuations at 46.1 °C

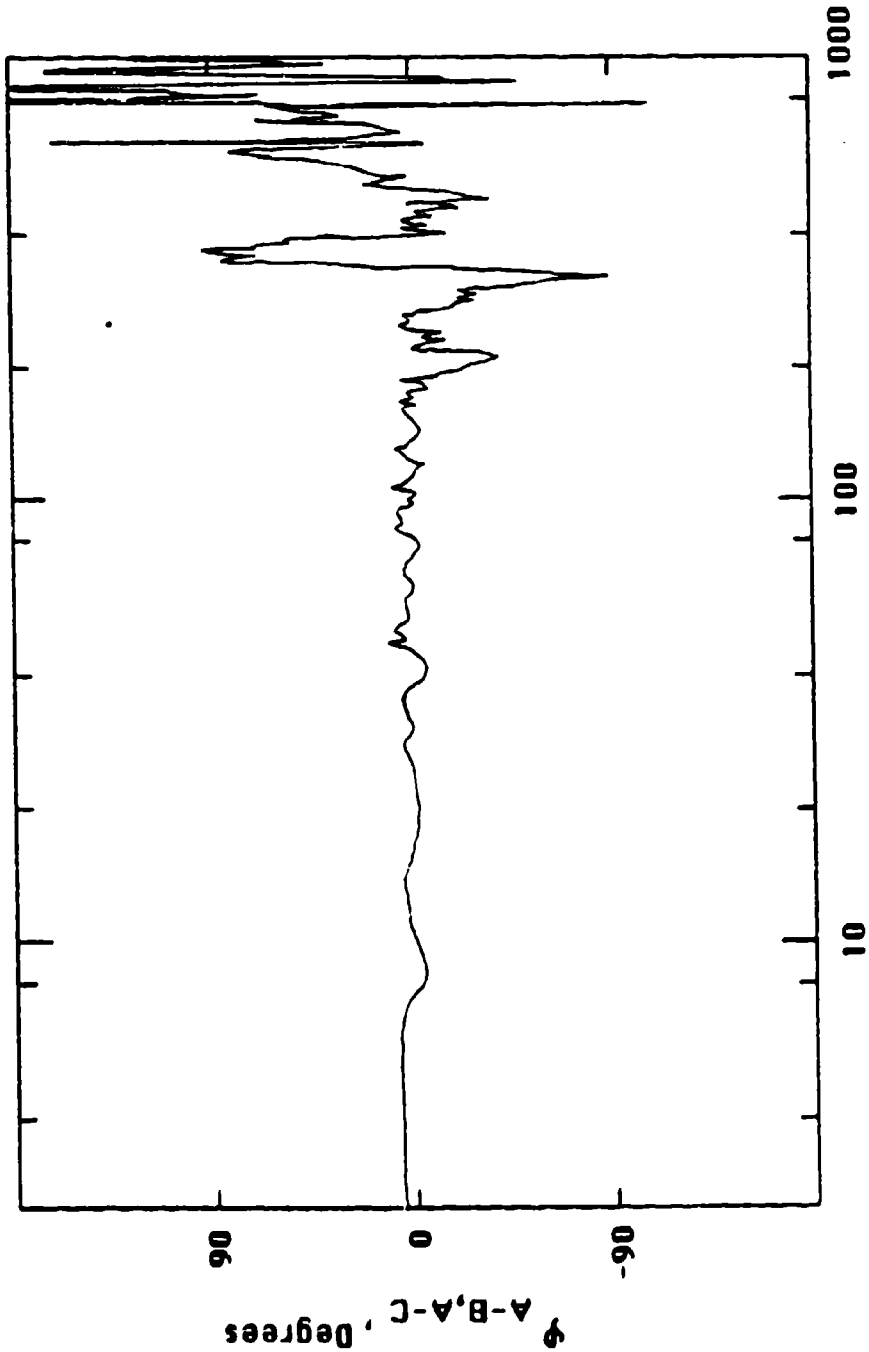

Figure 4.20: Typical Phase Response between Transducer Difference Signals at 35.0 °C.

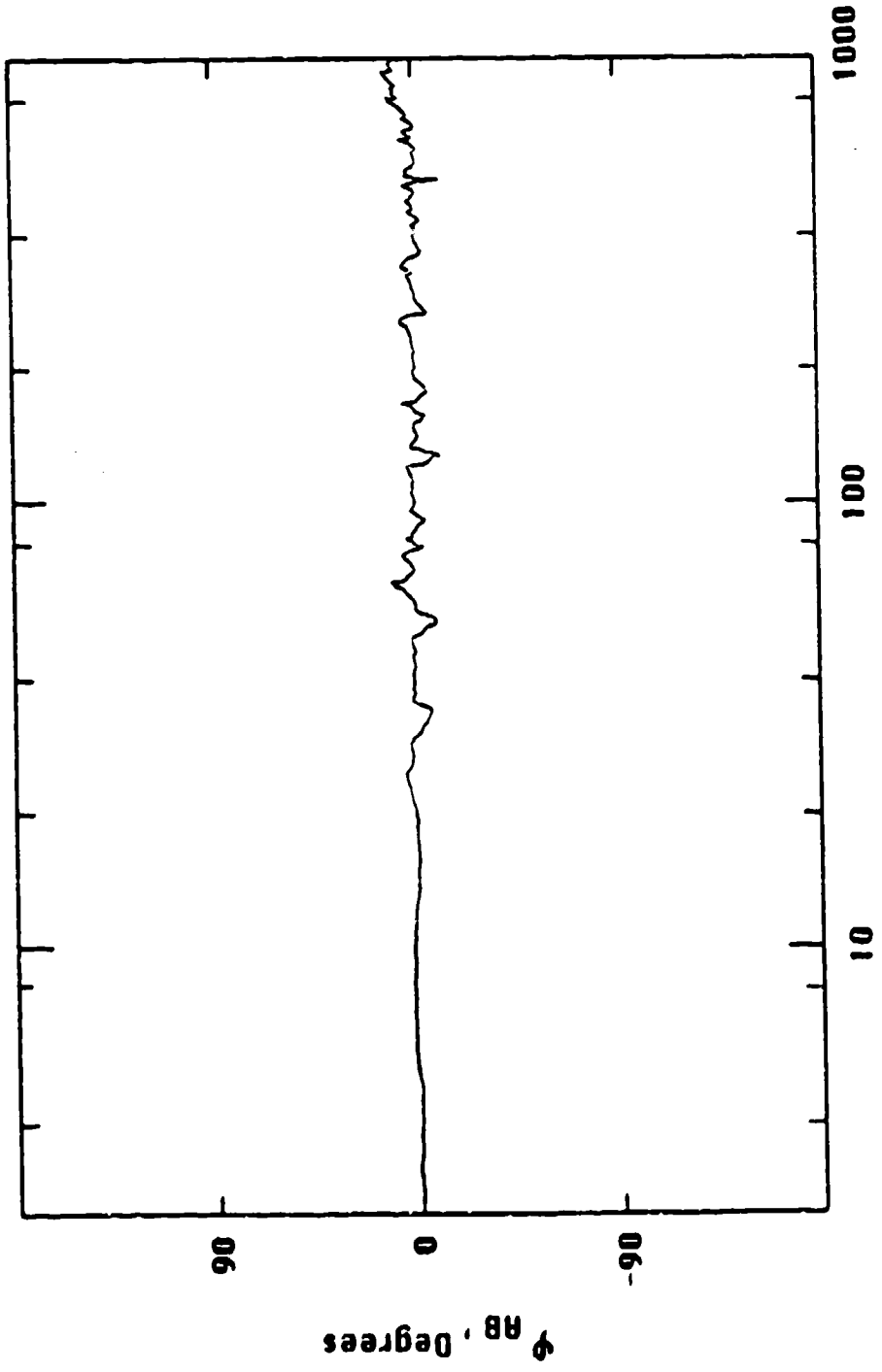

Figure 4.21: Typical Phase Response between Transducer Signals at 35.0°C.

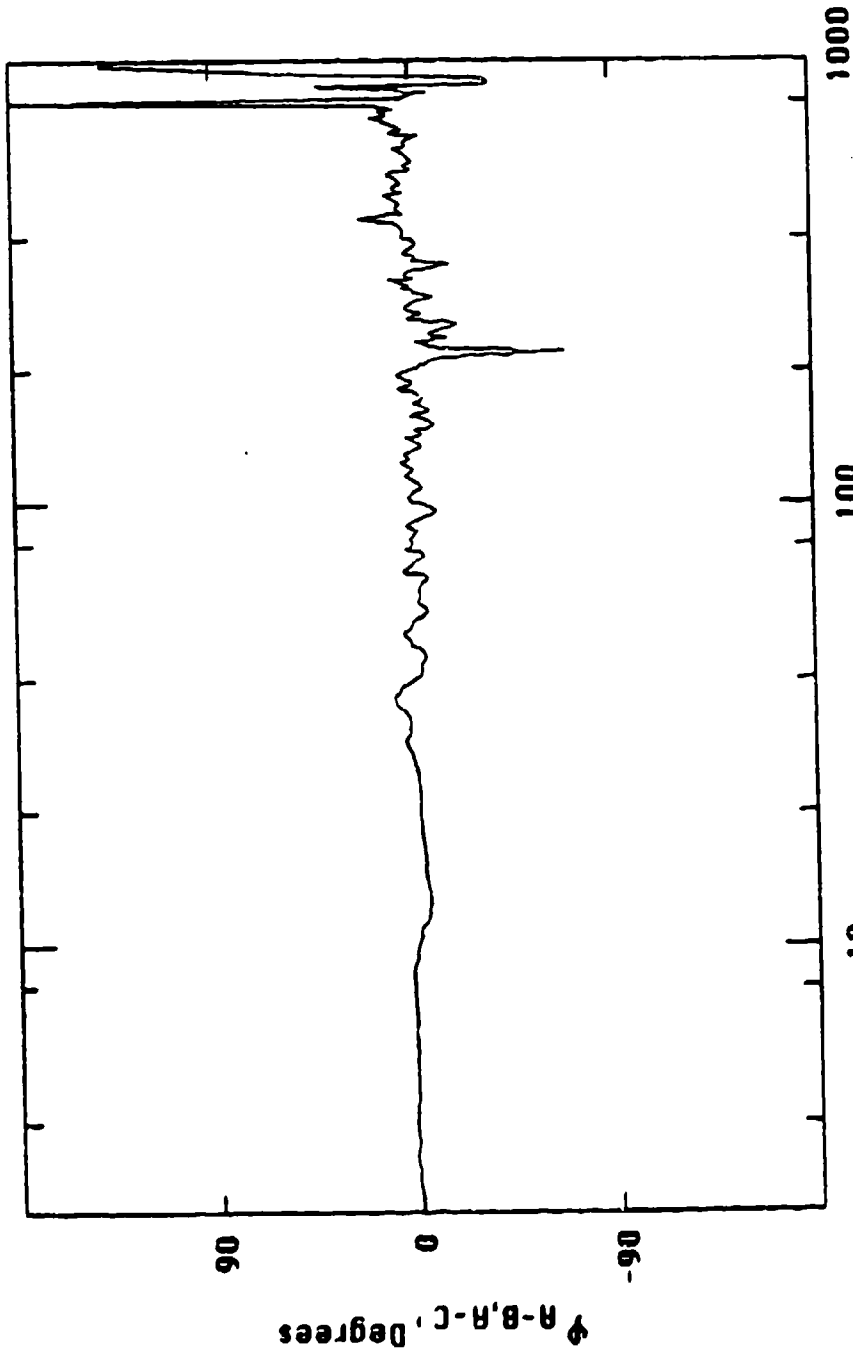

Figure 4.22: Typical Phase Response between Transducer Difference Signals at 46 1°C.

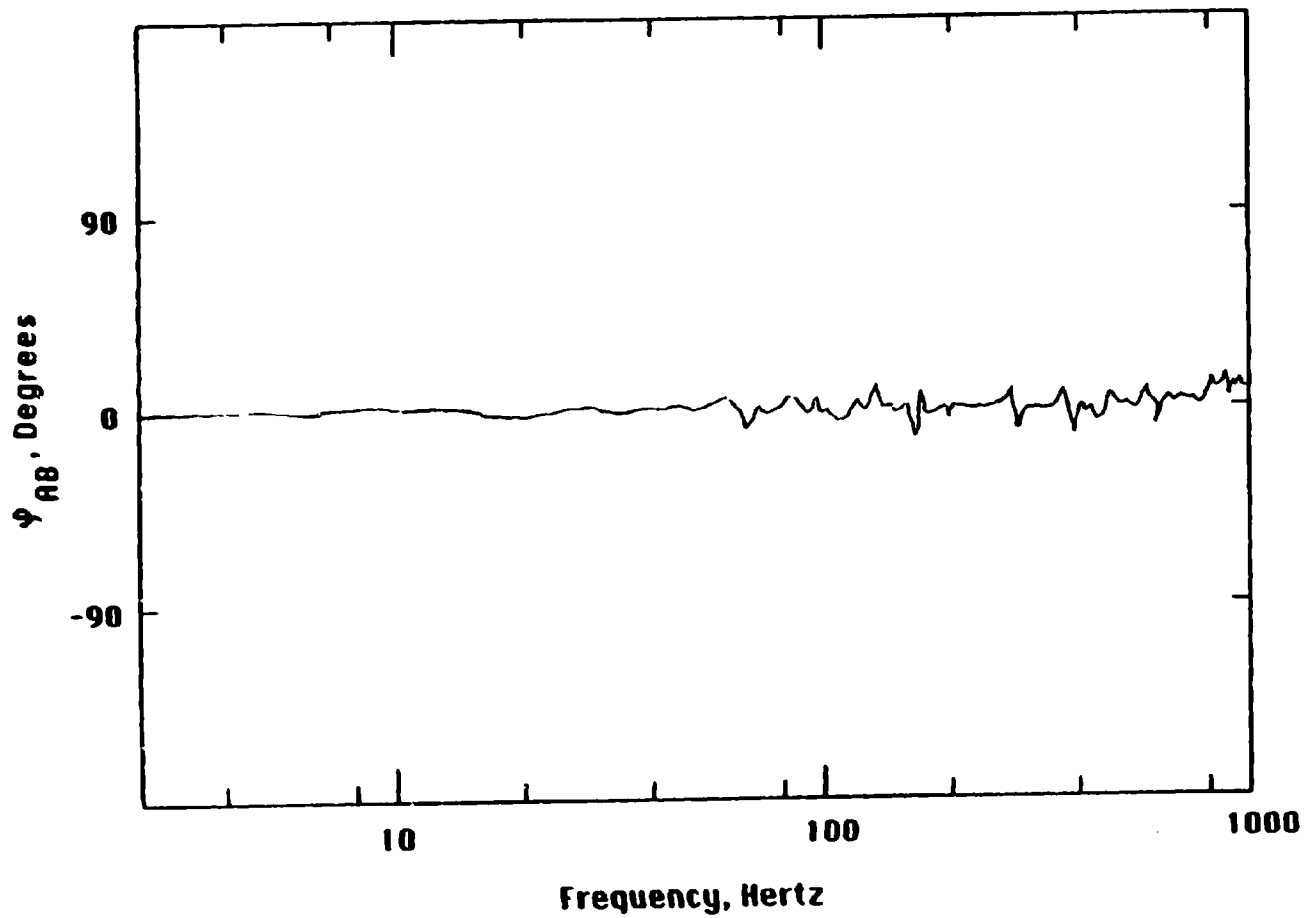

Figure 4.23: Typical Phase Response between Transducer Signals at 46.1°C.

These deviations at this lower tunnel temperature account for the more ragged appearance of the TBL pressure spectrum (Figure 4.10) at frequencies above 150 Hertz. (These deviations were earlier postulated as being related to the loss of the coherent structure in the vibrationally induced pressure field between transducers for frequencies above 150 Hertz.) The plots illustrating the measured phase difference between pressure sensors (Figures 4.21 and 4.23) show that the relative phase difference between pressure sensors is insignificant. This further substantiates that all acoustic noise in the facility propagates as plane waves, constant in phase and amplitude in any plane perpendicular to the flow of the test section for frequencies below 1000 Hertz.

Figure 4.24 shows the COP spectrum between the output of single transducer and its corresponding acceleration. Chapter 2 described how this particular spectrum represents the vibrational contamination present in the autospectrum of a single transducer. Although this measurement indicates a cause of possible contamination it does not indicate the source. That is, the COP spectrum does not show whether the noise source is entirely structure borne or, fluid/structure coupled. However, Figure 4.24 does show that vibrational effects dominate the high-frequency part of the autospectrum of a single transducer and that acoustical, fluid-borne noise contributes to most of $G_{AA}(f)$ below 150 Hertz.

Although not investigated in detail, it is speculated that a major source of noise--both acoustic and vibrational--is due to the tunnel's, pump/motor coupling and the pump. Excessive floor vibration can be felt at the initial start-up of the facility and during tunnel operation. Measurements of the motor and pump shaft misalignment were made and found to be quite excessive. An improved flexible coupling for the facility

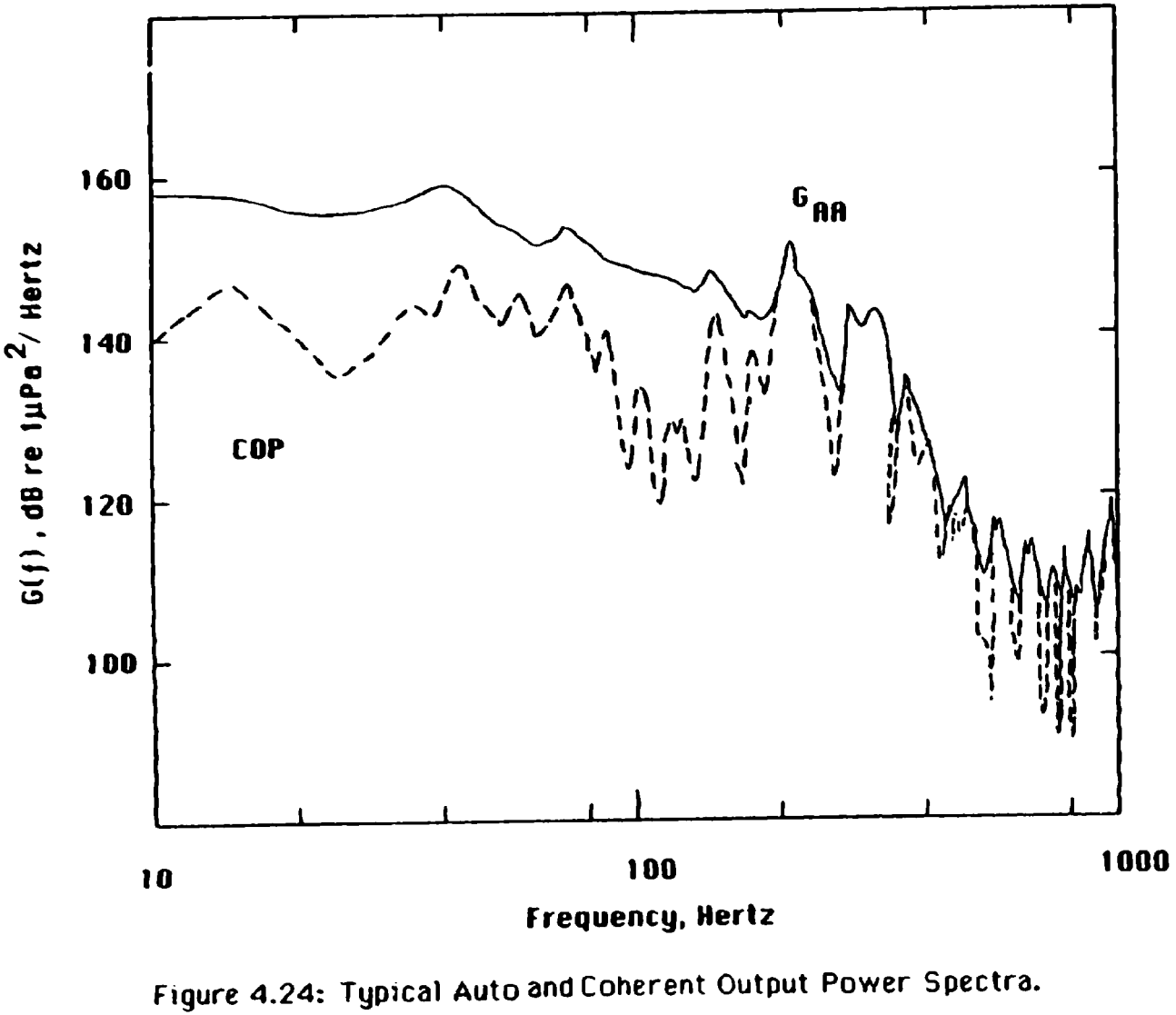

Figure 4.24: Typical Auto and Coherent Output Power Spectra.

has been designed and subsequent measurements of the COP spectrum and transducer cross-spectrum should be repeated after the new coupling is installed. This relatively easy implementation should reduce tunnel vibrational (and acoustic) noise levels significantly. Other quieting measures are also under investigation at this writing.

4.6 Conclusions and Areas of Future Research

The techniques employed in measuring and validating the TBL wall pressure spectra were of primary importance in this study. Without these novel signal-processing techniques, the ability to measure the wall pressure spectrum accurately, with conventional single point measurements, would have proved futile due to the excessive facility background noise.

Wall pressure spectra obtained for both pipe and flat plate flows have been compared with remarkable agreement. From these comparisons and selected scaling, the characteristic features of the wall pressure spectrum have been identified. That is, the inner flow parameters τ_w, and U_τ along with the viscosity (υ) of the fluid can be used to consistently characterize the TBL wall pressure fluctuations and their frequency content for both internal and external flows.

Due to the large viscous sublayer present in the glycerine turbulent boundary layer, the value of the normalized transducer diameter (d^+) ranged from 2.1 to 4.4, depending on the fluid bulk temperature. These are the smallest values of d^+ ever reported. From these results, a critical uppermost limit on the value of d^+ has been validated; namely, $d^+ < 20$ as speculated by previous investigators. This value of d^+ represents an upper limit for which proper resolution of the high-frequency content of the TBL pressure fluctuations can be achieved.

A simple measurement of the coherence function between difference signals has validated all the TBL pressure fluctuation measurement assumptions previously outlined in Chapter 2. From these results, measurement of the very low-frequency content (<10 Hertz) of the TBL wall pressure spectrum was obtained. The coherence function measurement, also provides a simple means to test the integrity of the TBL wall pressure spectrum (i.e. removal of vibration and acoustic noise), especially at very low frequencies.

An area of possible future research for the glycerine tunnel may include velocity and pressure correlation measurements. Because the wall pressure fluctuations are related to the fluctuating velocity field and, because the viscous sublayer is quite thick, detailed measurements of these types are possible. They would provide additional information on coherent structures including bursting frequencies and the scaling of these frequencies. A major issue in the study of coherent structures in turbulent boundary layers has been the scaling of the bursting frequency. This controversy centers about transducer spatial resolution. It has been shown that (conservative) d^+ values as small as 2.1 can be obtained in the glycerine tunnel, which would therefore make the glycerine tunnel a likely candidate to resolve this controversy.

APPENDIX 1

SPECTRAL DENSITY VIA THE FINITE FOURIER TRANSFORM

The two sided spectral density functions $S_{xx}(f)$, and $S_{xy}(f)$ are by definition, the Fourier transform of their auto and cross-correlation functions $R_{xx}(\tau)$, and $R_{xy}(\tau)$. However, they can also be represented as the expected value of their Fourier transformed time functions x(t) and y(t). Before proceeding with this proof a few fundamental definitions will be given.

A random process can be described as an ensemble of a real-valued time function and is denoted as $\{x_k(t)\}$ where, $-\infty < t < \infty$. The function, $x_k(t)$ is defined as the kth event of an entire ensemble in which N events occur or are observed. In practice, N is a statistically large finite number and is usually large enough to approximate infinity. The mean values of the stationary random processes $\{x_k(t)\}$ and $\{y_k(t)\}$, are described as:

$$\mu_x = E[x_k(t)] = \int_{-\infty}^{\infty} x(t)\, p(x)\, dx$$

$$\mu_y = E[y_k(t)] = \int_{-\infty}^{\infty} y(t)\, p(y)\, dy$$

where p(x) and p(y) are the probability density functions of x(t) and y(t), respectfully. For arbitrary fixed t and τ, let:

$$R_{xx}(\tau) = E[x_k(t)\; x_k(t + \tau)]$$

$$R_{yy}(\tau) = E[y_k(t)\ y_k(t+\tau)]$$

$$R_{xy}(\tau) = E[x_k(t)\ y_k(t+\tau)].$$

Now, consider the kth sample records $x_k(t)$ and $y_k(t)$ of stationary random processes $\{x_k(t)\}$ and $\{y_k(t)\}$. Let,

$$S_{xy}(f,T,k) = X_k^*(f,T)\ Y_k(f,T)/T \qquad (A.1)$$

where, $0 \leq t \leq T$ and,

$$X_k(f,T) = \int_0^T x_k(t)\, e^{-j2\pi ft} \qquad (A.2a)$$

$$Y_k(f,T) = \int_0^T y_k(t)\, e^{-j2\pi ft}. \qquad (A.2.b)$$

The above integral equations represent the finite Fourier transform of the records $x_k(t)$ and $y_k(t)$, respectfully. We now wish to show that,

$$S_{xy}(f) = \lim_{T\to\infty} E[\ S_{xy}(f,T,k)\ ]\ /\ T.$$

Substituting Equations A.2 into Equation A.1 and changing variables to avoid confusion results in,

$$S_{xy}(f,T,k) = 1/T \int_0^T \int_0^T x_k(\xi)\, y_k(\zeta)\, e^{-j2\pi f(\zeta - \xi)}\, d\xi\, d\zeta. \quad \text{(A1.3)}$$

Now, let $\tau = \zeta - \xi$ and $d\tau = d\zeta$ so the range of integration changes from (ξ,ζ) to (ξ,τ). Equation A1.3 now becomes,

$$S_{xy}(f,T,k) = \int_{-T}^{0} \left[1/T \int_{-\tau}^{T} x_k(\xi)\, y_k(\xi+\tau)\, d\xi \right] e^{-j2\pi f\tau}\, d\tau$$

$$+ \int_{0}^{T} \left[1/T \int_{0}^{T-\tau} x_k(\xi)\, y_k(\xi+\tau)\, d\xi \right] e^{-j2\pi f\tau}\, d\tau. \quad \text{(A1.4)}$$

Taking the expected value of both sides of Equation A1.4 and recalling that the definition of the cross-correlation function is,

$$R_{xy}(\tau) = E[x_k(t)\, y_k(t+\tau)]$$

Equation A1.4 becomes,

$$E[S_{xy}(f,T,k)] = \int_{-T}^{0} \left[1/T \int_{-\tau}^{T} R_{xy}(\tau)\, d\xi \right] e^{-j2\pi f\tau}\, d\tau$$

$$+ \int_{0}^{T} \left[1/T \int_{0}^{T-\tau} R_{xy}(\tau)\, d\xi \right] e^{-j2\pi f\tau}\, d\tau$$

$$= \int_{-T}^{T} (1 - |\tau| / T) R_{xy}(\tau) e^{-j2\pi f\tau} d\tau. \qquad \text{(A1.5)}$$

Taking the limit as T tends to infinity of Equation A1.5 results in the following expression,

$$\lim_{T\to\infty} E[S_{xy}(f,T,k)] = \int_{-\infty}^{\infty} R_{xy}(\tau) e^{-j2\pi f\tau} d\tau. \qquad \text{(A1.6)}$$

But from the definition of $S_{xy}(f,T,k)$, Equation A1.6 becomes,

$$S_{xy}(f) = \lim_{T\to\infty} E[X_k^*(f,T)\, Y_k(f,T)/T] = \int_{-\infty}^{\infty} R_{xy}(\tau) e^{-j2\pi f\tau} d\tau. \qquad \text{(A1.7)}$$

The above expression is the desired result for the cross-spectral density function. The other auto spectral density functions of x(t) and y(t) follow directly and are given by,

$$S_{xx}(f) = \lim_{T\to\infty} E[X_k^*(f,T)\, X_k(f,T)/T] = \int_{-\infty}^{\infty} R_{xx}(\tau) e^{-j2\pi f\tau} d\tau \qquad \text{(A1.8)}$$

$$S_{yy}(f) = \lim_{T\to\infty} E[Y_k^*(f,T)\, Y_k(f,T)/T] = \int_{-\infty}^{\infty} R_{yy}(\tau) e^{-j2\pi f\tau} d\tau. \qquad \text{(A1.9)}$$

From the above results the single-sided auto and cross-spectral density functions are,

$$G_{xx}(f) = 2 \lim_{T\to\infty} E[X_k^*(f,T)\, X_k(f,T)/T] = 2\int_{-\infty}^{\infty} R_{xx}(\tau)\, e^{-j2\pi f\tau}\, d\tau \qquad \text{(A1.10)}$$

$$G_{yy}(f) = 2 \lim_{T\to\infty} E[Y_k^*(f,T)\, Y_k(f,T)/T] = 2\int_{-\infty}^{\infty} R_{yy}(\tau)\, e^{-j2\pi f\tau}\, d\tau \qquad \text{(A1.11)}$$

$$G_{xy}(f) = 2 \lim_{T\to\infty} E[X_k^*(f,T)\, Y_k(f,T)/T] = 2\int_{-\infty}^{\infty} R_{xy}(\tau)\, e^{-j2\pi f\tau}\, d\tau. \qquad \text{(A1.12)}$$

The above expressions show the relationship between the cross and auto spectral density functions and the Fourier transforms of their time records $x_k(t)$ and $y_k(t)$. These expressions are exact and represent the true spectral functions for the limiting case of T.

APPENDIX 2

SOUND PROPAGATION IN CIRCULAR TUBES

The general wave equation in cylindrical coordinates is given as,

$$\frac{\partial^2\Phi}{\partial r^2} + \frac{1}{r}\frac{\partial\Phi}{\partial r} + \frac{1}{r^2}\frac{\partial^2\Phi}{\partial\varphi^2} + \frac{\partial^2\Phi}{\partial z^2} = \frac{1}{c^2}\frac{\partial^2\Phi}{\partial t^2} \qquad (A2.1)$$

In the above expression r, φ, and z are the usual spatial coordinates, t is the time variable and c, the sound speed of the medium. Solutions to Equation A2.1 will be of the form,

$$\Phi = R(r)\, Z(z)\, \Psi(\varphi)\, T(t). \quad (A2.2)$$

Substituting equation A2.2 into Equation A2.1 and using separation of variables; the wave equation for the radial dependency is given as,

$$\frac{1}{R}\frac{\partial^2 R}{\partial r^2} + \frac{1}{rR}\frac{\partial R}{\partial r} + k_r^2 - m^2/r^2 = 0. \qquad (A2.3)$$

In the above expression k_r, and m are separation constants. The standing wave solution to Equation A2.3 is given in terms of Bessel functions and Neumann functions of order m, such that;

$$R(r) = A\, J_m(k_r r) + B\, N_m(k_r r), \qquad (A2.4)$$

where A and B are constants. For wave propagation in a cylinder of outer radius a, the solution must be defined at r=0, therefore B must be

identically equal to 0. For a tube with rigid walls the velocity is zero at r=a. Therefore, the roots of Equation A2.4 are computed from (where $\gamma_{mv} = k_r a$),

$$\frac{\partial}{\partial r} J_m(k_r r) \Big|_{r=a} = k_r J_m'(\gamma_{mv}) = 0. \quad (A2.5)$$

Table A2.1 shows the first few roots of Equation A2.5.

Table A2.1: Roots of $J_m'(\gamma_{mv})$

m	v=0	v=1	v=2	v=3
0	0	3.83	7.02	10.17
1	1.84	5.33	8.54	11.71
2	3.05	6.71	9.97	13.71
3	4.20	8.02	11.35	14.59

For frequencies below the lowest non-zero mode (0,1) of propagation, only axial plane waves can propagate in the tube. Therefore, an expression for this lowest cutoff mode can be written as,

$$\gamma_{10} = \omega_{10} a / c = 1.84$$

where c, is the sound speed of the fluid and ω is the radian frequency. In terms of the lowest cutoff frequency, the above expression can be written as,

$$f_{10} = f_{CO} = 0.293\ c/a.$$

The above expression represents the uppermost frequency for which plane axial wave propagation exists in a rigid-walled tube. Higher order modes represent non-axial wave propagation and are excited at the tube termination or, from disturbances in the tube.

APPENDIX 3

RANDOM AND BIAS ERRORS IN THE CROSS-DIFFERENCE SIGNAL SPECTRUM

Essentially two types of errors occur in the analysis of random data. These types of errors are normally termed the "random" and "bias" errors of measurement.

Bias errors (ϵ_b) are independent of the data under analysis and result from the number of ways that data is analyzed and processed. For instance, data tapering, a process that involves various types of data weighting, has a number of errors associated with it. A major type of one of these errors (in the measured data) is due to the bandwidth associated with the analysis window. That is, the amplitude of a harmonic estimate is biased due to the broad-band noise included in the bandwidth of the analysis window's major lobe. Side lobes--associated with most types of analysis windows--also allow spectral leakage to "spill over" into the major lobe and can account for significant errors in the harmonic estimate if large amounts of higher frequency energy is present. These types of errors result in an constant increase (bias) in the true spectrum that would otherwise be observed if the analysis window had infinite resolution (i.e. zero bandwidth main lobe with no side lobes).

Random errors (ϵ_r) occur because averaging operations must occur over a finite extent or, for a limited sample size. The random scatter in the measured values that results from the finite sampling time are then referred to as "random" error.

Bendat and Piersol (1980) have derived various formulae that describe the bias and random errors inherent in the auto and cross-spectral density estimates and for the coherence function. These errors are tabulated below in Table A3.1.

Table A3.1: Estimation Errors in the Measured Spectral Density Functions.

Estimated Function	Bias Error, ϵ_b	Random Error, ϵ_r
Autospectrum, $G_{xx}(f)$	$-1/3\ (B_e/B_r)^2$	$1/\sqrt{n_d}$
Cross-spectrum, $G_{xy}(f)$	$-1/3\ (B_e/B_r)^2$	$1/\lvert\gamma_{xy}(f)\rvert\sqrt{n_d}$
Coherence, $\gamma_{xy}(f)$	Undefined	$\sqrt{2}\,(1-\gamma^2_{xy})/\lvert\gamma_{xy}\rvert\sqrt{n_d}$

In the above table B_e and B_r refer to the spectral resolution and half power point bandwidths, respectfully and n_d is the number of spectral averages taken.

For data acquired in the glycerine tunnel random errors in the estimate of the cross-difference signal spectrum (G_{tb1}) are approximately on the order of 12% or, 1.1 dB. The corresponding bias error due to the 2.5 Hertz analysis bandwidth (B_e) is negligible if the turbulent boundary layer pressure spectrum is approximated as band-limited white noise (i.e. B_r in this case will be the bandwidth of the data). The random error associated with the coherence function of the (pressure) transducer difference signals is estimated at 13% or, 1.2 dB. The bias error associated with a typical

autospectrum measured by a single transducer is difficult to estimate due to the sharp peaks that occur in spectrum (i.e. hard to define B_r). However, the random error associated with the autospectrum's 256 spectral averages is on the order of 6% or, 0.5 dB. Random errors associated with the cross-spectral (acoustic) measurements of two pressure sensors are not known, because a corresponding coherence function measurement was not taken. However, these random errors are not expected to be any greater than those associated with other spectral measurements and are at most between 10 to 12%.

APPENDIX 4

CORCOS' CORRECTIONS TO THE ESTIMATED TBL WALL PRESSURE SPECTRUM

Corcos (1963) proposed various correction factors, due to the attenuation of the high-frequency content of the turbulent boundary layer pressure spectrum (TBL) caused by its measurement with a finite-sized sensor. These correction are based on the similarity parameter $\omega a/U_c$ in which a is the transducer radius and U_c, the convection velocity of the pressure producing eddies. The following summarizes Corcos' results for a circular pressure sensor.

Table A4.1: Attenuation Factors for a Round Transducer.

$\omega a/U_c$	Φ_m/Φ	$10\log(\Phi_m/\Phi)$
0.05	0.9651	-0.15
0.10	0.9313	-0.31
0.15	0.8996	-0.46
0.20	0.8698	-0.61
0.30	0.8123	-0.90
0.40	0.7585	-1.20
0.50	0.7069	-1.50
0.60	0.6573	-1.82
0.70	0.6094	-2.15
0.80	0.5632	-2.49
0.90	0.5186	-2.85
1.00	0.4758	-3.23

In the above table Φ_m is the measured TBL wall pressure spectrum with a transducer of radius a and, Φ is the true spectrum, measured by a point transducer.

The frequency range of the TBL wall pressure spectrum measured in the glycerine tunnel was from 1 Hz, to 800 Hz (50 dB down point). This range, corresponded to normalized transducer radii ($\omega a/U_c$) of 7.9×10^{-4} to, 0.63. From these values and the corresponding corrections given in Table A4.1, corrections to the TBl wall pressure spectrum are for the most part less than 1dB and therefore insignificant, considering the accuracy of measurement. In closing, if the true parameter describing the high frequency resolution of the TBL wall pressure spectrum is $d^+(= u_\tau d/\upsilon)$, as Chapter 4 suggests, then, the above corrections based on the similarity parameter $\omega a/U_c$ should not apply.

BIBLIOGRAPHY

Bakewell, Jr., H. P. "An Experimental Investigation of the Viscous Sublayer in Turbulent Pipe Flow," Ph.D Thesis, The Pennsylvania State University (1966).

Bendat, J. S., A. G. Piersol Engineering Applications of Correlation and Spectral Analysis, Wiley and Sons, New York 1980, pp. 15-77.

Bendat, J. S., A. G. Piersol Random Data: Analysis and Measurement Procedures, Wiley and Sons, New York 1971, p 82.

Blackwelder, R. F., R. E. Kaplan "On the Wall Structure of the Turbulent Boundary Layer," Journal of the Acoustical Society of America, 76:89 (1976).

Blake, W. K. "Turbulent Boundary Layer Wall Pressure Fluctuations on Smooth and Rough Walls," Journal of Fluid Mechanics, 44:637 (1970).

Blake, W. K., D. M. Chase "Wavenumber-Frequency Spectra of Turbulent Boundary Layer Pressure Measured by Microphone Arrays," Journal of the Acoustical Society of America, 49:862 (1971).

Blake, W. K. "Aero-Hydroacoustics For Ships Volume II," David Taylor Naval Ship Research Center, Rep. No. DTNSRDC-84/010 (June 1984).

Bull, M. K., J. L Willis "Some Results of Experimental Investigations of the Surface Pressure Field Due to a Turbulent Boundary Layer," Dept. Aero.-Astroeng., Univ. Southampton, Rep. 99. (1961).

Bull, M.K. "Wall Pressure Fluctuations Associated With Subsonic Turbulent Boundary Flow." Journal of Fluid Mechanics, 28:719 (1967).

Bull, M. K., A. S. W. Thomas "High Frequency Wall-Pressure Fluctuations in Turbulent Boundary Layers," Physics of Fluids, 19(4):597 (1976).

Chase, D. M. "Modeling the Wavevector-Frequency Spectrum of Turbulent Boundary Layer Wall Pressure," Journal of Sound and Vibration, 70:29 (1980).

Corcos, G. M., J. W. Cuthbert "On the Measurement of Turbulent Pressure Fluctuations with a Transducer of Finite Size," Univ. of Cal. Inst. Eng. Research, Rep. Ser. 82, No. 112 (Nov. 1959).

Corcos, G. M. "Resolution of Pressure in Turbulence," Journal of the Acoustical Society of America, 35:192 (1963).

Corcos, G. M. "The Structure of the Turbulent Pressure Field in Boundary-Layer Flows," Journal of Fluid Mechanics, 18:353 (1964).

Emmerling, R. "The Instantaneous Structure of the Wall Pressure Under a Turbulent Boundary Flow," Max-Planck-Institut Fur ü Strömungsforschug, Rep. No. 9/1973 (1973).

Farabee, T. M., E. F. Geib, Jr. "Measurement of Boundary Layer Pressure Fields with an Array of Pressure Transducers in a Subsonic Flow," David Taylor Naval Ship Research Center, DTNSRDC Rep. 76-0031 (March 1976).

Ffowcs-Williams, J. E. "Boundary Layer Pressures and the Corcos Model: a Development to Incorporate Low-Wavenumber Constraints," Journal of Fluid Mechanics, 125:9 (1982).

Galib, T. A., A. Zardina "Turbulent Pressure Fluctuations with Conventional Piezoelectric and Miniature Piezoresistive Transducers,"108th Meeting of the Acoustical Soc. of Am., Mpls., Mn., J.A.S.A. Suppl. 1, 76 (Fall 1984).

Geib, Jr., F. E. "Measurements on the Effect of Transducer Size on the Resolution of Boundary-Layer Pressure Fluctuations," Journal of the Acoustical Society of America, 46:253 (1969).

Gordon, C. G. "Noise Generation by Fluid Flow Through Pipes," Conference of the ASME Winter 1969 Meeting.

Greshilov, E. M., M. A. Mironov "Experimental Evaluation of Sound Generated by Turbulent Flow in a Hydrodynamic Duct," Sov. Phys. Acoust., 29(4):275 (1983).

Haddle, G. P., E. J. Skudrzyk "The Physics of Flow Noise," Journal of the Acoustical Society of America, 46:130 (1969).

Harris, F. J. "On the Use of Windows for Harmonic Analysis With the Discrete Fourier Transform," Proceedings of the IEEE, 66(1) (January 1978).

Herzog, S., J. L. Lumley "Determination of Large Eddy Structures in the Viscous Sublayer," Unpublished 1979.

Hinze, J. O. Turbulence, an Introduction to its Mechanism and Theory, McGraw Hill, New York, 1959.

Hodgson, T. H. "Pressure Fluctuations in Shear Flow Turbulence," College of Aeronaut., Cranfield Note No. 129 (1962).

Hodgson, T. H. "On the Dipole Radiation From a Rigid and Plane Surface," Proceedings Purdue Noise Conference (1971).

Horne, M. P., R. J. Hansen "Minimization of the Farfield Acoustic Effects in Turbulent Boundary Layer Wall Pressure Fluctuation Experiments," 1981 Symp. on Turbulence, Univ. of Mo.-Rolla.

Kraichnan, R. H. "Pressure Field Within Homogeneous Anisotropic Turbulence," Journal of the Acoustical Society of America, 28:1-64 (1956a).

Kraichnan, R. H. "Pressure Fluctuations in Turbulent Flow over a Flat Plate," Journal of the Acoustical Society of America, 28:378 (1956b).

Lighthill, M. J. "On Sound Generated Aerodynamically, I: General Theory," Proc. R. Soc. (London), A-211:564 (1952).

Lighthill, M. J. "On Sound Generated Aerodynamically, II: Turbulence as a Source of Sound," Proc. R. Soc. (London), A-221:1 (1954).

Lauchle, G. C. "Noise Generated by Axisymmetric Turbulent Boundary Layer Flow," Journal of the Acoustical Society of America, 61(3):694 (1977).

Lauchle, G. C. Unpublished notes from a short course on, Underwater Acoustics, The Pennsylvania State Univ.

Lilley, G. N. "Pressure Fluctuations in an Incompressible Turbulent Boundary Layer," College of Aeronaut., Cranfield Rep. 133 (1960).

Lilley, G. N., T. H. Hodgson "On Surface Pressure Fluctuations in Turbulent Boundary Layers," AGARD Rep. 276 (1960).

Lilley, G. N. "A Review of Pressure Fluctuations at Subsonic and Supersonic Speeds," Arch. Mechanics Stosow, 16:301 (1964).

Maestrello, L. "Measurement of Noise Radiated by Boundary Layer Excited Panels," Journal of Sound and Vibration, 2:100 (1965a).

Maestrello, L. "Measurement and Analysis of the Response Field of Turbulent Boundary Layer Excited Panels," Journal of Sound and Vibration, 2:270 (1965b).

Maestrello, L. "Use of Turbulent Model to Calculate the Vibration and Radiation Responses of a Panel, with Practical Suggestions for Reducing the Sound Level," Journal of Sound and Vibration, 5:407 (1967).

Martin, N. C., P. Leehey "Low Wavenumber Wall Pressure Measurements Using a Rectangular Membrane as a Spatial Filter," Journal of Sound and Vibration, 52:95 (1977).

Meecham, W. C. "Surface and Volume Sound from Boundary Layers," Journal of the Acoustical Society of America, 37:516 (1965).

Nishi, R. Y., J. H. Stockhausen, E. Evensen — "Measurement of Noise on an Underwater Towed Body," Journal of the Acoustical Society of America 48:753 (1970).

Patrick, H. B. L. — "Turbulent Boundary Layer Wall-Pressure Fluctuations on an Axisymmetric Body." Naval Ocean Systems Center, Tech. Rep. No.149 (1977).

Schewe, G. — "On the Structure and Resolution of the Wall-Pressure Fluctuations Associated with the Turbulent Boundary-Layer," Journal of Fluid Mechanics, Vol. 134:311 (1983).

Schlichting, H. — Boundary-Layer Theory, 7th Edition McGraw-Hill, New York 1979, pp. 596-602.

Schloemer, H. H. — "Effects of Pressure Gradients on Turbulent Boundary Wall Pressure Fluctuations," U.S. Navy Underwater Sound Lab., Rept No. 747 (1966).

Skudrzyk, E. S., C. P. Haddle — "Noise Production in a Turbulent Boundary Layer by Smooth and Rough Surfaces," Journal of the Acoustical Society of America, 532:19 (1960).

Skudrzyk, E. G. — The Foundations of Acoustics: Basic Mathematics and Basic Acoustics, Springer-Verlag, Wein-New York 1971, pp. 428-431 (1971).

Tam, C. K. W., — "Intensity, Spectrum, and Directivity of Turbulent Boundary Layer Noise," Journal of the Acoustical Society of America, 57:25 (1975).

Vecchio, E., C. A. Wiley — "Noise Radiated from a Turbulent Layer," Journal of the Acoustical Society of America, 53:596 (1973).

Wambsganss, M. W., J. A. Jendrzejczyk, W. P. Lawrence — "Wall Pressure Fluctuations on a Cylinder in Annular Water Flow," Argonne National Laboratory, Tech. Mem. ANL-CT-79-38, (May 1979).

Willis, J. — "Measurement of the Wavenumber/Phase Velocity Spectrum of the Wall Pressure Beneath a Turbulent Boundary Layer," Journal of Fluid Mechanics, 45:65 (1970).

Willmarth, W. W. — "Wall Pressure Fluctuations in a Turbulent Boundary Layer," Journal of the Acoustical Society of America, 28:1048 (1956).

Willmarth, W. W., C. E. Wooldridge — "Measurements of the Fluctuating Pressure at the Wall Beneath a Thick Turbulent Boundary Layer," Journal of Fluid Mechanics, 14:187 (1962).

Willmarth, W. W., F. W. Roos — "Resolution and Structure of the Wall Pressure Field Beneath a Turbulent Boundary Layer," Journal of Fluid Mechanics, 22:81 (1965).

Willmarth, W. W. — "Pressure Fluctuations Beneath Turbulent Boundary Layers," Ann. Rev. of Fluid Mech., 134:311-328 (1975).

Wilson, R. J., B. Jones, R. Roy — "Measurement Techniques of Stochastic Pressure Fluctuations in an Annular Flow," Sixth Symposium on Turbulence, Univ. Missouri-Rolla (October 1979).

Witting, J. M. "A Spectral Model of Pressure Fluctuations at a Rigid Wall Bounding an Incompressible Fluid, Based on Turbulent Structures in the Boundary Layer." Noise Control Eng. Journal. 26:28 (1986).